

Eisosome Biogenesis and Organization

by

Karen Elizabeth Moreira

DISSERTATION

Submitted in partial satisfaction of the requirements for the degree of

DOCTOR OF PHILOSOPHY

in

Cell Biology

in the

GRADUATE DIVISION

of the

UNIVERSITY OF CALIFORNIA, SAN FRANCISCO

Approved:

Jeffrey S. Cox

Jan 11, 2010

M. Zentgraf

01.11.10

Peter Weid

Jan 11, 2010

Committee in Charge

UMI Number: 3390106

All rights reserved

INFORMATION TO ALL USERS

The quality of this reproduction is dependent upon the quality of the copy submitted.

In the unlikely event that the author did not send a complete manuscript and there are missing pages, these will be noted. Also, if material had to be removed, a note will indicate the deletion.



UMI 3390106

Copyright 2010 by ProQuest LLC.

All rights reserved. This edition of the work is protected against unauthorized copying under Title 17, United States Code.



ProQuest LLC
789 East Eisenhower Parkway
P.O. Box 1346
Ann Arbor, MI 48106-1346

ACKNOWLEDGEMENTS

I would like to thank the mentors that that guided me trough my graduate career and made this journey more amiable: Marc Shuman, Barbara Panning, Robert Farese, Elizabeth Blackburn, Holly Ingraham, Sandy Johnson, Allan Balmain, Ben Cheyette, David Agard, Geeta Narlikar, Joe DeRisi. A special thanks to Carol Gross who was very instrumental to my acceptance to UCSF and watched my every step. To Peter Walter, for being nurturing and supporting and providing me with tools to advance in science and in life. To my collaborator and mentor, Tobias Walther, for teaching me that synergy, perseverance and hard work are tickets to success in the sciences. To my collaborators for sharing the excitement and agony that this project has brought to us, Pablo Aguilar, Florian Fröhlich, and Sebastian Schuck who worked closely with me on the Pen1 story. Next I would like to thank current and former members of the Walter lab, special thanks to Tomas Aragon, Sebastian Bernales, and Alex Engel, for being great friends and very encouraging. To Shannon Behrman and Claudia Rubio for their friendship, companionship and support. To my close friends, ‘the musketeers’, for sharing the good and the bad moments every step of the way: Isla Cheung, Rowena Suriben and Han Li.

Finally I would like to thank my family in particular my husband Jesus Betancourt for being my rock and source of support, energy and understanding the dedication to my work. I would like to dedicate this work to my grandmother, Elsa Flores Paniagua, she raised me and encouraged me to become an independent and strong woman and to pursue my goals fearlessly, I wish you were here to see the final product; you are always in my heart.

The text of Chapter 2 is a reprint of the material as it appears in *Molecular Biology of the Cell*. The research was directed and supervised by Peter Walter. Tobias Walther and Karen Moreira collaborated closely in designing the experiments, performing the experiments, and writing the manuscript. Pablo Aguilar was also collaborated in various parts of the experimental design and writing of the manuscript.

The text of Chapter 3 is a reprint of the material as it appears in *The Journal of Cell Biology*. The research was directed and supervised by Peter Walter and Tobias Walther. Karen Moreira carried out the genome-wide genetic visual screen, experimental design, and imaging, scoring of entire set, secondary imaging of candidate genes and contributed to writing the manuscript. Quantification and scoring of individual candidates was done in collaboration between Karen Moreira, Tobias Walther, and Pablo Aguilar. Florian Fröhlich carried out the characterization of Nce102, endocytosis assay, isolation of detergent-resistant membranes, and wrote the majority of the manuscript. He also collaborated with Nina Hubner and Matthias Mann to carry out SILAC and mass spectrometry on Pil1.

EISOSOME BIOGENESIS AND ORGANIZATION

KAREN MOREIRA

ABSTRACT

The plasma membrane is a highly dynamic organelle controlling the traffic of molecules, nutrients, and ions into and out of the cell according to need. We discovered a novel protein complex required for proper membrane integrity and marks sites of endocytosis, termed ‘eisosome’. Eisosomes are static assemblies that distribute uniformly in a punctate pattern under the plasma membrane. We currently do not understand the mechanism of formation by which they are inherited to maintain stability, uniform size, distribution and organization. We explored the rules of eisosome formation and distribution focusing on the role of Pil1, one of the main components, in their formation and organization. In addition, we conducted a genomic-wide visual screen to identify genes required for proper eisosome organization. Eisosome formation happens *de novo* in daughter cells in a polarized fashion with an initial lag phase. Lowering Pil1 levels reduces eisosome density to maintain a minimal size while increased Pil1 levels results in larger eisosomes while maintaining the set density. This is not true when Pil1 is removed from cell cycle control. We show that the temporal expression level of Pil1 during G2/M phase of the cell cycle controls eisosome size and set density.

The genome-wide screen identified two novel eisosome components, Nce102 and Pen1. Deletion of either gene results in reduced eisosome assembly and increased Pil1 localization to the cytoplasm but their modes of action are different. Nce102 moves into and out of eisosomes in response to sphingolipid levels, and found to negatively regulate Pkh signaling and eisosome assembly. Nce102 deletion causes an increase in Pil1 phosphorylation mediated by the Pkh kinases and a nonphosphorylatable mutant of Pil1 is resistant to it. Pen1 was found to be an eisosome nucleator, its deletion results in a delayed aberrant eisosome formation and plasma membrane deformities. Its deposition in small buds lacks a lag phase and it precedes Pil1. Its association to the membrane is independent of Pil1, but Pil1 is needed to stabilize its localization to eisosomes. In addition, Pen 1 overexpression results in overnucleated long shaped eisosomes and a mutation on the second phenylalanine rescues this phenotype.

TABLE OF CONTENTS

Chapter 1	Introduction	p. 1
Chapter 2	Pil1 Controls Eisosome Biogenesis	p. 15
Chapter 3	A Genome-Wide Screen for Genes Affecting Eisosomes Reveals Nce102 Function in Sphingolipid Signaling	p. 60
Chapter 4	Pen1 Promotes Eisosome Nucleation and Elongation	p. 121
References		p. 147

LIST OF TABLES

2-S1	Strains used in biogenesis study	p. 58
2-S2	Coordinates for eisosome position in biogenesis study	p. 59
3-S1	Strains used in Nce102 study	p. 120
4-8	Strains used in Pen1 study	p. 146

LIST OF FIGURES

2-1	Eisosomes are assembled de novo	p. 42
2-2	Eisosome assembly occurs in a polar fashion	p. 43
2-3	Eisosome density is constant and regulated to a set-point	p. 45
2-4	Eisosomes are distributed randomly	p. 46
2-5	Eisosomes are formed in a continuous process	p. 48
2-6	Eisosome number and size is controlled by the levels of Pil1	p. 49
2-7	Pil1 expression is cell cycle regulated	p. 51
2-8	Pil1-GFP expression from the <i>CUP1</i> promoter	p. 53
2-9	Pil1 expression from the <i>CUP1</i> promoter in LSP1-GFP cells	p. 54
2-S1	Pil1 and Lsp1 behave identically during de novo eisosome formation	p. 56
3-1	A functional genomic screen reveals genes required for eisosome organization	p. 96
3-2	Nce102 is required for normal plasma membrane organization	p. 97
3-3	Nce102 localizes to both MCC and non-MCC domains in the plasma membrane	p. 98
3-4	Nonphosphorylatable Pil1 is resistant to <i>nce102Δ</i>	p. 100
3-5	Pil1 phosphorylation is increased in <i>nce102Δ</i> cells	p. 101
3-6	Mutation of Pkh kinases is epistatic to <i>nce102Δ</i>	p. 103
3-7	Nce102 and sphingolipids act in the same pathway	p. 104
3-8	Overexpression of Nce102 suppresses eisosomes disassembly after sphingolipid synthesis block	p. 106
3-9	Nce102-GFP localization depends on sphingolipid levels	p. 107
3-10	Model for Nce102 function in sphingolipid sensing	p. 109

3-S1	A visual screen for genes affecting Pil1-GFP	p. 110
3-S2	Mass spectrometric analysis of Pil1 shows increased Pil1 phosphorylation in <i>nce102Δ</i> and myriocin-treated cells compared with wild-type cells	p. 112
3-S3	Relationship of Nce102 with sphingolipid metabolism	p. 114
3-S4	Localization of Nce102-GFP in response to altered sphingolipid levels or mutations of Pil1 or Pkh kinases	p. 116
3-S5	Pkh2 and Nce102 colocalization depends on sphingolipid synthesis	p. 118
4-1	Pen1 is required for normal eisosome and membrane organization	p. 137
4-2	Pen1 colocalizes with eisosomes and its deposition precedes that of Pil1	p. 138
4-3	Pen1 localizes to the plasma membrane independent of Pil1 and Nce102	p. 140
4-4	Pen1 overexpression causes eisosomes to nucleate into rods	p. 141
4-5	Eisosome brightness increases with increased Pen1 expression levels	p. 143
4-6	Pen1 nucleating function is compromised in <i>pen1(F2A)</i> mutant cells	p. 144
4-7	Eisosome nucleation and assembly model	p. 145

CHAPTER 1

INTRODUCTION

The plasma membrane is a highly dynamic and complex organelle that functions to protect the cell from the outside environment. The plasma membrane contains various receptors that sense extracellular conditions, as well as transporters and channels needed to traffic of molecules such as nutrients, ions and catabolites. While all of these exchanges happen at the cell surface, the composition of the plasma membrane is dynamically regulated, with endocytosis of specific proteins playing a prominent role. It is still not fully understood how these events are orchestrated to maintain membrane homeostasis, but with a tremendous membrane flux through the endocytic pathway of roughly 1% turnover / min, the nature of the process poses the need for a tight organization of events at the plasma membrane.

Some big questions in the field are, how the dynamic trafficking from the plasma membrane is organized and controlled, and how particular cargo 'know' to enter a specific endocytic event. An interesting clue arising from studies in budding yeast is the existence the eisosome. Eisosomes are organized structures with a defined location at the plasma membrane around which rapid endocytosis occurs (Walther et al., 2006). The following thesis explores the framework of eisosome biogenesis, the processes that affect their organization and their effects on plasma membrane organization. In this introduction, I will begin with a historical view of the development of the idea membrane compartmentalization followed by the description of the types of membrane domains found in *Saccharomyces cerevisiae*. I will then introduce the discovery of eisosomes and their connection to endocytosis. Also, I will discuss what was known about the effects of phosphorylation and Pkh signaling on eisosome organization. Finally I will discuss in an outlook the possible role of eisosomes in endocytosis.

Historical view of membrane compartmentation.

The two-dimensional fluid lipid bilayer model, originally proposed by Singer and Nicholson in 1972, became the classical way of depicting membranes. It consisted of transmembrane proteins sprinkled through the plasma membrane diffusing freely in a two dimensional pattern, without any organizational link to specific cellular processes (Singer and Nicholson, 1972). It is well known that distinct lipids undergo phase separation in synthetic lipid bilayers at equilibrium, raising the question of whether such lateral segregation of lipids occurs in the plasma membrane under physiological (and, by definition, non-equilibrium) conditions. Based on differential extraction of lipids and proteins from biological membranes by non-ionic detergents, and in an effort to explain pronounced compositional differences between the apical and basolateral surface domains of epithelial cells, Kai Simons and colleagues proposed just such a hypothesis more than a decade later. The observation of sphingolipid sorting to the apical domain of epithelial cells (van Meer et al., 1997; Simons and van Meer, 1988) and eventually the biochemical studies of sphingolipid, GPI-anchored proteins and cholesterol interactions, lead to the concept of lipid rafts and lateral protein/lipid segregation at the plasma membrane (Brown and Rose, 1992; Hanada et al., 1995; Simons and Ikonen, 1997). In particular, they posited the existence of phase-separated domains in the plasma membrane that are enriched in sphingolipids and cholesterol, and exist effectively as stable 'rafts' floating in a uniform 'sea' of other mixed lipids (largely phosphatidyl choline). Defining the physical properties of these proposed lipid rafts - their size, how many types there are, and whether or not they exist as stable structures- is a matter of

continuing investigation and debate. Nevertheless, it is increasingly clear that lateral heterogeneity does exist at some level in the plasma membrane, and that heterogeneity in lipid composition contributes to diverse physiological processes (Simons and Toomre, 2000; Brown and London 1998; Munro, 2003; van Meer et. al., 2008; Mayor and Rao, 2004). In the present work, I will use the term 'lipid raft' as a shorthand for these still-mysterious inhomogeneities of the plasma membrane, which are defined operationally by being enriched in sphingolipids and certain sterols.

Membrane compartments in yeast.

Mammalian lipid rafts are primarily rich in cholesterol, sphingolipids (Rietveld and Simmons, 1998). These structures are evolutionary conserved, as the equivalent to lipid rafts were also found in yeast membranes, as regions that are rich in ergosterol and glycosphingolipids (Kübler et al., 1996; Bagnat et al., 2000). Although these microdomains are estimated to be in the nano scale range, 5-100nm, (Prior et al., 2003; Sharma et al., 2004; Lenne et al., 2006; Eggelin et al., 2009) Tanner and collaborators identified two mutually exclusive membrane compartments (MC's) (Malinksa et al., 2003). Tanner eventually termed these domains after the resident proteins found to localize in there. One of them is "MCP" for membrane compartment occupied by proton ATPase Pma1. This compartment forms one connected network of channels with islands in between. The islands compose the second domain, which is the "MCC" for membrane compartment occupied by the proton/arginine symporter Can1. This compartment forms stable patches with a diameter of ~300nm that are distributed uniformly on the plasma membrane and are colonized by a number of permeases such as Fur4, Tat2 and Hup1 in

addition to the transmembrane protein Sur7, protein associated to sphingolipid synthesis, plasma membrane and cell wall integrity, and endocytosis (Young et al., 2007; Alvarez et al, 2008 and 2009). In addition, it was found that these two compartments are highly dynamic and the localization of some proteins to their home compartment can be disrupted by a change in membrane potential (Grossmann, et al., 2007). But the functional importance of this compartmentation was shown by the observation that both Pma1 and Can1 need to be associated into rafts to be effectively shuttled to and maintained at the plasma membrane. Mutations that affect sphingolipid and ergosterol synthesis result in their rapid turnover due to retargeting to the vacuole for degradation (Lee et al, 2002; Eisencolb et al., 2002; Malinska et al., 2003). Therefore, the lipid environment of a protein tightly determines the correct trafficking and fate of membrane proteins.

One main difference between the MCP and MCC is the characteristic stability of MCCs. FRAP (fluorescence recovery after photobleaching) experiments have shown that Pma1 molecules diffuse freely through the MCP, while Can1 patches remain immobile during cell growth (Malinska et al., 2003 and 2004). This stability is not attributed to the interaction with microtubules or actin cables since treatments with nocodazole (microtubule destabilizing drug) or latrunculin A (depolymerizes F-actin) did not affect their pattern. In addition, MCCs were still visualized in protoplasts after treatment with zymolase to hydrolyze the cell wall; ruling out the dependence of cell wall and membrane protein interactions to maintain stability of this compartment (Malinska et al, 2004). Subsequently, our group discovered another group of proteins that shares the spatial distribution and stability of MCCs in *Saccharomyces cerevisiae*. These proteins form

large assemblies underlying the plasma membrane at MCCs. We termed these eisosomes, derived from the Greek, 'eis' meaning into or portal and 'soma' meaning body (Walther et al., 2006).

The discovery of eisosomes.

Eisosomes are large, uniformly-sized complexes at the cell periphery that form a distinct punctate pattern that when visualized by fluorescence microscopy colocalize with MCCs. Their main components are cytoplasmic proteins that reside below this plasma membrane compartment although the transmembrane protein associated to eisosomes, Sur7, also resides in MCCs (Grossmann et al., 2007). Eisosome patches are highly uniform and estimated to be composed of a few thousands copies of identical subunits. FRAP experiments show that there is no exchange of subunits between eisosomes and like MCCs they are not affected by disruption of actin fibers, microtubule destabilization, or cell wall hydrolysis (Walther et al., 2006; Moreira et al., 2008). Eisosomes are thought to play a structural role to help define the membrane domain. Unlike MCCs, their stability is not disturbed by a change membrane potential, as Sur7 remains associated (Grossmann et al., 2007).

Eisosomes are mainly composed of two highly homologous phosphoproteins, Pil1 and Lsp1. These proteins were originally found in a large-scale study to form a complex with two partially redundant kinases, Pkh1 and Pkh2 (Ho et al, 2002) and negatively regulate their signaling (Zheng et al., 2004). Pil1 and Lsp1 share 72% sequence identity and have no apparent homology to known functional domains. Each eisosome contains 2000-5000 copies of each Pil1 and Lsp1. Despite their similarity, Pil1 has unique

properties not shared with Lsp1 and emerged early on as the major component important for eisosome organization. Deletion of *Pil1*, but not of *Lsp1* or *Sur7*, results in a collapse of eisosomes into 3-4 'remnants' per cell at the periphery for both *Lsp1*-GFP and *Sur7*-GFP with some *Lsp1* becoming cytoplasmic and some *Sur7* becoming uniformly distributed along the plasma membrane. In addition, the collapse of eisosome organization affected the plasma membrane integrity, as electron micrographs show that $\Delta pil1$ cells contain large aberrant invaginations seen with the same frequency in which eisosome remnants are detected by fluorescence microscopy (Walther et al., 2006). This deformity at the plasma membrane is likely to correspond to MCCs because filipin staining shows that sterols are concentrated there. Sterols are enriched in MCCs; these and MCC resident proteins also became distributed along the plasma membrane with a few bright remnants along the periphery in $\Delta pil1$ cells (Grossmann et al., 2007). This findings show that eisosomes organize subdomains at the plasma membrane and that their proper distribution is important to maintain protein and lipid compartmentation.

How eisosomes contribute to membrane structure became evident by elucidating the function associated with them. We found that eisosomes mark static sites of endocytosis (Walther et al., 2006). Endocytosis is a basic cellular process that is used to internalize nutrients, signaling receptors, and ensure appropriate membrane composition by recycling plasma membrane components. Despite multiple studies about the spatiotemporal dynamics of assembling an endocytic event and the importance of actin patches to drive these events, it is still not known where or how these events are triggered along the plasma membrane. Eisosomes were the first report of a specialized compartment in yeast that serves as a habitual harbor for the endocytic machinery. The

first clue came from the fact that Sur7 had been identified as an overexpression suppressor of an endocytic effector Rvs167 mutant strain. In particular, Sur7 can suppress the actin cytoskeleton disorganization in these mutants (Sivandon et al., 1997). The uptake of lipid was monitored with the fluorescent lipid dye FM4-64, enters the cell by endocytosis; and the uptake of protein cargo was monitored by fluorescently tagged hexose transporter Hxt2, internalized by endocytosis during high-glucose availability. The internalization of both FM4-64 and Hxt2 colocalized nicely with an eisosome. In addition, internalization was redirected to eisosome remnants in $\Delta pil1$ cells. We also observed that endocytic effectors Sla1 and Abp1 visited eisosomes and eisosome remnants more frequently than random spots at the cell periphery. This evidence suggested that the endocytic machinery assembled at eisosomes and that eisosomes, therefore, function as endocytic portals. Moreover, the endocytic rate in *PILI* deleted cells was compromised and was decreased by half (Walther et al., 2006). An uncontrolled continuous triggering of endocytic events and resulting in a continuous tugging of the membrane at eisosome remnants may contribute to the membrane deformity seen in *PILI* deleted cells. One can imagine that the influx of membrane components may exceed the efflux at these sites, making it impossible to restore membrane homeostasis. Therefore, having these portals uniformly distributed throughout the cell periphery is important to ensure membrane integrity and serve as a convenient docking site for efficient recruitment of the endocytic machinery and cargo internalization.

The role of Pil1 and Lsp1 in Pkh signaling.

As it was noted before, Pil1 and Lsp1 are modulators of Pkh signaling. The yeast Pkh kinases are the yeast homologs of the mammalian 3-phosphoinositide-dependent protein kinase 1 (PDK1) and have two known substrates, Pkc1-MAP Kinase and protein kinases Ypk1 and Ypk2. These targets regulate the cell wall integrity pathway, and actin repolarization during heat stress (Inagaki et al., 1999; Casamayor et al., 1999; Delley et al., 1999). Pkhs are known to be regulated by long chain bases (LCBs), dihydrosphingosine (DHS) and phytosphingosine (PHS) (Sun et al., 2000). LCBs are important regulators during heat stress when they transiently increase (Dickson et al., 1997; Jenkins et al., 1997). LCBs are also required for efficient endocytosis and actin patch polarization, and this process is mediated through the Pkhs. (Munn and Riezman, 1994; Zanolary et al., 2000; Friant et al., 2001; deHart et al., 2002). All of these findings point to a functional connection between Pkhs and eisosomes. Both Pil1 and Lsp1 are targets of Pkhs *in vivo* and *in vitro*, however the presence of LCBs affects their phosphorylation differently. They were named as Pil1 for phosphorylation is inhibited by LCBs; and Lsp1 for LCBs stimulate phosphorylation (Zhang et al., 2004). Zang et al. proposed a homeostatic model in which basal low levels of LCBs maintained Pil1 and Lsp1 in an inhibitory state to downregulate Pkh signaling. However, upon increase of LCBs during heat shock this inhibitory block was removed by a change in phosphorylation state, thus activating Pkh signaling. After this transient increase in LCBs ceases, then Pil1 and Lsp1 return to their inhibitory state to turn the signal back off. This model proposes that Pil1 and Lsp1 play a direct role in cell signaling and their localization at the cell periphery positions them conveniently to receive environmental

cues. We still do not understand however, how the eisosomes influence the endocytic functions of Pkhs and LCBs.

Effects of Pkh signaling and Pil1 phosphorylation on eisosome organization.

With increasing evidence to the importance of eisosome organization for proper protein segregation, the question of how this organization is achieved became more exciting. Since Pil1 is the main organizer of eisosomes, we explored the role of Pil1 phosphorylation and Pkh signaling in eisosome organization. It was noted before that Pkh1 but in particular Pkh2 had a punctate localization at the cell periphery very reminiscent to eisosomes (Roelants et al., 2002). We found that Pkhs did not only colocalize with eisosomes, but that they also modulated the assembly state of Pil1 into eisosomes. LCB and ceramide levels also affected the assembly state of eisosomes, and this response was mediated by Pkhs. We identified 11 phosphorylation sites on Pil1, four of which were modulated by Pkh signaling, S45, S59, S230 and T233. Eisosome disassembly was induced by hyperphosphorylation of Pil1 and can be mimicked by a phosphorylation mutant. Disassembly was also induced by overexpression of Pkh-kinases and increasing Pkh1 activity after reduction of LCBs either by mutations in the synthesis pathway or by using drug inhibition of LCB biosynthetic enzymes. On the other hand, eisosome assembly was induced by hypophosphorylation of Pil1 and can be mimicked by an unphosphorylatable form of Pil1. Reducing Pkh-kinase activity by mutations or upon addition of LCBs also lead to increased eisosome assembly (Walther et al., 2007). Our study, however, was challenged by a group that found three different forms of Pil1 phosphorylation, and showed that increased phosphorylation of Pil1 led

to eisosome disassembly, while decreased phosphorylation caused aberrant eisosome assembly (Luo et al., 2008). These discrepancies can be reconciled by considering that different phosphorylation mutant combinations and conditions were studied, and modifications of different residues on the protein may result in a different outcome.

What these findings have in common is that they suggest that changing levels of LCBs are sensed by Pkh-kinases to regulate the assembly state of eisosomes and possibly regulate their function on endocytosis. The conditions, under which phosphorylation states were tested were extreme cases, were all-or-none states of Pil1's phosphorylation status. It is likely that under physiological conditions the effects of Pkh signaling may be subtler.

One model proposed by our group is that Pkhs can sense the composition of the plasma membrane locally. Alternatively, LCBs function as second messengers and their reduction alerts eisosomes that conditions have changed and a particular cargo is ready for internalization. In this way phosphorylation of Pil1 may trigger an eisosome to fire an endocytic event. These findings open the door for future studies on the function of eisosomes.

Outlook: possible eisosome functions in endocytosis.

Genetic interactions and functional studies to date suggest that eisosome function in endocytosis may have to do with actin recruitment (Walther et al, 2006). Actin plays an important role in endocytosis in yeast and mammals (for a review see Robertson et al., 2009; Girao et al., 2008). Although endocytosis is a broad process and there are a wide variety of mechanisms in mammalian cells, I will focus on the most studied and the only form of endocytosis described in yeast cells, clathrin-mediated endocytosis. The

spatiotemporal features of endocytosis and the involvement of cortical actin patches at different steps were first studied by real-time fluorescence microscopy (Kaksonen et al., 2003). The internalization process was described as a modular event consisting of three main steps (Kaksonen et al, 2005). *Step 1*, is a non-motile phase in which the membrane is prepared for internalization; cargo and the coat modules (clathrin, Sla2, Pan1 and Sla2) are recruited to the membrane. In addition, an actin polymerization activator, Las17 is also put in place, but remains inhibited by one of the coat proteins (Sla1) until everything is ready to move on to the next step (Warren et al., 2002). This step is not known to involve actin, and the coat module prepares the membrane for the change in curvature. *Step 2*, is know as membrane invagination. This is a very slow inward movement of ~200 nm. The membrane is internalized by the pulling force of actin polymerization (the actin module) which is activated by a WASP/myo module. The WASP/myo module consists of Las17, type I myosin Myo5 and Bbc1; they remain non motile at the plasma membrane and serve as an anchor where they promote actin polymerization to make the vesicle. Yeast invaginations have been shown by electron microscopy to be tubular structures, rather than the classical flask shape seen in mammalian cells, and estimated to be about 50 nm wide and up to 150 nm long (Idrissi et al., 2008). Finally, *step 3* is where the scission event happens. This is a fast movement where the amphiphysins that contain membrane-deforming BAR domains, Rvs161 and Rvs167, which help to tubulate membranes for scission. Subsequently the vesicle moves inward ~100 nm, presumably due to the scission force, and then is quickly moved away from the membrane while the coat module is removed (Kaksonen et al., 2005 and 2006; Alastair et al, 2009).

Where and how eisosomes fit in this process is yet to be determined. However,

there are many genetic interactions between eisosomal components and proteins in the coat and amphiphysin modules that raise interesting ideas. Pil1 has been shown to be synthetic-lethal with a Pan1 temperature sensitive mutant, synthetic-sick with Sla1 deletion, and it suppresses the growth defect of a temperature sensitive mutation of Sla2 (Walther et al., 2006). This suggests that Pil1 may have a redundant role with some of these coat proteins. The coat proteins form a complex that not only recruits cargo but also mediates actin recruitment and activation. Sla1 can bind to both clathrin and actin, and mediates their interaction with Sla2. Together these two proteins bind Pan1, which is an activator of the actin nucleation complex Arp2/3. These events are coordinated with the inhibitory effect of Sla1 to another actin polymerization activator Las17 (Tang et al., 2000; Rodal et al., 2003; Wesp et al, 1997; Newpher and Lemmon 2006; Gourlay et al., 2003). This coordination may ensure the efficient internalization of the vesicle once the cargo is ready. Therefore, one possible role of Pil1 in endocytosis is to oversee the fidelity of the activation of actin polymerization, thereby ascertaining that polymerization only occurs after cargo has been loaded.

Lsp1 can suppress the low endocytic rate of Rvs161 deletion mutant. And Sur7 was identified as an overexpression suppressor of several defects in Rvs161 and Rvs167 deletion mutants including an actin patch polarization defect (Walther et al., 2006; Sivadon et al., 1997). These BAR domain proteins have been implicated in the scission of the vesicles, probably due to their tubulation properties (Peter et al, 2004). Their deletion causes invaginations to bounce back and not be internalized; however, some scission still occurs. Myosin I protein Myo5 helps the process (Jonsdottir and Li et al, 2004). Together suggests, these observations suggest that Lsp1 and Sur7 may overcome

the need for the amphiphysin module by changing the membrane properties to make a Myo5 mediated scission more efficient. Alternatively, they may be able to tubulate the membrane themselves to achieve scission. This model is supported by unpublished results and personal communication with Tobias Walther, that Lsp1 may have a BAR domain like structure. This preliminary result may answer how eisosomes, in particular Pil1 and Lsp1 since they are so similar, may affect plasma membrane structure, and how they are tethered to the plasma membrane.

But studies of endocytosis in yeast are still in infancy. There are numerous parallel endocytic pathways in mammalian cells known now, yet all yeast work has focused on only the clathrin-dependent pathway. Thus it is plausible that, eisosomes may be found to coordinate a novel and parallel type of endocytosis in yeast that still has to be discovered. Although this thesis does not answer some of these functional questions, it provides a structural framework for eisosome biogenesis and explores the processes that affect their organization. Thus it provides powerful molecular tools to study eisosome function in endocytosis.

The material in Chapter 2 was originally published online November 26, 2008 and appeared in print February 20 (*Mol Biol Cell*. 20(3):809-18), Copyright © 2008 by The American Society for Cell Biology. The article is available online at:

<http://www.molbiolcell.org/cgi/content/full/20/3/809>

CHAPTER 2

PIL1 CONTROLS EISOSOME BIOGENESIS

Pil1 Controls Eisosome Biogenesis

Karen E. Moreira^{*}, Tobias C. Walther^{*,#}, Pablo S. Aguilar, and Peter Walter

Howard Hughes Medical Institute, and

Department of Biochemistry and Biophysics,

University of California at San Francisco,

San Francisco, CA 94158,

USA

* These authors contributed equally to this work

Corresponding author; current address:

Organelle Architecture and Dynamics,

Max Planck Institute of Biochemistry,

Am Kopferspitz 18

82152 Martinsried, Germany

ABSTRACT

The molecular composition of plasma membranes is constantly remodeled by endocytosis and exocytosis. Eisosomes are large cytoplasmic protein assemblies that localize to specialized domains on the yeast plasma membrane. They are of uniform size and immobile, and their disruption leads to large aberrant plasma membrane invaginations and endocytic defects. It is unknown how eisosomes are formed or inherited and what governs their size, distribution, and location. Here we show that eisosomes are formed *de novo* in the bud of dividing cells. They colonize newly formed membrane at a fixed density in a polarized wave proceeding from the bud neck to the bud tip and become anchored at the site of their formation. Pil1, one of the two main eisosome subunits, emerges as the central regulator of eisosome biogenesis that determines both size and location of eisosomes. Lowering Pil1 expression leads to normal-sized eisosomes at a reduced density, suggesting that eisosomes must be of a minimal size. Conversely, raising Pil1 expression leads to larger eisosomes at a fixed density, suggesting that under these conditions eisosome nucleation sites are limiting. Pil1 expression is regulated by the cell cycle, which synchronizes eisosome formation with plasma membrane growth. Our results establish a first framework of the molecular principles that define eisosome assembly and distribution.

INTRODUCTION

All communication and exchange of metabolites such as nutrients and catabolites with the environment occurs across the cell's plasma membrane, which must dynamically adapt its molecular composition to changing conditions. As such, the plasma membranes of all eukaryotic cells are constantly remodeled by endocytosis and exocytosis. To accommodate these processes effectively, the plasma membrane is highly organized and laterally divided into domains of different composition and function. Plasma membrane organization has been characterized in many cell types and has been most extensively studied in polarized epithelial cells and neurons (Broadie, 2004; Rodriguez-Boulan et al., 2005). Specialized areas of the plasma membrane, such as the neuromuscular junction or the neuronal synapse, form zones of active endocytosis and exocytosis that are spatially separated, and disruption of this organization leads to impairment of membrane traffic (Koh et al., 2004; Marie et al., 2004).

Similar organizational features are found even in unicellular yeasts, such as *Saccharomyces cerevisiae*. In this organism, recent analysis of protein and lipid distribution revealed that the plasma membrane is laterally inhomogeneous. Examples include the polar distribution of ergosterol-rich domains to the shmoo tip during the formation of mating projections (Bagnat and Simons, 2002), the polarized distribution of plasma membrane proteins that are involved in the directed targeting of secretory vesicles to the bud tip (Valdez-Taubas and Pelham, 2003), and the non-uniform distribution of plasma membrane proteins, such as Can1 and Sur7, into punctate domains (Grossmann et al., 2007; Malinska et al., 2003; Malinska et al., 2004). Recently, we discovered large immobile structures, called eisosomes (from the Greek "eis" meaning "into" or "portal"

and “some” meaning “body”), that organize these latter domains and showed that they mark sites of endocytosis (Walther et al., 2006).

Eisosomes have fascinating features (Walther et al., 2006). They are large macromolecular assemblies of relatively uniform size, each composed of a few thousand copies of two principal subunits, Pil1 and Lsp1. They lie underneath the plasma membrane and localize in a punctate pattern that is not reminiscent of any other organelle, but colocalize with specialized membrane domains of unique protein and lipid composition (Grossmann et al., 2007). Eisosomes distribute evenly over the cell cortex, but the principles guiding this distribution are unknown. Deletion of *PILI* leads to clustering of the remaining eisosome components to one or a few spots (“eisosome remnants”) that are associated with grossly aberrant plasma membrane invaginations and causes a reduction of the endocytic rate (Walther et al, 2006). Eisosomes are immobile and, remarkably, do not exchange subunits with free cytoplasmic pools of Lsp1 or Pil1, indicating that after initial assembly, they are not subject to dynamic remodeling at the level of exchange of their major structural subunits. How eisosomes assemble, achieving both their uniform size and even distribution, is unknown. To gain first insights into eisosome biogenesis, we describe here the formation of eisosomes in dividing cells and define the rules that govern their formation.

RESULTS

Eisosomes form *de novo* and, after an initial lag phase, colonize the bud as a polar wave initiating at the bud neck

To begin to determine the rules that guide eisosome biogenesis, we first asked two simple questions: i) are new eisosomes derived by division of existing eisosomes or are they assembled *de novo*? And, ii) are they pre-assembled at some site in the cell and transported to their final location or do they form *in situ*? To distinguish between these possibilities, we fused *GFP* to *PIL1* at its endogenous genomic locus and observed the formation of new eisosomes by 3D confocal time-lapse microscopy with different time intervals (Supplemental Movie 1; Fig. 1). A qualitative inspection of the data shows that small buds do not contain eisosomes (Fig. 1a, middle left panel). As the buds grow beyond a critical size, eisosomes form in a wave that starts close to the bud neck (Fig. 1a, central panel) and continues in a polar fashion towards the bud tip (Fig. 1a, middle right panel). During these analyses, we never observed an eisosome forming in the mother cell, nor did we find evidence for division of preexisting eisosomes. We also never saw movement of eisosomes, excluding a model invoking transport of eisosomes to the sites of their deposition. Rather, all newly formed eisosomes were immediately immobile, indicating that they form at the sites where they are anchored.

Quantitative analyses validate and refine these conclusions. For example, we counted the number of eisosomes in buds of various sizes and plotted these numbers against the buds' surface area. The data in Figure 1b are well described statistically by a hockey-stick regression, which fits the data to a linear function preceded by a lag phase. This analysis shows that eisosomes are absent from buds with less than $17 \mu\text{m}^2$ surface area. After this lag, their number grows proportionally to the bud's surface area.

To rule out that the observed lag phase might be artifactually caused by a delay in the appearance of fluorescence due to delayed maturation of the GFP fluorophore, we visualized eisosomes by indirect immunofluorescence over the same time course, using a polyclonal antibody that recognizes GFP independent of its folding or fluorescence maturation state (Fig. 1a, lower panels). This analysis showed an indistinguishable eisosome distribution during the formation of new buds, demonstrating that the Pil1-GFP fusion is a faithful marker of eisosomes in these experiments.

Also consistent with our observations from time-lapse microscopy, quantitative analysis shows that eisosomes form in a polar wave originating at the bud neck. We counted eisosomes in small, medium, and large sized buds (small: 0-17 μm^2 , medium 17-60 μm^2 , and large >60 μm^2 in surface area, respectively), for each bud assessing eisosome distribution in three zones of equal length along the polarity axis, defined as neck (“N”), middle (“M”), and tip zone (“T”), respectively. As shown in Figure 1c, medium sized buds show a strongly polarized distribution of eisosomes within the bud, with 4-fold more eisosomes in the neck than in the tip zone. The polar distribution becomes less pronounced as the bud grows and eventually diminishes, as seen in the approximately even distribution in large buds. We repeated this quantification on immunofluorescence images of cells stained with anti-GFP antibodies and confirmed that it parallels the deposition pattern of live cells detecting GFP fluorescence (Fig. 1d). By this analysis also, small buds contained no eisosomes (Fig. 1d), again confirming that GFP accurately reports on eisosome disposition in our experiments.

As a further control, we tagged the second principal eisosome core component, Lsp1, with GFP and analyzed its distribution. We found that the number of Lsp1-GFP

marked eisosomes per bud when plotted against the bud surface area is very similar to eisosomes marked by Pil1-GFP, first showing a lag phase and then a steady increase of eisosome number proportional to surface area (Pearson Correlation = 0.925, Supp. Fig. 1a). In addition, the distribution of Lsp1 eisosomes in the three different regions of growing buds, as analyzed in Figures 1c and 1d for Pil1, is indistinguishable from the distribution of Pil1 (Supp. Fig. 1b). In time-lapse microscopy experiments following the kinetics of Lsp1-GFP localization compared to Pil1 tagged with mCherry, we did not observe a significant difference in localization or kinetics of deposition between Pil1 and Lsp1, indicating that, within the precision of our measurements, both subunits assemble synchronously.

The apparent lack of eisosomes in small buds ($< 17 \mu\text{m}^2$ surface area) could be due to a cell cycle-regulated switch in expression or assembly, or it could be due to a time lag between the formation of new plasma membrane and new eisosomes. To distinguish between these possibilities, we arrested cells at a specific stage in the cell cycle, G2, by inactivating a drug-sensitized mutant of Cdc28 kinase (*cdc28-AS2*) with low levels of a cognate inhibitor, 1NM-PP1 (Bishop et al., 2000). Under these conditions, bud growth continues in a polar fashion for extended periods of time because the switch from polar to isotropic growth that normally occurs after the transition to M phase does not take place (Lew et al., 1993). This defect results in formation of a cylindrical rather than the normal spherical shape of the bud. As expected, the G2-arrested *cdc28* mutant cells extended elongated buds (Fig. 2a, “DIC”). The cells formed new eisosomes in the bud (Fig. 2a, “Pil1-GFP”). Indeed, eisosome formation still proceeded in a wave-like pattern starting at the bud neck, which because of the elongated shape of the buds resulted in an even

more striking appearance than that observed in wild-type cells. Eisosome formation never caught up with the bud tip during the time course of the experiment. Eisosomes counting revealed that their number was roughly proportional to the cell length (Fig. 2b), which for a cylindrical shape in approximation is proportional to the surface area. Together these observations suggest that eisosome formation proceeds at the same rate as plasma membrane growth and that the transition past G2/M phase *per se* is not required for their formation.

Thus the results presented so far suggest that: i) eisosomes are assembled *de novo*, ii) they are formed *in situ*, iii) their formation proceeds in a wave-like pattern, with new eisosomes being assembled next to existing ones, leading to the polar colonization of the newly formed plasma membrane, and iv) there must be intricate regulation of the process to achieve a constant eisosome number per membrane surface area.

Eisosome number is proportional to the cell surface area

The data in Figure 1b show that in the colonized regions of the cell surface the number of eisosomes linearly correlates ($P = 0.0002$) to the surface area. By contrast, a fit of the eisosome count to cell volume shows poor correlation ($P = 0.43$). These observations suggest that eisosome density is tightly controlled and linked to plasma membrane expansion.

To seek further evidence for eisosome density control, we sought experimental conditions under which the cell surface area would change. To this end, we arrested yeast cells with the microtubule depolymerizing drug nocodazole, which blocks budding and causes isotropic growth (non-polar growth enlarging the plasma membrane in all

directions) yielding large, round cells. Incubation with nocodazole leads to an increase of cell surface area that is first apparent after ~ 3 hours and reaches 2.5-fold after 5.5 hours (Fig. 3b). Remarkably, we found that the eisosome density of these giant yeast cells remains constant when compared to the density observed in wild type mother cells (Fig. 3c, $t = 0$; 0.33 ± 0.06 eisosomes/ μm^2 surface area) between 0.32 and 0.34 eisosomes/ μm^2 surface area as the cells grow (Fig. 3c).

In these experiments, we reproducibly observed a ~20% “overshoot” of increased eisosome density at the onset of cell growth (Fig. 3b, 3 h), yet one hour later (Fig. 3b, 4 h) this trend was reversed, returning the density back to the starting value. A similar situation was observed during the cell cycle of normally growing cells, where the density briefly reached 0.5 eisosomes/ μm^2 in large buds before returning to the set value in mother cells (Fig. 1b, eisosome density for small buds = 0.01 ± 0.04 eisosomes/ μm^2 surface area; for medium buds = 0.32 ± 0.2 eisosomes/ μm^2 surface area and for large buds = 0.5 ± 0.13 eisosomes/ μm^2 surface area). A possible interpretation of these results is that there is a set point of eisosome density that is maintained by feedback regulation. When eisosome density becomes smaller than the set point after an initial increase in cell size, the regulatory loop overshoots leading to a transient increase in eisosome density.

Eisosomes are arranged randomly

The wave-like appearance of newly made eisosomes suggests that eisosomes form next to existing ones, perhaps at specific distances and thus resulting in a spatial pattern on the plasma membrane. Since eisosomes are immediately immobilized at the location where

they are formed, their distribution pattern in cells reflects possible constraints imposed during their biogenesis, such as the distribution of putative nucleation sites. On first principle, eisosomes could be i) randomly distributed with respect to each other, ii) fixed on a regular grid, or iii) distributed non-randomly with less obvious constraints, such as preferred distance or orientation. To distinguish between these scenarios, we acquired complete 3D stacks of images of individual yeast cells and assigned polar coordinates to individual eisosomes (Supp Table 2). Figure 4a shows a representative stack. We then calculated the distances between all eisosomes on the surface of the cells and calculated the pair-wise correlation function $g(r)$ to determine whether there are any constraints on the distribution of eisosomes. In brief, this function gives the ratio of the density of eisosomes at any distance from any given eisosome to the average density of eisosomes over the entire surface. If eisosomes were randomly distributed, the local density would be the same everywhere and $g(r)$ would be constant; if eisosomes were positioned at the nodes of a regular grid, the local density would have preferred distances and $g(r)$ would have an oscillating form.

Figure 4b shows a comparison between the experimentally determined $g(r)$ (*red* line) and a function derived for the same number of simulated random distributions of points on a sphere (*blue* line). With the important exception of the single point representing the smallest distance bin (0 - 0.5 μm), the two functions do not differ from each other significantly, indicated by the overlap of the standard errors, providing positive evidence that eisosomes are randomly distributed over the surface of the cell. By contrast, the closest distance measured between eisosome centers, 0.5 μm , shows a clear under-representation of eisosomes: it is 4-fold less likely to find an eisosome at that

distance than is predicted from a random distribution. Thus eisosomes appear to be distributed randomly but are restricted to a minimal distance from one another.

To understand better the nature of distance constraints on eisosome distribution, we experimentally forced new eisosomes assembly on an already colonized cell membrane.

As demonstrated above, this scenario does not occur under normal physiological conditions, where eisosomes are exclusively formed at the newly assembled plasma membrane in the bud. However, the experiments discussed above, arresting cells in M phase by nocodazole arrest, showed that the cell surface grew 2.5-fold, yet maintained the same density of eisosomes (Fig. 3b, 3c). Therefore, new eisosome assembly must occur under these conditions at the already eisosome-covered plasma membrane. To observe these events, we imaged cells after 3 hours of nocodazole treatment, a time when the effect of the arrest on cell size became first apparent. As shown in Figure 4c, we observed that, as the plasma membrane expanded, gaps in the eisosome pattern formed. The gaps expanded as the cells grew further and after a variable amount of time new eisosomes formed in the gaps. Similar to eisosome insertion during budding, the formation of these new eisosomes in arrested cells occurred *de novo* and not by a division or preassembly-transport mechanism.

Pil1 controls eisosome number and size

Regulation of eisosome number must be coordinated with control of eisosome size, which, given the large size of these macromolecular assemblies, is maintained within a remarkably narrow window, only varying within a factor of two (Walther et al., 2006).

To begin addressing how such tight control is achieved, we analyzed confocal 3-D time-

lapse movies of yeast cells expressing GFP-tagged Pil1 (Fig. 5a). We then selected individual eisosomes in the recorded movies and ascertained that they had reached a steady level of fluorescence, indicating that they had reached a final state of Pil1 assembly. We then went back to preceding frames and quantitated the fluorescence intensities to derive the kinetics of assembly of individual eisosomes. The graph in Figure 5b shows four representative examples of eisosome growth. The data show that the formation of individual eisosomes is characterized by a steady linear increase of fluorescence that takes on average 40 ± 4 min to reach steady state. Pil1 assembly into eisosomes therefore appears to occur as a continuous process of subunit addition.

To gain mechanistic insights into the process, we focused on *PIL1*, since deletion of genes encoding other known eisosome components, such as the highly homologous *LSP1* or the combined deletion of the *SUR7* gene family members has no dramatic effect on eisosome size or number (T.C.W. and P.W, unpublished data). By contrast, deletion of *PIL1* disrupts eisosome formation, size and density, causing clustering of the remaining eisosome components to one or a few loci at the cell periphery (Grossmann et al., 2007; Walther et al., 2006). To control the amount of Pil1 expressed in cells, we generated diploid yeast cells bearing one, two, three, or four copies of *PIL1-GFP* (Fig. 6a) that replace the wild type gene. To assess the relative expression level of Pil1-GFP in these strains, we performed quantitative Western blotting against GFP, measured Pil1 protein levels relative to Pgk1 levels, the constitutively expressed 3-phosphoglycerate kinase, and normalized the signal to wild type diploid cells. This analysis showed that the Pil1 expression level parallels the gene dose in the diploid strains (Fig. 6b left panel).

Consistent with the notion of a “set-point” of eisosome density, the bigger diploid yeast cells bearing two or more copies of *PILI-GFP* displayed an almost identical density of eisosomes on the cell surface as haploid cells (0.39 ± 0.07 eisosomes per μm^2 for diploids versus 0.33 ± 0.06 for haploids). By contrast, decreasing the gene dose to one-half of normal (i.e., one *PILI-GFP* copy per diploid cell) resulted in a significant decrease in eisosome density, yet each eisosome was assembled to a normal size as judged by their Pil1-GFP intensity (Fig. 6c and 6d; Pil1-GFP/Pgk1 levels <1 , blue diamonds). This observation suggests a minimal eisosome size is maintained independent of the amount of available Pil1; under conditions of limiting Pil1 availability, fewer eisosomes assemble at this minimal size. To obtain further evidence for this notion, we generated a haploid strain bearing a “dampened” allele of *PILI-GFP*. In this construct, the 3'UTR was deleted, resulting in a destabilized *PILI-GFP* mRNA and reduced Pil1 expression to roughly 45% of the wild type (Fig. 6b right panel). Consistent with the observations made in *PILI/pil1Δ* diploid cells, we found that reduction of Pil1 expression levels also lead to a decrease of eisosome density and the size of individual eisosomes remained unchanged (Fig. 6b and 6c, Pil1-GFP/Pgk1 levels <1 , green squares).

By contrast, overexpression of Pil1-GFP by increasing the gene dose by 1.5 and 2-fold maintained eisosome density at the set-point (0.33 ± 0.11 and 0.40 ± 0.06 eisosomes/ μm^2 , respectively), yet their sizes (as assessed by Pil1-GFP fluorescence per eisosome) increased proportional to the gene dosage (Fig. 6c and 6d, Pil1-GFP/Pgk1 levels >1 , blue diamonds; ANOVA P values <0.0001). These results suggest that if Pil1 is available in excess, nucleation sites become limiting and eisosomes grow larger to use

up the available Pil1 building blocks. Together, these data establish Pil1 as a regulator of eisosome formation, both with regard to number and size.

Cell cycle regulation of *Pil1* determines the polar formation of eisosomes

As yeast cells grow, their plasma membrane expands non-linearly. We have estimated the size of the plasma membrane by measuring cell size microscopically throughout the cell cycle and calculated the rate of membrane addition from the derivative ($d[\text{membrane increase}]/d[\text{time}]$) of these data (Fig. 7a, plotted as the *green* curve). This analysis shows that most membrane addition occurs at the G2/M transition, when the rate of bud expansion peaks. We then determined the rate of total fluorescence change in cells expressing Pil1-GFP (Fig. 7a, *red* curve) and found that Pil1 synthesis also occurs in cell cycle-regulated bursts. As apparent from the similarity of the curves, plasma membrane expansion and Pil1-GFP expression correlate well through the cell cycle. Consistent with this observation, inspection of published microarray gene expression data (Spellman et al., 1998) reveals that *PILI* mRNA abundance is cell cycle regulated. Clustering analysis of genes showing expression patterns similar to *PILI* identifies *SICI* as the gene with the most similar expression pattern. *SICI* is an inhibitor of the Cdc28-cyclin kinase complex, and its expression serves as a marker for the G2/M transition (Fig. 7b; (Oehlen et al., 1998)). The strong similarity between *PILI* and *SICI* expression patterns was observed in experiments utilizing a variety of cell cycle synchronization methods, such as release from α -factor arrest, release from *cdc28^{ts}* and *cdc15^{ts}* arrests, as well as by elutriation (Fig. 7b). To confirm the conclusions derived from the published high-throughput data sets, we arrested yeast cells in G1 by incubation with α -factor for 3

hours, washed the cells in fresh YPD to release the block, and took samples at 10 min intervals as cells progressed through one and a half subsequent cell cycles. Northern blot analysis of these samples showed that *PILI* mRNA levels oscillate with a three-fold increase in amplitude through the cell cycle (Fig. 7c).

These data show that the expression of Pil1 occurs in 20 minute bursts that correlate with the phase of the cell cycle when eisosome formation initiates, e.g., when the small bud starts first acquiring eisosomes. Interestingly, *LSP1* shows no cell cycle regulation while *SUR7* does (Spellman et al., 1998), however, neither *LSP1* nor *SUR7* gene deletions display a dramatic effect on eisosome organization. These observations underline the proposed role of Pil1 in controlling eisosome biogenesis and suggest that cell cycle regulation of *PILI* mRNA contributes to the regulation of eisosome formation.

To test the importance of cell cycle regulation of Pil1 expression and eisosome biogenesis, we placed *PILI-GFP* under control of the *CUPI* promoter, which can be regulated by the addition of copper to the growth medium. Importantly, *CUPI* is not cell cycle regulated (Spellman et al., 1998). We found that at 25 μM CuSO_4 , Pil1 was expressed in the cell population at similar levels as in wild type cells, as assessed by quantitative Western blotting (Fig. 8b). Moreover, eisosome morphology and deposition looked normal, and eisosome density was within error at the set-point of wild type cells (0.43 \pm 0.09 eisosomes per μm^2 at 25 μM CuSO_4).

Based on the results in Fig. 8b, we chose 25 μM CuSO_4 as a concentration that resulted in a cellular Pil1 level comparable to that of wild type cells. In marked contrast to wild type cells, we found that under these conditions eisosomes formed in small buds and showed no apparent polarization of deposition (Fig. 7d). Thus taken together, the

data suggests that the cell cycle regulation of *PIL1* expression is required for the wave-like colonization of newly made plasma membrane seen in wild type cells.

In light of the results presented above, we were surprised to find that eisosome density increased as more Pil1 was produced under the higher CuSO_4 concentration conditions (Fig. 8c), whereas the size of individual eisosomes (as measured by integrating Pil1-GFP fluorescence intensity) increased only slightly (ANOVA P value < 0.0001, Fig. 8d). Overexpression of Pil1 therefore can have qualitatively different consequences: increasing the gene dosage which retains cell cycle control lead to larger eisosomes at wild type density (Fig. 6), whereas increasing Pil1 expression from a heterologous promoter which eliminates cell cycle control lead to wild type size eisosomes at an increased density. Formally however, we cannot rule out that the observed difference results more indirectly from the different ploidy of the cells.

To test whether Pil1 expression under the *CUPI* promoter directed assembly of other eisosome components in small buds, we followed the expression of Lsp1-GFP, in a strain in which endogenous (untagged) *PIL1* was placed under the control of the *CUPI* promoter (Fig. 9). Consistent with the parallel experiments following Pil1-GFP in Figure 8, we observed a reduction in Lsp1 containing eisosome density ($0.24 \pm 0.06 \mu\text{m}^2$) as Pil1 abundance was titrated down. Moreover, eisosome size was similar to that found in wild type cells (data not shown). Lsp1-labeled eisosome density increased to wild type levels as Pil1 abundance was raised to wild type levels (Fig. 9a). We did not observe a significant increase in size or density of Lsp1-labeled eisosomes when Pil1 levels were increased, however, despite the increase in Pil1-labeled eisosomes observed in Figure 8c (data not shown).

We measured the levels of Pil1 and Lsp1-GFP by quantitative Western blotting and found that the expression of Lsp1-GFP decreased when Pil1 levels decreased, indicating that Lsp1 is unstable if it cannot assemble with Pil1. By contrast, Lsp1-GFP levels plateau as Pil1 levels increased (Fig. 9b), indicating that Lsp1 becomes limiting under these conditions. In parallel experiments, we did not observe Lsp1-GFP in small buds when Pil1 was expressed from the *CUP1* promoter (Fig. 9c). We conclude that Pil1 provides the upper limit for the density of Lsp1 containing eisosomes, yet its early deposition in small buds is not sufficient to recruit the early deposition of Lsp1. This observation implies that Lsp1 deposition is governed by an unknown process coupled to the cell cycle, perhaps requiring a certain cell cycle-dependent phosphorylation state.

Discussion

Eisosomes are large macromolecular assemblies underlying the plasma membrane that help sequester a subgroup of plasma membrane proteins into discrete membrane domains, which co-localize with sites of endocytosis (Grossmann et al., 2007; Walther et al., 2006). They are present in cells in relatively constant numbers and built of 2000 - 5000 copies each of Pil1 and Lsp1, their two major subunits. Here we describe a series of experiments and observations that establish a basic framework of eisosome biogenesis. In particular, we found that eisosomes are formed *de novo*, colonizing the plasma membrane of the growing bud in a wave-like fashion. We currently do not know the molecular mechanism that leads to the polar eisosome deposition: either active nucleation sites form after a lag time as newly deposited membrane matures, or deposition is excluded from the very bud tip, perhaps because it is too crowded by other molecular

machinery. Their deposition results in a remarkably constant density that is maintained in both haploid and diploid cells, as well as under conditions of aberrant cell growth during G1 cell cycle arrest. From this and previous studies, Pil1 emerges as the central player of eisosome organization: i) among the known eisosome components, *PIL1* is regulated in a cell cycle dependent manner that synchronizes eisosome assembly with membrane expansion, ii) lowering or increasing the gene dose of *PIL1* leads to a reduction in eisosome number or increase in eisosome size, respectively, and iii) deletion of *PIL1* (but not of *LSP1*) leads to a collapse of eisosome remnants (Grossmann et al., 2007; Walther et al., 2006).

Modulation of Pil1 levels suggests that eisosomes have a minimal size. When the relative expression level of *PIL1* was reduced, both Pil1 and Lsp1 labeled eisosome size leveled off at the expense of eisosome density. In addition Lsp1-GFP levels decreased instead of assembling larger Lsp1 containing eisosomes. One possible explanation of this finding is that eisosomes have a regular structure - perhaps a toroid or an icosahedron - that is not stable when it cannot be formed completely, and thus provides a maximum limit for the assembly of other eisosome components, resulting in the destabilization of eisosome components in excess of Pil1. In addition, we did not find a difference in the kinetics of deposition between Pil1 and Lsp1 under wild type conditions, suggesting that these two components are assembled into eisosomes at the same time. As such, eisosomes provide an interesting paradigm for molecular self-assembly, and it will be intriguing to determine the molecular design principles that govern the assembly of Pil1 and other components into eisosomes. Equally surprising, we found that when Pil1 levels were increased moderately, any excess of Pil1 was incorporated into eisosomes leading to

gradual size increases, while their density on the plasma membrane remained constant. Thus the capping mechanism that restricts incorporation of excess Pil1 subunits into eisosomes can be overcome—maybe forming additional “layers” onto their minimal structure. Pil1 assembly in small buds was not sufficient to recruit Lsp1 to the small buds, suggesting additional regulatory mechanisms can affect the assembly of other eisosome components. While remarkably tight under conditions where Pil1 expression remained cell cycle controlled, eisosome density was not constant when Pil1 was expressed at elevated levels from the copper-regulated promoter. These observations suggest that the mechanism that limits eisosome nucleation is normally restricted to the timing of new bud formation to prevent additional nucleation in the mother cell. Continuously elevated expression of Pil1 in the copper regulated strains overcomes this regulation, resulting in more nucleation sites. We do not know if eisosome components other than Pil1 are also recruited to these new nucleation sites. Similarly, the tight regulation of *PILI* expression normally leads to a relatively uniform eisosome size, despite the fact that eisosomes can, in principle, grow larger as shown in the strains with increased *PILI* copy number. Thus, our results suggest that the cell cycle regulation of Pil1 contributes to the fidelity of eisosome size, eisosome density, and orderly eisosome deposition in the wave-like pattern observed in growing buds.

The cell cycle regulation of *PILI* is likely to be direct. A cursory inspection of the *PILI* promoter revealed the presence of a binding site for the cell cycle regulated transcription factor Swi5 located 410 base pairs upstream of the *PILI* open reading frame. Swi5 is known to activate the transcription of genes in G2 phase and the G2/M boundary after phosphorylation by Cdc28 kinase. This argues that at least some of the

regulation of Pil1 is directly mediated by the cell cycle via binding of Cdc28 activated Swi5 to a binding site in the *PILI* promoter. In addition, we conclude from the effects on eisosome assembly when Pil1 is expressed from a heterologous promoter that posttranscriptional and cell cycle-regulated control may also have a role in eisosome assembly. Either way, a checkpoint-like feedback overrules the cell cycle control to ensure that the eisosome density remains constant (disrupted here experimentally in the copper regulated strains). Evidence for this notion comes from the observation that cells arrested at different points in the cell cycle maintain a constant eisosome density. Under these conditions the newly formed eisosomes are generated in apparent gaps in the plasma membrane that open up as the cells expand.

Since eisosome density does not increase under conditions of excess Pil1, when expressed under its endogenous promoter, it is likely that nucleation sites on the plasma membrane are limiting. The observed wave of eisosome colonization in which all new eisosomes form adjacent to preexisting ones would be consistent with short filamentous structures that may link eisosomes, binding to existing ones with one end and providing nucleation sites for new eisosomes at their other end. Thus eisosomes may form at vertices of a meshwork of yet to be identified filamentous proteins, perhaps resembling in its characteristics the spectrin networks that underlie membrane systems in metazoan cells. A mechanism utilizing filamentous spacers could explain the constant eisosome density on the cell surface and account for the minimal distance observed between eisosomes. In G1 arrest cells, which grow isotropically, the network may rupture allowing assembly of new filaments in the gaps that then form new nucleation sites. Alternatively, eisosome formation may be inhibited in a zone surrounding pre-existing

eisosomes, thus determining eisosome density by exclusion. These two mechanisms are not mutually exclusive, and currently available data do not allow us to distinguish between them.

The plasma membrane domains associated with eisosome are specialized both in protein and lipid composition (Grossmann et al., 2007; Malinska et al., 2003; Malinska et al., 2004)). Moreover, Pil1 and Lsp1 are differentially phosphorylated in response to an increase of long chain bases, which are the precursors of sphingolipids, by Pkh1/2, two kinases that localize to eisosomes (Luo et al 2008; Walther et al., 2007; Zhang et al., 2004). Perturbation of the Pil1 phosphorylation status affects Pil1 assembly into eisosomes: specifically, eisosomes disassemble if Pil1 is hyperphosphorylated, and more Pil1 assembles into eisosomes if Pil1 is hypophosphorylated. The phosphorylation status of Pil1 therefore may be an additional factor that modulates eisosome assembly, possibly using the membrane's lipid composition as a controlling feature. Alternatively, however, Pil1 phosphorylation may primarily serve under physiological conditions to effect local structural rearrangements within an eisosome to regulate, for example, its activity to recruit endocytic effectors. As such, phosphorylation events may not globally affect assembly/disassembly properties as observed upon extreme hypo- and hyperphosphorylation observed under experimental conditions (Walther et al., 2007).

By providing on the plasma membrane a constant density of specialized domains, eisosomes may ascertain an even distribution of potential endocytic sites. This organization principle is important because mutations in many parts of the system, such as in Pkh1/2 and eisosome components, show endocytic defects, impairing the rate and the localization of endocytic events. *pillΔ* strains, for example, show large, aberrant

plasma membrane invaginations. A massing of many endocytic sites in close proximity may result in too much actin pulling force at the same place, thereby deforming the membrane in a disorganized and uncontrolled fashion. The organization provided by constant density and minimal distance between eisosomes might serve to avoid such chaotic events by guaranteeing sufficient spatial separation between individual endocytic events.

MATERIALS AND METHODS

Yeast strains

Genotypes of all strains used in this study are listed in Supplementary Table 1. The Pil1-GFP and Lsp1-GFP strains were described previously (TWY110 and TWY113 respectively, Walther et al., 2006). Diploid yeast strains expressing various amounts of Pil1 were generated by mating of Pil1-GFP strains with a *pillA* strain (TWY580) or a Pil1-GFP strain of opposite mating type (to generate TWY576). In addition, an extra copy of Pil1-GFP was cloned onto a pRS306 plasmid and integrated into one (TWY581) or both URA (TWY578) loci. To generate the DAMP allele of Pil1-GFP (KEM101), a KAN-selection marker was integrated directly after the open reading frame in TWY 110 as previously described (Schuldiner et al., 2005). The *Cdc28* mutant strain (KEM100) was generated by integrating the plasmid pRS406 carrying the *cdc28-as2* allele in the URA locus of TWY110. The *cdc28-as2* plasmid was generated by David Morgan's laboratory (Ubersax et al., 2003) and was a generous gift from Gustavo Pesce. The copper inducible strains KEM102 and KEM103 were made by replacing the endogenous promoter of *PIL1* with the *CUP1* promoter in TWY110 and TWY113. This was done by homologous recombination using a PCR-based modification (Janke et al., 2004).

Microscopy

Live cell microscopy was performed by mounting yeast cells on concanavalin A covered coverslips. Images were taken at room temperature on a Zeiss LSM510 confocal microscope and on a Nikon TE2000U inverted microscope with a Yokogawa CSU22 Spinning Disk Confocal from Solamere Technology Group. Images were processed with ImageJ (<http://rsb.info.nih.gov/ij/index.html>) and MATLAB.

Immunofluorescence was performed as described previously (Brickner et al, 2004). Cells were fixed in 4% formaldehyde for 45 minutes at room temperature. Then spheroblasted with lyticase and detergent extracted with 0.01% Triton X-100. Cells were probed with 1:200 rabbit polyclonal anti-GFP (Invitrogen, #A6455 rabbit polyclonal antibody against full length GFP) in WT buffer (1% nonfat dry milk, 0.5mg/ml BSA, 150 mM NaCl, 50mM HEPES pH 7.5) for 1 hour at room temperature, followed by secondary, goat anti- rabbit-Alexafluor 488 (Invitrogen, #A11034) antibody diluted at 1:200 in WT buffer for 1 hour also at room temperature. Slides were mounted using Vectashield (Vector Laboratories, Burlingame, California, United States), and imaged with a Zeiss LSM510 confocal microscope.

For surface area calculation we treated yeast cells as a spheroid shape, determined the major (a) and minor axes (b) and calculated the surface area using the standard

formula $S = 2\pi a^2 + 2\pi \left(\frac{ab}{e}\right) \sin^{-1} e$, where $e = \sqrt{1 - \frac{b^2}{a^2}}$. Mother and nocodazole arrested

cells were approximated to a sphere shape, $S = 4\pi r^2$.

The measurements of eisosome distribution in the 3-d reconstructed images showed that the radii varied within 10% (Supp Table 2), validating our strategy to approximate yeast cells as spheres for the purpose of this analysis.

Molecular Biology

For gene expression analysis, total RNA was extracted with acidic phenol and blotted for Northern analysis. Blots were probed with a radio-labeled probe representing 500 bp of the *PIL1* mRNA amplified with primers 5'-cgatgtttccgacatcactg and 5'-gtgcgctttcagcatcaata

Quantitative Western blots were done by preparation of cell extracts in 8M urea 50mM HEPES pH 7.4. Pil1-GFP was detected by a chemifluorescence method (ECF) using an antibody against GFP (Invitrogen #A6455 rabbit polyclonal antibody against full length GFP recognizing both the native and denatured protein) at 1:10,000 dilution; or a rabbit polyclonal antibody against full length Pil1 at 1:10,000 dilution (Walther et al., 2007); or a monoclonal mouse antibody against Pgk1 (Invitrogen, #A6457) at 1:5,000 dilution, followed by an alkaline phosphatase-labeled secondary antibody (Amersham Biosciences) diluted at 1:5,000. The blots were incubated with an ECF Substrate, which when dephosphorylated fluoresces, and were then scanned in a Typhoon 9400. Individual bands were quantified using ImageQuant TL.

ACKNOWLEDGMENTS

We thank Mark Segal for help with the statistical analysis of eisosome density. We also thank Ken Dill, David Gliden, Arne Gennerich and the Walt(h)er labs for valuable

discussions, and Gustavo Pesce for providing reagents. Data for this study were acquired at the Nikon Imaging Center at UCSF. TCW was supported by the International Human Frontiers Science Program (HFSP) and the German Research Association (DFG - WA 1669/2-1). KEM is a recipient of an aging training grant from NIH/NIA. In addition, this work was supported by grants from the NIH to PW. PW is an Investigator of the Howard Hughes Medical Institute.

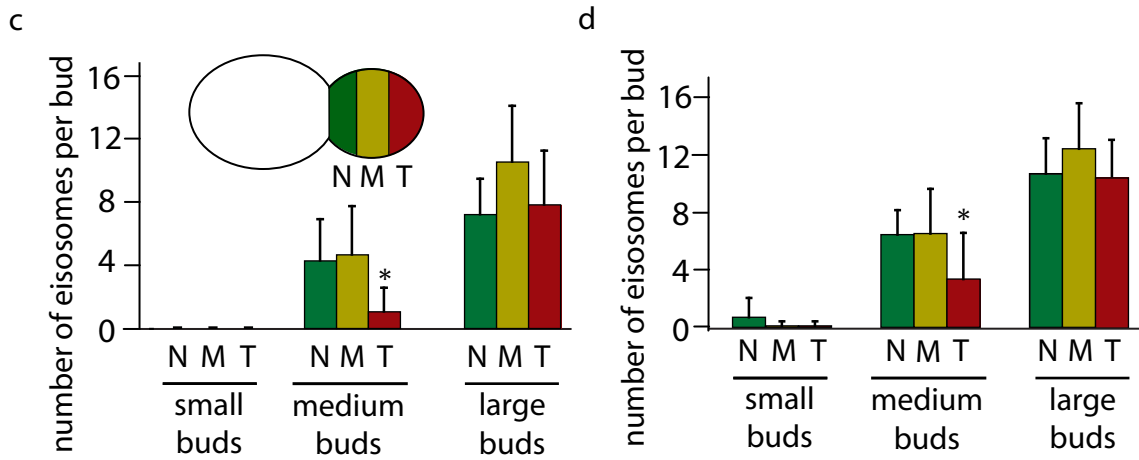
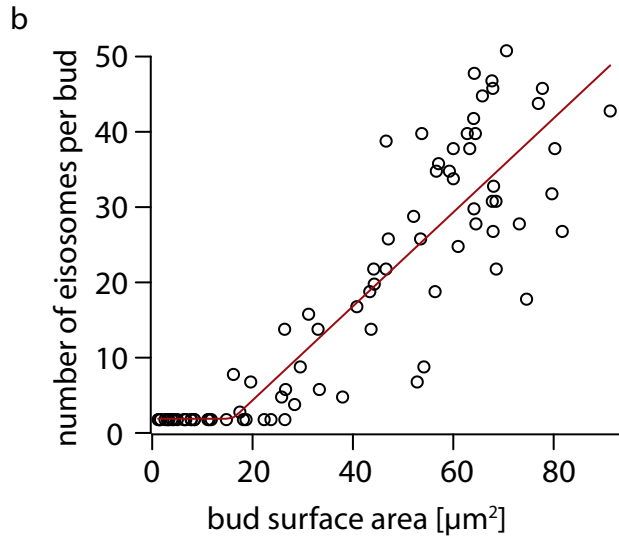
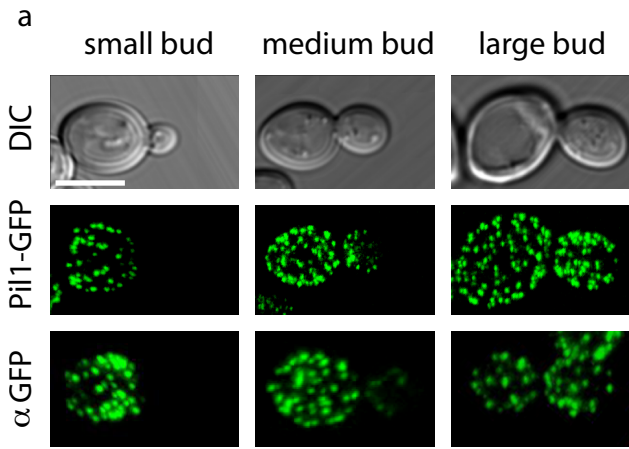


Figure 1. Eisosomes are assembled de novo. (a) Pil1-GFP accurately reflects the localization of eisosomes. Pil1-GFP fluorescence pictures (top row) are compared with immunofluorescence staining of Pil1-GFP with an antibody against GFP. The scale bar is 5 μm . (b) Eisosomes are formed after an initial lag phase and their number is directly proportional to cell surface area. Eisosomes were visualized in three-dimensional confocal stacks of cells expressing Pil1-GFP. The number of eisosomes per bud was counted and plotted against the surface area of the bud, $n = 83$. Eisosome number was fit to a hockey stick progression using R (<http://cran.r-project.org/>) according to (Bacon and Watts, 1971). (c) Eisosomes are formed in a polar fashion. Confocal stacks of cells with small ($0-17\mu\text{m}^2$), medium ($17-60\mu\text{m}^2$) and large ($>60\mu\text{m}^2$) sized buds were recorded. The buds were segmented along the axis of cell polarity into three equal regions (N= bud neck, M= middle, T= bud tip) and the number of eisosome was counted for each region, $n = 95$. (*) The number of eisosomes was significantly lower in the T region compared to the N and M regions (ANOVA P value < 0.001). (d) Similar as in (c) number of eisosome was counted for images after immunofluorescence staining of Pil1-GFP with antibody against GFP $n = 43$. (*) Similar to (c), the number of eisosomes was significantly lower in the T region compared to the N and M regions (ANOVA P value < 0.001). The strain used in all panels is TWY110.

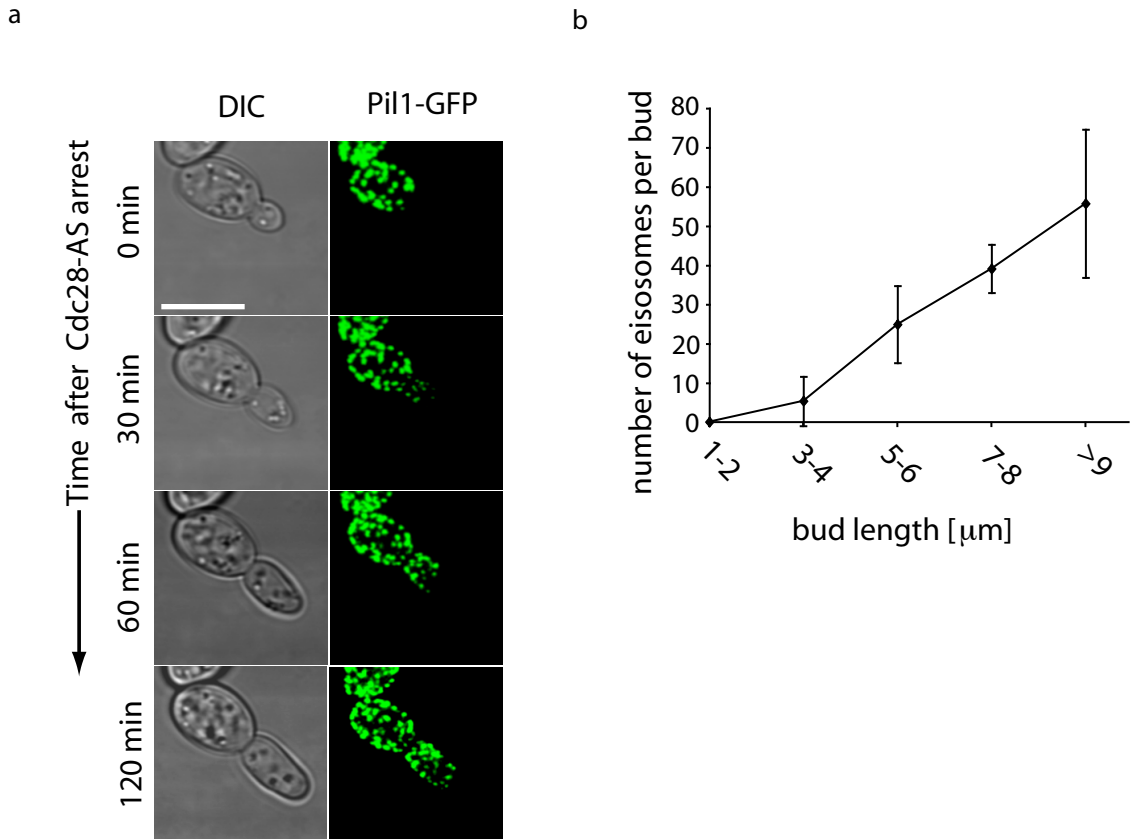


Figure 2. Eisosome assembly occurs in a polar fashion. (a) Cells expressing Pil1-GFP and harboring a drug-sensitized *cdc28* allele (KEM100) were incubated with 10 μM of the inhibitor 1NM-PP1 (Bishop et al., 2000) and followed over time by confocal live-cell microscopy at room temperature. Representative three dimensional projection images are shown. The scale bar is 5 μm . (b) Quantitation of eisosome number from experiments described in (a) plotted against bud length along the axis of polarization, $n = 75$.

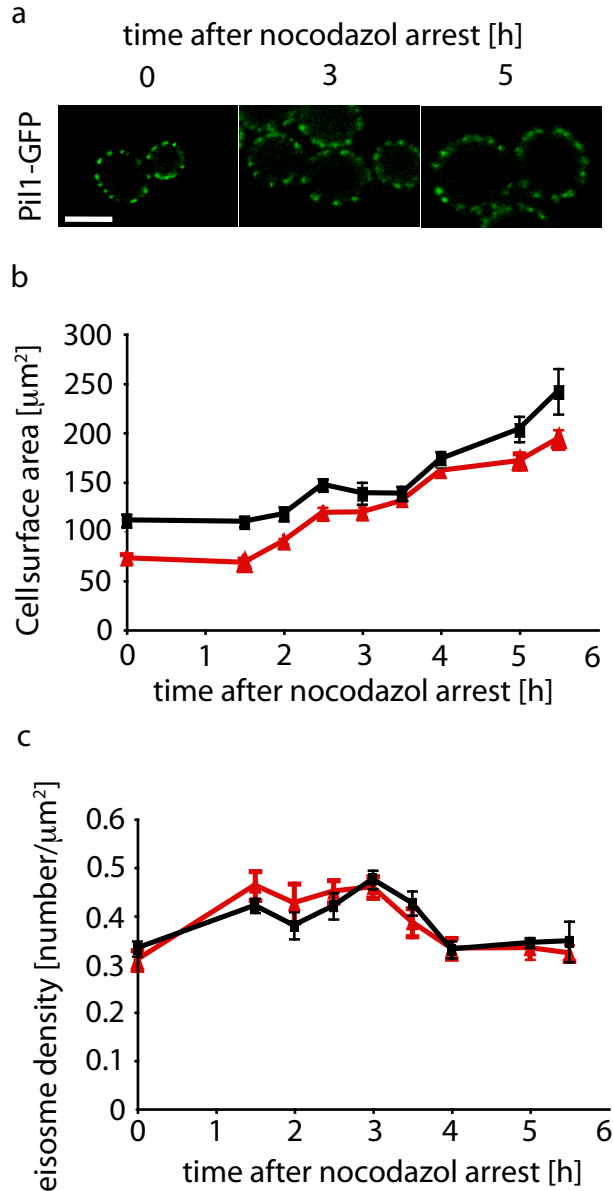


Figure 3. Eisosome density is constant and regulated to a set-point. (a) Cells expressing Pil1-GFP (TWY110) were arrested in M-phase by the addition of 30 μM nocodazole at 30°C and followed over time by confocal life cell microscopy. Representative images are shown. The scale bar is 5 μm . (b) Increase of yeast cell surface area over time after nocodazole-arrest in daughter cells (red lines) and mother cells (black lines). (c) Development of eisosome density over time after nocodazole arrest in daughter cells (red lines) and mother cells (black lines). The error bars indicate standard deviations from the mean, $n = 112$.

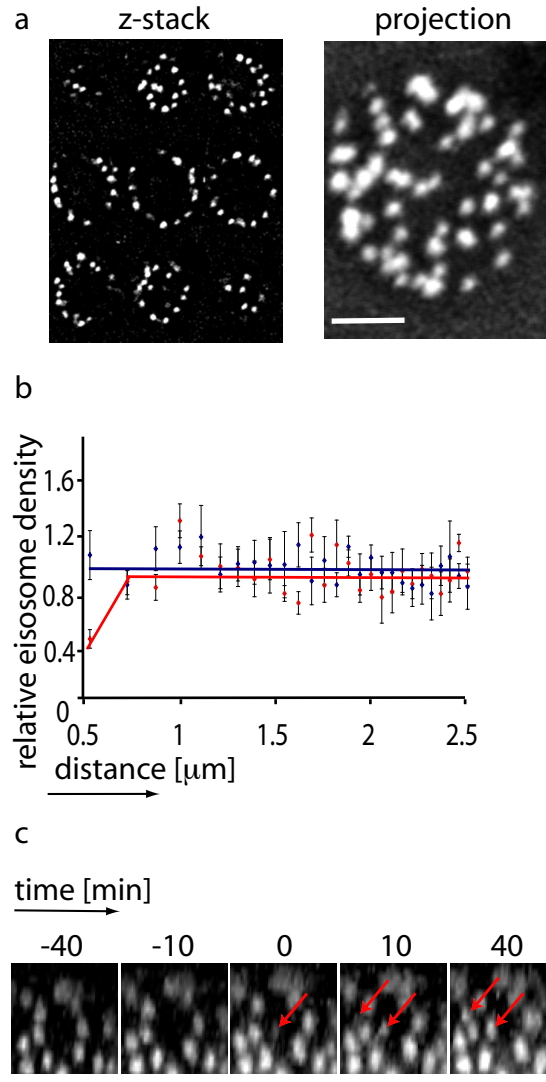


Figure 4. Eisosomes are distributed randomly. High resolution confocal stacks were acquired for strain TWY110 and representative images are shown in (a). The coordinates of the centers of all eisosomes of a cell were determined (Supp Table 2) and the distribution of the density of eisosomes related to the distance from the center of an eisosome was calculated. Five independent measurements were taken, each with an average of 39 eisosomes. The resulting values were averaged and are shown as a red line in (b). The blue line shows the result for the same analysis performed on simulated random coordinates. (c) De novo eisosome formation in nocodazole-arrested cells occurs in apparent gaps. Cells (TWY110) were treated as described in Figure 3, and the formation of new eisosomes in the mother cells was followed by confocal live-cell

microscopy at room temperature. A representative optical surface section is shown. Arrows indicate the formation of new eisosomes between already existing ones on the mother cell plasma membrane. The scale bars shown in panels (a) and (c) are 2 μ m.

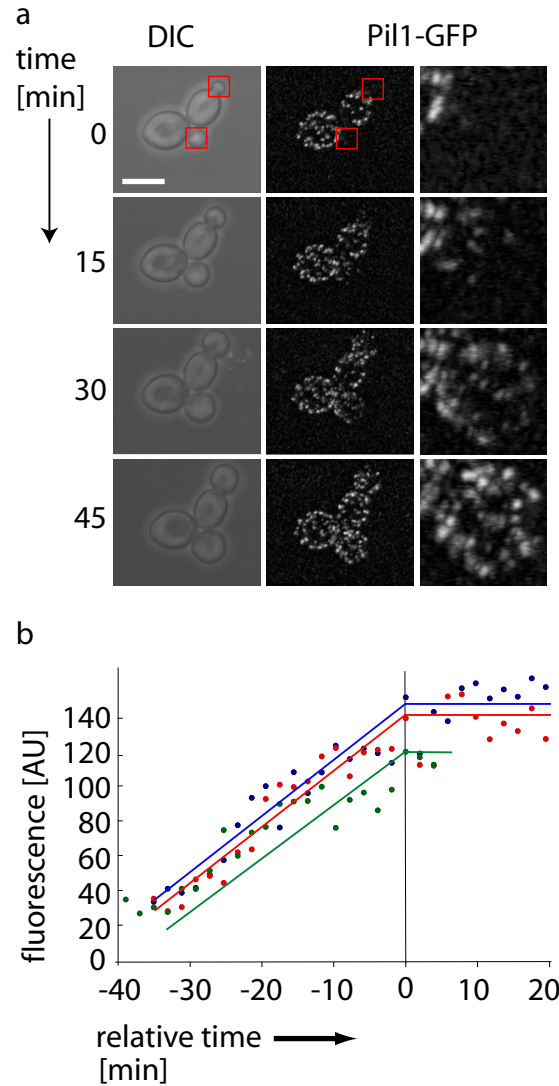


Figure 5. Eisosomes are formed in a continuous process. (a) Formation of eisosomes over a complete cell cycle was followed by confocal time-lapse microscopy of cells expressing Pil1-GFP (TWY110) at room temperature. Representative images are shown. The scale bar is 5 μm . (b) The rate of eisosome formation is constant. The increase of fluorescence of individual eisosomes was quantified over time. The vertical line indicates the time when each eisosome has reached its final fluorescence intensity.

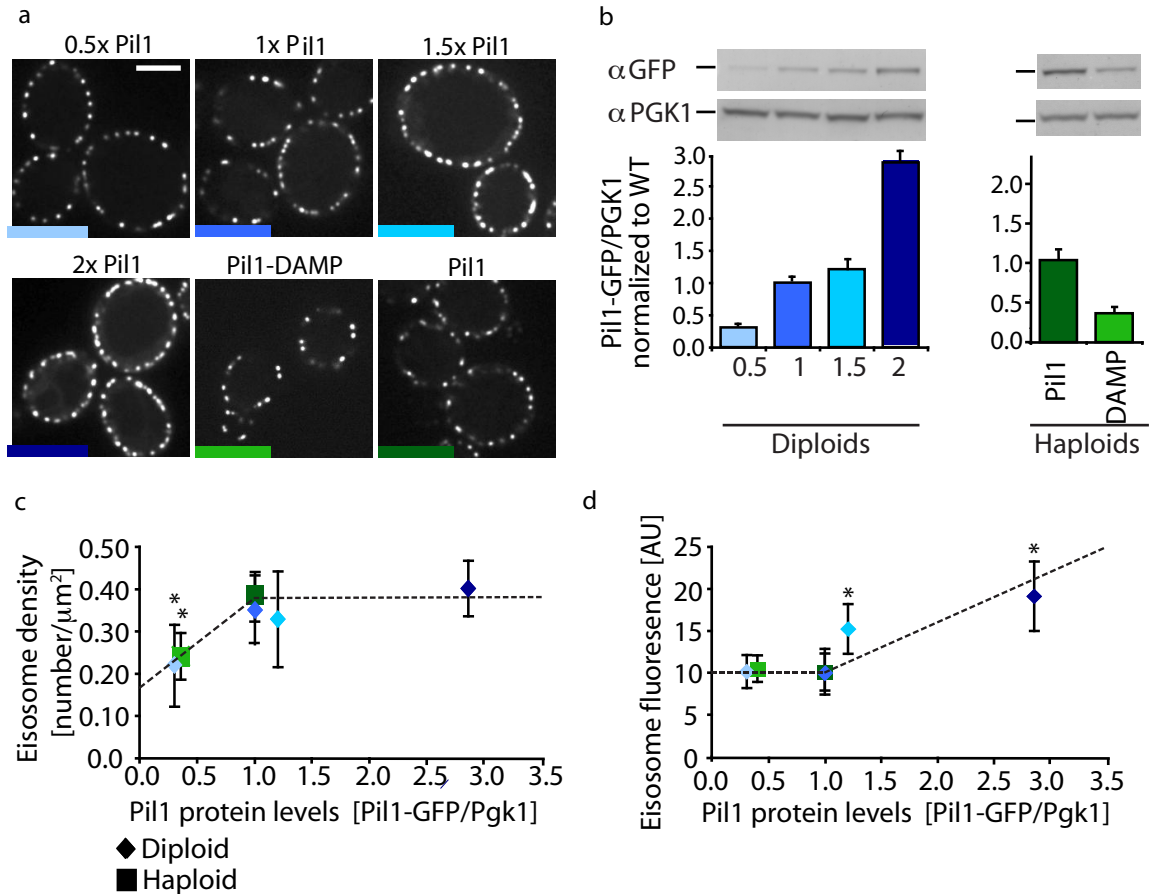


Figure 6. Eisosome number and size is controlled by the levels of Pil1. (a) Diploid cells were engineered to express either one (TWY580), two (TWY576), three (TWY581), or four copies (TWY578) of Pil1-GFP, and images were acquired by spinning disk confocal microscopy. Pil1-GFP expression was decreased in haploid cells by expressing a destabilized form of PIL1 mRNA by deletion of the Pil1-GFP mRNA 3' untranslated region ("Pil1-DAMP", KEM101). The scale bar is 5 μm . (b) Western blot against GFP of diploid cells with increasing copies of Pil1-GFP, and wild type haploid cells expressing one copy of Pil1-GFP, and against Pgk1, the constitutively expressed 3-phosphoglycerate kinase are shown (top). The graph shows the quantification of Pil1-GFP protein levels relative to Pgk1 and normalized to the wild type diploid protein level levels (bottom left, blue bars) or to the wild type haploid protein levels (bottom right, green bars), $n = 3$. Error bars show the standard deviation from the mean. (c) Eisosome density was calculated for cells such as shown in (a) and plotted as a function of Pil1

protein levels, measured by Pil1-GFP/Pgk1 ratios, which are normalized to the wild type diploid protein levels (blue diamonds) or wild type haploid protein levels (green squares). (*) ANOVA P values < 0.0001 for samples with densities lower than wild type. (c) The relative fluorescence intensity was measured and plotted as a function of protein levels as described in c. The error bars indicate the standard deviations from the mean. Diploid cells (blue diamonds) “0.5” n = 9, “1” n = 16, “1.5” n = 17, “2” n = 22, and haploid cells (green squares) “Pil1” n = 17, “DAMP” n = 28. Dashed lines represent trend lines.

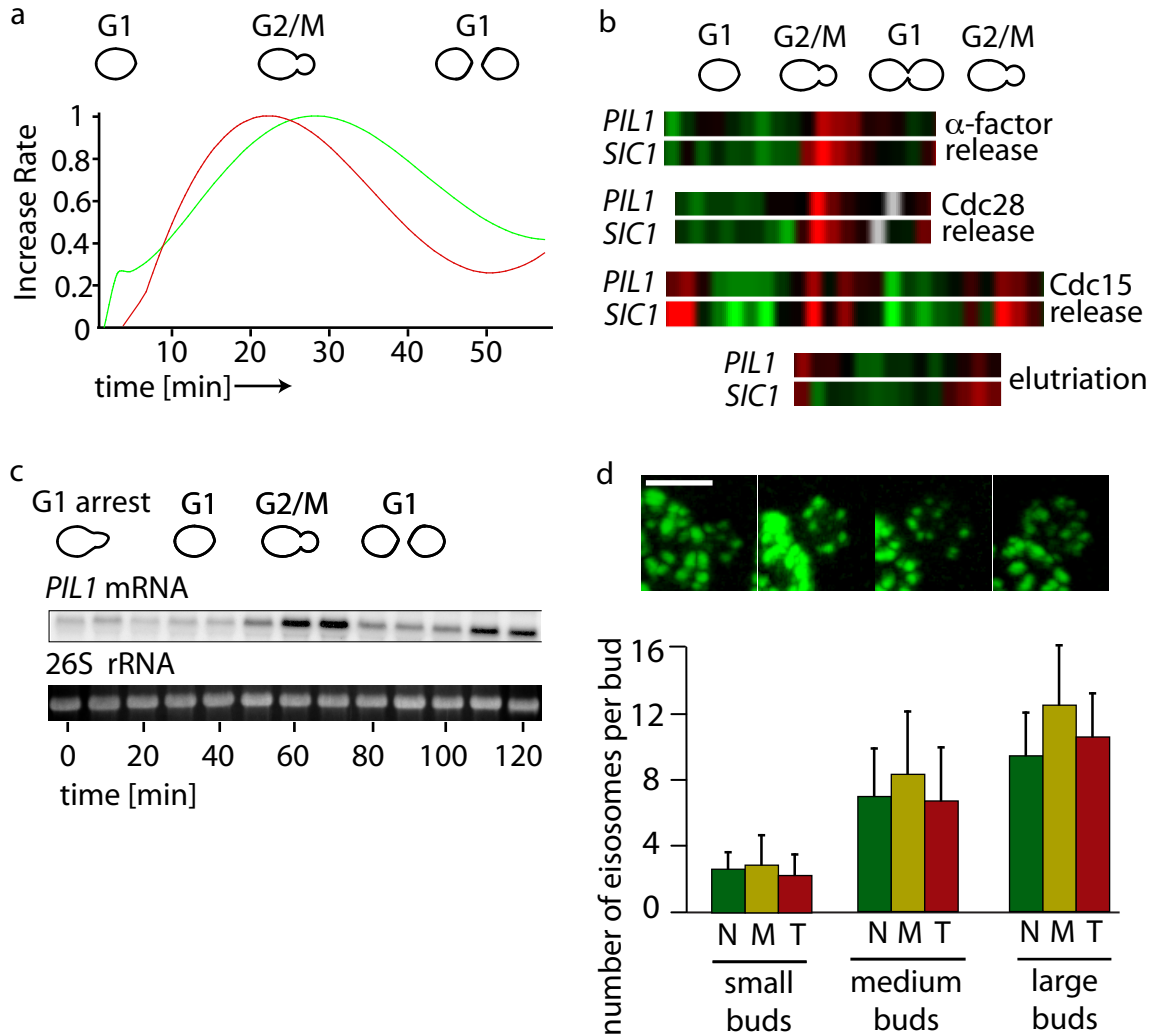


Figure 7. Pil1 expression is cell cycle regulated. Cells (TWY110) were followed over an entire cell cycle by confocal live-cell imaging. The increase in cell surface over time was calculated from the images, and the total GFP fluorescence per cell was measured. The derivatives of the resulting curve fits indicating rate of change in surface area (red) and rate of change of GFP fluorescence (green) are displayed. The curves show that Pil1-GFP expression correlates with membrane growth. (b) Data mining revealed the strong cell cycle regulation of PIL1 in several different synchronization methods (Spellman et al., 1998). Expression higher than the mean is shown in red and lower than the mean is shown in green. (c) PIL1 mRNA expression is cell cycle controlled. MATa cells (CRY2) were arrested in G1 phase of the cell cycle by addition of α -factor for an

hour and then released. Total RNA from the indicated time points was extracted and analyzed for PIL1 mRNA levels by Northern blotting. The respective cell cycle stage is indicated graphically above the time points. (d) Delay in eisosome deposition is explained by PIL1 cell cycle control. Confocal 3D reconstructions of small buds expressing PIL1 under the CUP1 promoter, KEM102 (top). Eisosomes are present in small buds. Confocal stacks of cells grown in the presence of 25 μ M CuSO₄ concentration (bottom). The scale bar is to 2 μ m. Small, medium and large sized buds were recorded as in Figure 1. The buds were segmented along the axis of cell polarity into three equal regions and the number of eisosome was counted for each region (n = 159).

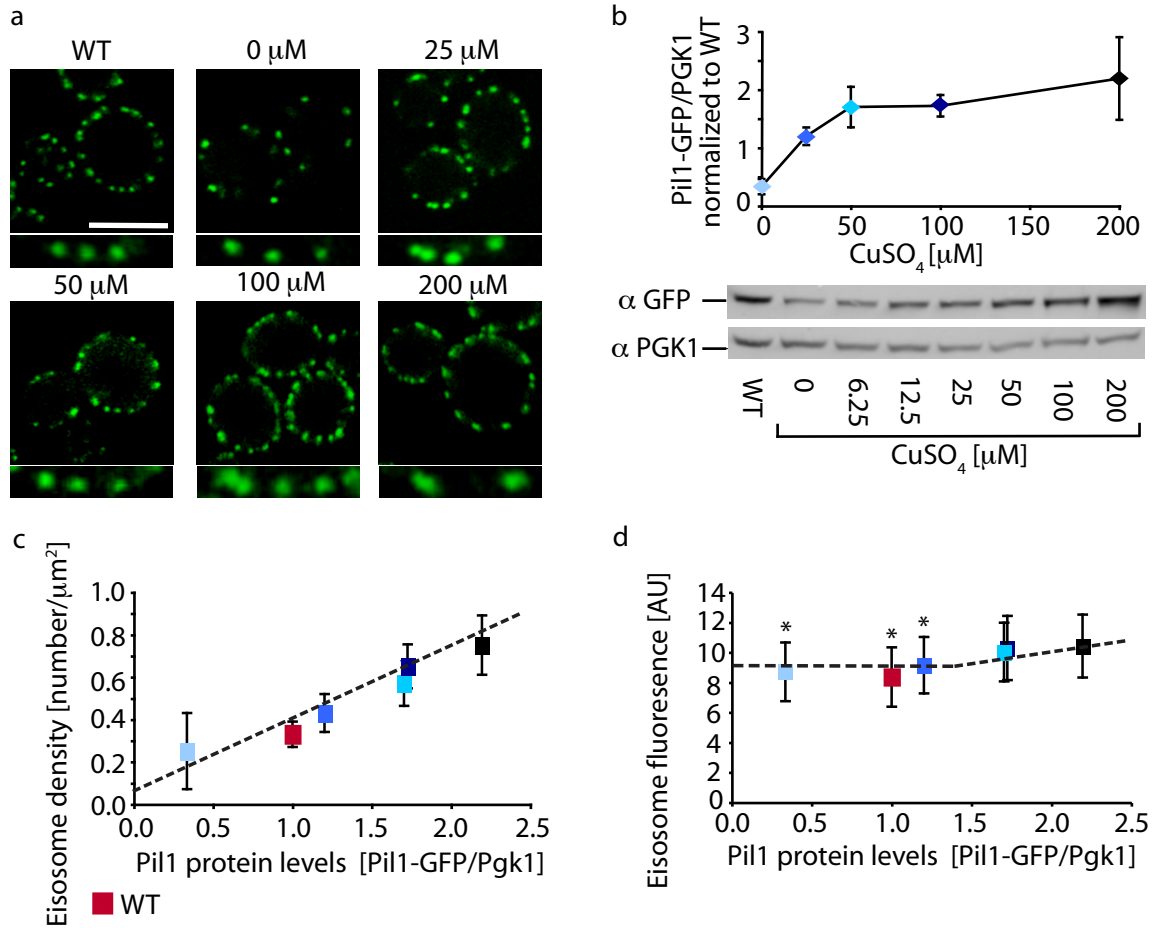


Figure 8. Pil1-GFP expression from the CUP1 promoter. (a) Confocal cross sections of cells grown at increasing concentrations of CuSO_4 at 30°C for 4h, cells expressing Pil1-GFP driven from the CUP1 promoter (KEM102) are shown. The scale bar is $5\ \mu\text{m}$. (b) Titration of CuSO_4 of cells expressing Pil1-GFP under control of the CUP1 promoter. The original Western blots and the quantification of relative abundance of Pil1-GFP as measured by Pil1-GFP/ Pkg1 ratios normalized to wild type protein levels are shown ($n = 3$). (c) Eisosome density was measured and plotted as a function of Pil1-GFP protein levels as measured in b. (d) Fluorescence intensities of Pil1-GFP in individual eisosomes was measured and plotted against Pil1 protein levels as measured in b. Cup strains KEM102 = blue squares and diamonds and wt strain TWY110 = red square. Dashed lines represent trend line. (*) ANOVA P values = 0.147. The error bars indicate the standard deviation from the mean ($n = 56$ at each CuSO_4 concentration).

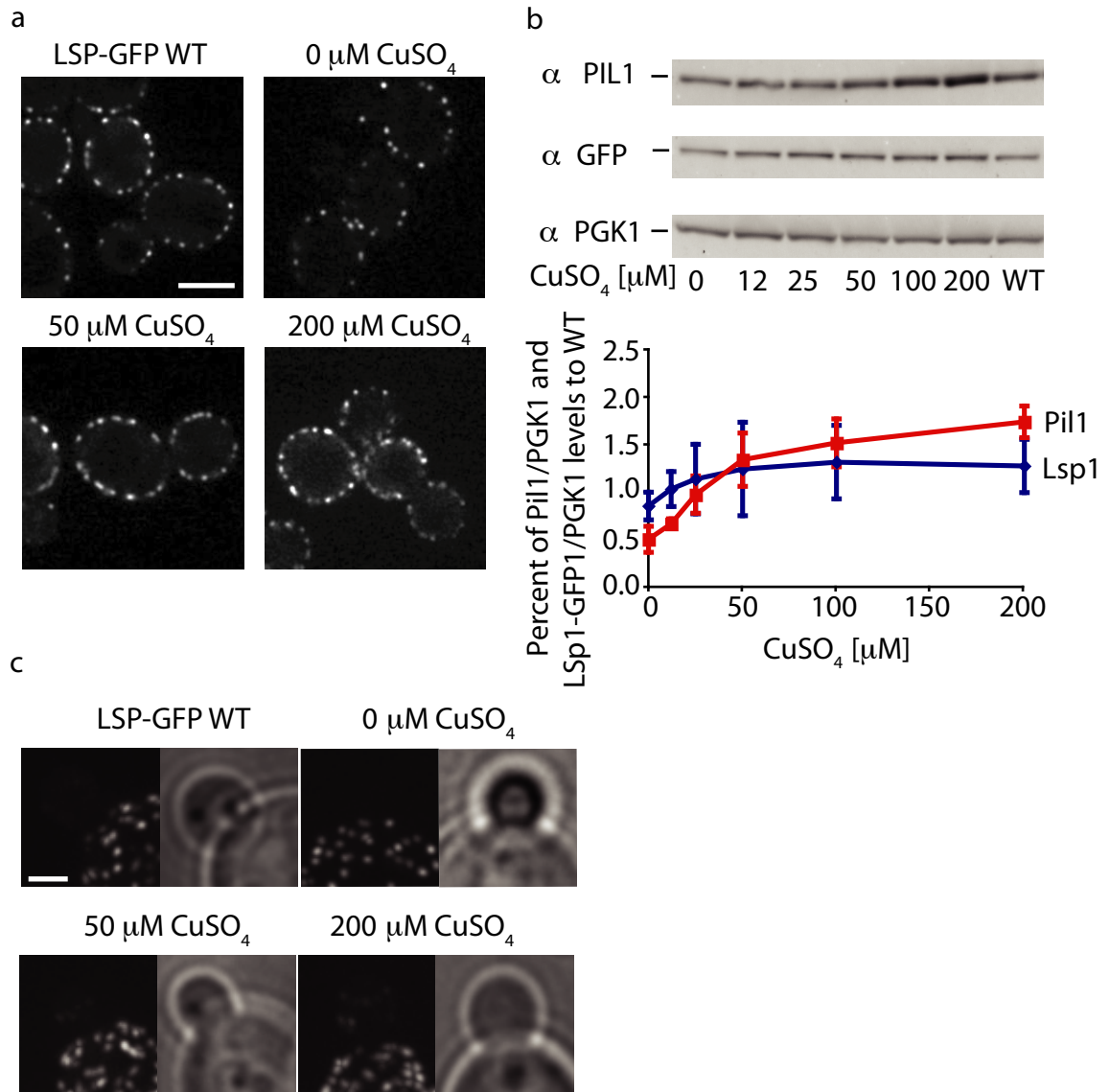
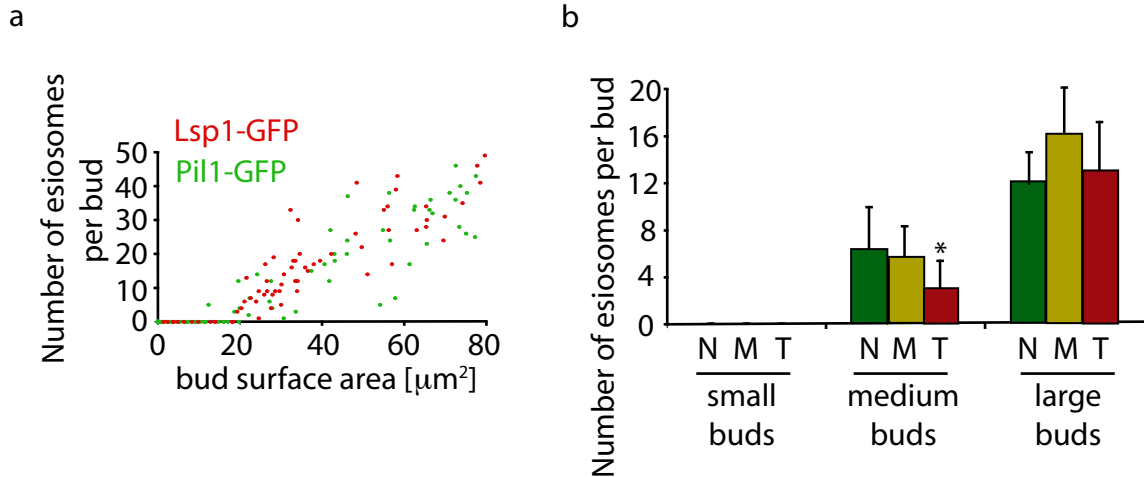


Figure 9. Pil1 expression from the CUP1 promoter in LSP1-GFP cells. (a) Spinning disk confocal cross sections of cells grown at increasing concentrations of CuSO_4 at 30°C for 4h, expressing Pil1 driven from the CUP1 promoter in LSP1-GFP cells (KEM103) are shown and Lsp1-GFP with Pil1 under its endogenous promoter (Lsp1-GFP wild type, TWY113). The scale bar is 5 μm . (b) Titration of CuSO_4 of cells expressing Pil1 under control of the CUP1 promoter. Shown are the original Western blots and the quantitation of relative abundance of Pil1 to Pkg1 and Lsp1-GFP to Pkg1 normalized to wild type levels of Pil1 and Lsp1-GFP respectively, $n = 3$. Error bars

indicate the standard deviation from the mean. “WT” lane contains extracts from Lsp1-GFP (TWY113) cells with Pil1 under its endogenous promoter, (c) Lsp1 eisosome deposition in small buds does not follow Pil1 deposition. Shown are 3D reconstructions of small buds in cells expressing Lsp1-GFP and Pil1 under its endogenous promoter, TWY113 (left panel, “Lsp1-GFP WT”) and Lsp1-GFP with Pil1 under the CUP1 promoter, KEM103. The scale bar is 2 μ m.



Supplemental Figure 1: Pil1 and Lsp1 behave identically during de novo eisosome formation (a) Number of eisosomes where counted in cells expressing either Lsp1-GFP, TWY113 (red) or Pil1-GFP, TWY110 (green) and are shown as a function of the bud cell surface. (b) Eisosome deposition as visualized by Lsp1-GFP is polarized. Cells expressing Lsp1-GFP (TWY103) were analyzed analogously to Figure 1c.

Supplemental Movie 1: Eisosome formation during the cell cycle. Yeast cells expressing Pil1-GFP (TWY110) were immobilized on tissue culture dishes and followed by 3-D microscopy over time. Projections from a single stack are shown. The left panel shows the fluorescence signal from Pil1-GFP, the right panel shows the corresponding transmission light image; time intervals between two stacks are 97 sec.

Supplemental Table I. Strains used in this study.	
Strain	Genotype
CRY1 ^{a,b}	<i>MATα ade2-1 can1-100 his3-11,15 leu2-3,112 trp1-1 ura3-1</i>
CRY2 ^{a,b}	<i>MATα ade2-1 can1-100 his3-11,15 leu2-3,112 trp1-1 ura3-1</i>
TWY110 ^c	<i>MATα PIL1-GFP::HIS3</i>
TWY113 ^c	<i>MATα LSP1-GFP::HIS3</i>
TWY580	<i>MATα/MATα PIL1-GFP::HIS3/pil1Δ ::KAN^R; "0.5x"</i>
TWY576	<i>MATα/MATα PIL1-GFP::HIS3/PIL1-GFP::HIS3 ; "1x"</i>
TWY581	<i>MATα/MATα PIL1-GFP::HIS3/PIL1-GFP::HIS3 URA3::PIL1-GFP/URA3; "1.5x"</i>
TWY578	<i>MATα/MATα PIL1-GFP::HIS3/PIL1-GFP::HIS3 URA3::PIL1-GFP/URA3::PIL1-GFP; "2x"</i>
KEM100	<i>MATα PIL1-GFP::HIS3 Cdc28-AS2:: URA3</i>
KEM101	<i>MATα DAMP-PIL1-GFP::HIS3</i>
KEM102	<i>MATα NAT::pCUP1-PIL1-GFP::HIS3</i>
KEM103	<i>MATα LSP1-GFP::HIS3; NAT::pCUP1-PIL1</i>

^aAll strains used in this study were derived from CRY1 and CRY2, these strains are wild-type W303

^bWilcox et al. 1992

^cWalther et al. 1996

Supplementary Table 2. Coordinates for eisosome position (n = 5 cells)

Eisoosme No.	Cell #1			Cell #2			Cell #3			Cell #4			Cell #5		
	X	Y	Z	X	Y	Z	X	Y	Z	X	Y	Z	X	Y	Z
1	3.92	3.2	0.84	1.72	2.76	0.7	1.84	3.24	1.26	3.12	3.44	0.98	3.24	3.08	0.7
2	3.8	3.88	1.26	3.16	4.04	0.84	2.24	3.44	1.26	3.24	2.24	1.26	2.12	2.76	0.98
3	4.4	3.4	1.4	1.92	1.64	0.98	1	3.16	1.68	2.56	3	1.12	2.64	4.04	0.98
4	4.36	3.32	1.12	1.48	3.76	0.98	3.32	3.88	1.54	4.12	3.24	1.26	3.48	2.24	1.12
5	3.08	1.24	1.82	2.04	4.68	1.12	1.56	3.92	1.54	2.2	2.36	1.26	4	2.32	1.4
6	4.04	1.52	1.68	4.08	3.6	1.26	1.76	4.52	1.82	2.56	3.84	1.26	3.24	1.52	1.54
7	4.88	2.64	1.68	2.88	4.76	1.12	3.24	4.56	1.82	3.16	4.2	1.26	3.36	4.88	1.82
8	2	1.52	2.24	2.72	4.72	0.7	3.24	2.12	1.82	4.52	4.08	1.54	4.36	2.52	1.82
9	5	2.04	2.1	0.84	3.4	1.68	3.72	2.96	1.96	1.64	2.6	1.54	2.6	4.96	2.1
10	1.72	3.84	1.96	4.52	2.68	1.82	2.56	4.8	1.96	1.6	3.4	1.68	2.72	1	2.1
11	1.28	3.04	2.24	4.12	1.28	1.96	2.4	1.24	2.1	2.68	1.36	1.96	2.24	1	2.24
12	6.44	4.44	2.24	2.96	5.56	2.1	3.92	3.72	2.1	1.6	2.12	1.68	0.96	2.24	2.24
13	4.08	1.12	2.38	1.44	1.24	2.66	3	1.48	2.38	4.52	2.28	1.96	1.64	4.56	2.38
14	5.24	3.44	2.52	3.92	4.96	3.36	1.48	5.16	2.8	4.8	3.44	1.68	4.76	3.04	2.52
15	3.76	4.6	2.52	2.32	0.72	2.8	4.04	4.4	2.52	4.68	4.6	1.96	0.64	2.84	2.66
16	2.68	4.6	2.52	0.68	1.92	2.94	0.28	2.64	2.8	1.84	4.56	3.5	2.2	5	2.8
17	4.68	1.32	2.52	0.4	2.56	2.8	4.28	2.6	3.08	2.92	5.12	2.24	5.04	3.96	2.8
18	1.36	2.44	3.22	1.6	1.48	3.08	0.32	3.28	2.94	1.88	1.28	2.24	4.24	1.8	3.92
19	6.44	5.04	2.94	0.8	3.52	3.78	3.76	1.92	2.8	3.2	0.96	3.5	4.28	4.64	3.36
20	6.44	5.44	2.66	6	5.88	3.08	4.44	3.52	2.8	1	1.84	2.52	0.68	3.56	3.36
21	3.44	0.8	3.36	3.32	1.04	3.92	0.56	4.32	3.5	5.08	3	3.92	1.28	4.44	3.64
22	5.28	4.08	3.5	4.64	2.6	3.64	3.4	1.36	3.78	0.72	2.72	2.94	2.16	0.72	4.06
23	4.24	4.72	3.36	0.68	3.4	3.22	4.48	2.04	3.36	1.36	4.24	2.94	0.96	4.04	4.06
24	2.8	4.64	3.64	4.52	3.48	3.22	2.4	5.72	4.06	4	5.44	3.08	4.48	2.6	4.2
25	2.44	4.32	4.34	4.6	3.64	3.22	2.16	1	4.62	2.36	5.16	3.22	3	4.92	4.2
26	3.96	0.76	4.06	4.4	3.76	4.06	4.16	5.12	4.2	4.68	5.08	3.5	2.52	0.96	4.76
27	2.76	1	4.2	2.08	4.92	3.22	1.76	5.6	4.48	3.92	1.16	3.64	0.64	2.76	4.76
28	5.4	3.88	3.92	2.56	6.56	3.22	1.04	4.96	4.62	3.32	5.48	3.78	3.68	4.08	5.04
29	1.76	3.52	4.34	1	2.64	3.92	1.32	1.88	5.46	1.12	3.76	4.2	3.6	3.68	5.32
30	5.32	1.64	4.62	1.24	4.8	3.78	0.52	2.64	4.9	1	3.52	3.92	2.72	3.96	5.6
31	1.92	1.96	4.76	1.52	2.48	4.62	0.64	4.12	5.04	4.52	2.16	4.76	3.2	3.4	5.74
32	5.08	4.12	4.76	2.4	4.72	4.9	0.68	3.56	5.32	2.4	1.04	4.76	2.8	2.8	6.02
33	3.6	1.04	5.04	3.84	2.12	4.62	0.84	3.12	5.46	1	2.56	4.76			
34	2.48	2.12	5.46	4.52	2.4	4.2	1.96	1.72	5.6	3.8	5.16	4.76			
35	2.44	2.76	5.74	3.64	4.24	4.76	1.8	5.16	5.6	1.84	1.44	5.04			
36	5.16	2.84	5.6	2.4	4.48	4.34	2.64	5.36	5.6	2.64	4.8	5.04			
37				2.32	2.6	5.04	2.84	2.36	6.16	3.76	1.68	5.18			
38				2.56	4.44	4.76	3.36	4.64	6.16	1.52	3.12	5.32			
39				2.28	3.52	5.18	1.56	3.12	6.3	4.72	3.76	5.04			
40				3.28	3.56	5.18	2.72	4.4	6.44	3.64	4.56	5.46			
41				2.04	4.12	5.04				2.92	2	5.6			
42										4.04	3.24	5.6			
43										2.2	3.76	5.6			
44										2.4	2.56	5.74			
45										3.56	2.88	5.74			
46										2.8	3.88	5.74			
47										3.08	2.92	5.88			

Chapter 3 is reproduced from The Journal of Cell Biology, 2009, originally published June 29;185(7):1227-42. Copyright © 2009 by The Rockefeller University Press. This article is available online at:

<http://jcb.rupress.org/cgi/content/full/185/7/1227>

CHAPTER 3

A GENOME-WIDE SCREEN FOR GENES AFFECTING EISOSOMES REVEALS NCE102 FUNCTION IN SPHINGOLIPID SIGNALING

A genome wide screen for genes affecting eisosomes reveals Nce102 function in sphingolipid signaling

Florian Fröhlich^{1#}, Karen Moreira^{2#}, Pablo S. Aguilar³, Nina C. Hubner⁵, Matthias Mann⁵, Peter Walter^{2,4} and Tobias C. Walther^{1*}

1. Organelle Architecture and Dynamics, Max Planck Institute of Biochemistry, Martinsried, Germany

2. Department of Biochemistry and Biophysics, University of California at San Francisco, San Francisco, USA

3. Institute Pasteur, Montevideo, Uruguay

4. Howard Hughes Medical Institute

5. Proteomics and Signal Transduction, Max Planck Institute of Biochemistry, Martinsried, Germany

These authors contributed equally to this work

* Corresponding author; current address:

Organelle Architecture and Dynamics,

Max Planck Institute of Biochemistry,

Am Kopferspitz 18

82152 Martinsried, Germany

ABSTRACT

The protein and lipid composition of eukaryotic plasma membranes is highly dynamic and regulated according to need. The sphingolipid-responsive Pkh kinases are candidates for mediating parts of this regulation, as they affect a diverse set of plasma membrane functions, such as cortical actin patch organization, efficient endocytosis, and eisosome assembly. Eisosomes are large protein complexes underlying the plasma membrane and help to sort a group of membrane proteins into distinct domains. In this study, we identify Nce102 in a genome-wide screen for genes involved in eisosome organization and Pkh kinase signaling. Nce102 accumulates in membrane domains at eisosomes where Pkh kinases also localize. The relative abundance of Nce102 in these domains compared with the rest of the plasma membrane is dynamically regulated by sphingolipids. Furthermore, Nce102 inhibits Pkh kinase signaling and is required for plasma membrane organization. Therefore, Nce102 might act as a sensor of sphingolipids that regulates plasma membrane function.

INTRODUCTION

The plasma membrane is highly dynamic and crucial for communication of cells with their environment. It transduces numerous extracellular signals and transports molecules in and out of the cell. To accommodate these diverse tasks, it is highly organized, and plasma membrane processes are tightly coordinated, both spatially and temporally (Simons and Toomre, 2000; Anderson and Jacobson, 2002; Simons and Vaz, 2004). How the abundance of most lipids and proteins in the plasma membrane is regulated is largely unknown.

In the yeast *Saccharomyces cerevisiae*, the plasma membrane is laterally organized into spatial domains that have different protein and lipid composition. One type of domain harbors several integral membrane proteins, such as the arginine transporter Can1 and members of the Sur7 family of proteins and was accordingly termed membrane compartment occupied by Can1 (MCC). MCCs were suggested to contain a distinct lipid composition enriched in ergosterol, as visualized by staining with filipin, a fluorescent marker binding this lipid (Malinska et al., 2003; Grossmann et al., 2007).

Yeast mother cells possess 25–45 MCCs that can be visualized as discrete foci in the plasma membrane. MCCs are mutually exclusive with a second domain, marked by the plasma membrane ATPase Pma1, termed membrane compartment occupied by Pma1 (MCP; Malinska et al., 2003, 2004). The organization of the plasma membrane in distinct spatial domains is at least in part mediated by large protein complexes termed eisosomes (Walther et al., 2006). Eisosomes lie underneath each MCC forming a punctate, distributed pattern in the cell cortex. When the gene encoding the major eisosome component Pil1 is deleted, MCCs and all remaining eisosome proteins investigated so far

coalesce into one or a few punctae per cell (Walther et al., 2006; Grossmann et al., 2007). In addition to concentrating at such eisosome remnants, a significant fraction of MCC transmembrane proteins, such as Sur7, localizes uniformly in the plasma membrane. Similarly, the ergosterol marker filipin loses its normal punctate eisosome localization in *pill1Δ* cells, distributes more evenly over the plasma membrane surface, and enriches at eisosome remnants (Grossmann et al., 2007).

One possible function of MCCs and eisosomes is to regulate protein and lipid abundance by sorting them into distinct, spatially separated pools where they are stabilized or from which they can be endocytosed selectively. Consistent with this notion, disruption of MCCs leads to increased turnover of some proteins normally localized there (Grossmann et al., 2008). The precise molecular function of eisosomes is still unclear, but it was suggested that they regulate sites of endocytosis based on their colocalization with endocytic intermediates visualized by the lipophilic dye FM4-64 and a hexose transporter GFP fusion protein (Walther et al., 2006). A clue of how eisosomes might be regulated is provided by the discovery that Pkh kinases localize at eisosomes and that Pil1 and Lsp1 are Pkh kinase substrates (Zhang et al., 2004; Walther et al., 2007; Luo et al., 2008).

Pkh kinases regulate physiology and plasma membrane functions such as actin patch organization, endocytosis, and eisosome assembly (Inagaki et al., 1999; Sun et al., 2000; Friant et al., 2001; deHart et al., 2002; Liu et al., 2005; Grosshans et al., 2006; Daquinag et al., 2007; Walther et al., 2007; Luo et al., 2008). These responses are mediated by their targets, including Ypk1 and Ypk2 (homologues of the mammalian serum glucocorticoid kinase), Sch9 (homologue of human AKT kinase), Pkc1 (atypical protein kinase C), and myosin-I. In addition, Pkh kinase phosphorylation of Pil1 regulates

the assembly state of eisosomes (Walther et al., 2007; Luo et al., 2008).

Pkh kinases are regulated by sphingoid long chain bases such as phytosphingosine (PHS) and dihydrosphingosine, which are precursors in sphingolipid synthesis (Zhang et al., 2004). However, it is not known how Pkh kinases sense and respond to long chain bases. Pkh kinases and several other kinases of the signaling module are regulated by levels of long chain bases in vitro, but whether this is relevant in vivo and whether it is the only way to control Pkh kinase activity is not clear (Zhang et al., 2004; Liu et al., 2005).

In this study, we visually screened for genes that affect eisosome organization either directly or through altering Pkh kinase activity. We identified the transmembrane protein Nce102 as part of the sphingolipid–Pkh signaling network. Our functional experiments suggest that Nce102 might act as a sphingolipid sensor that modulates Pkh kinase activity to regulate plasma membrane organization and function.

RESULTS

Nce102 is required for normal eisosome organization

To identify genes required for eisosome assembly and organization, we screened by fluorescence microscopy a systematic gene deletion collection into which we introduced GFP-labeled Pil1 fusion protein (Pil1-GFP; Fig. S1 a; Tong et al., 2001). To determine the effect of individual mutations on eisosomes, we grew the library in 96-well plates to mid-log phase and imaged cells with an automated microscope. Visual inspection of the images led to identification of 88 genes that affect eisosomes (Fig. 1 a).

To obtain quantitative data for the identified mutants, we collected confocal

images and quantitated the number of eisosomes per cell, the cytosolic fluorescence signal representing unassembled Pil1-GFP, the integrated fluorescence on the cell surface, the size of individual eisosomes, and the percentage of cell surface covered with eisosomes (Fig. S1 a). The relative values for these parameters were used to cluster the genes according to the similarity of their phenotypes (Fig. S1 b).

For example, deletion of genes encoding subunits of the NatC complex involved in N-terminal protein acetylation (*MAK3*, *MAK10*, and *MAK31*) showed a similar phenotype characterized by fewer eisosomes, increased cytoplasmic Pil1-GFP, and little change in the size of remaining eisosomes.

In addition, several hits (*YMR031C*, *YMR086W*, and *MSC3*) are good candidates for genes encoding previously not recognized eisosome components because they localize in a punctuate pattern at the cell periphery similar to eisosomes, and at least Ymr031c and Ymr086c were copurified with Pil1 (Huh et al., 2003; Grossmann et al., 2008; Deng et al., 2009).

In this study, we focused on Nce102 because it is the only hit in our screen previously found as a transmembrane plasma membrane protein (Cleves et al., 1996). To confirm the role of Nce102 in eisosome formation, we investigated the localization of Pil1-GFP in *nce102Δ* compared with wild-type cells. Consistent with the systematic genome-wide screen, confocal images showed a clear reduction of eisosome number and a wider spacing of remaining eisosomes (Fig. 1 b). Quantitation revealed that deletion of *NCE102* results in a twofold decrease of eisosome number per mother cell and concomitant increase of cytosolic signal (Fig. 1 c).

Nce102 is required for membrane organization

Eisosomes organize MCCs, and mutation of *PILI* results in mislocalization of all tested MCC components (Walther et al., 2006; Grossmann et al., 2007, 2008). Because *NCE102* deletion has a strong effect on eisosomes, we asked whether *NCE102* is also required for plasma membrane organization. Indeed, compared with wild-type cells in which the MCC marker Sur7-GFP was organized in distinct domains, *nce102Δ* cells showed only few clusters and more uniform localization of Sur7-GFP throughout the plasma membrane (Fig. 2 a). Furthermore, we observed a consistent but less pronounced phenotype on the MCP marker Pma1, which localized more uniformly in *nce102Δ* cells compared with its normal localization in structured plasma membrane domains (Fig. 2 b).

Next, we asked whether Nce102 influences the formation of endocytic intermediates formed as foci at eisosomes by using the lipophilic tracer FM4-64 (Vida and Emr, 1995; Walther et al., 2006). FM4-64 foci formed after short chase periods of 1 min and colocalized with eisosomes in both wild-type and *nce102Δ* cells (Fig. 2 c). However, when we quantitated the number of foci, we found their number greatly reduced in *nce102Δ* cells (median = 1 foci/cell; Fig. 2 d, right) compared with wild-type cells (median = 4 foci/cell; Fig. 2 d, left). Together, this shows that normal plasma membrane organization requires Nce102.

Nce102 localizes to the plasma membrane at MCC

To answer how Nce102 functions, we first investigated its subcellular localization. In agreement with a recent study that identified Nce102 as an MCC component, we found Nce102-GFP localizing in the plasma membrane and accumulating in foci reminiscent of

MCCs (Fig. 3 a; Grossmann et al., 2008). This notion was further confirmed by colocalization of Nce102 with plasma membrane markers but not, for example, with cortical ER markers (unpublished data).

To test whether Nce102 foci are MCCs, we investigated their localization in respect to Sur7 tagged with the red fluorophore RFP-mars (Fischer et al., 2004), an MCC marker. Nce102 foci completely overlapped with Sur7-marked MCCs (Fig. 3, a and b) with significant levels of Nce102-GFP also diffusely localized in the remainder of the plasma membrane. As MCCs are membrane domains located over eisosomes, we additionally investigated Nce102-GFP localization in respect to eisosomes marked by Lsp1-mars and found that Nce102-GFP foci and eisosomes colocalize perfectly (Fig. 3, c and d). Because Nce102 is a multipass transmembrane domain protein, it is most likely located in the MCC and partially in the remainder of the membrane.

One hallmark of proteins localizing to eisosomes or MCCs is that they collapse to one or a few eisosome remnants in *pillA* cells (Walther et al., 2006; Grossmann et al., 2007). Indeed, Nce102-GFP localization in *pillA* cells also closely resembles that of MCC proteins such as Sur7. Most of Nce102-GFP localizes to one or a few eisosome remnants in *pillA* cells, whereas the remaining portion shows a uniformly distributed signal throughout the plasma membrane (Fig. 3 e).

Nce102 acts negatively on Pil1 phosphorylation

Because eisosome organization is sensitive to Pil1 phosphorylation, we expected to find genes in our screen that directly affect the architecture, assembly, or stability of eisosomes and genes involved in signaling that modifies Pil1 phosphorylation. In fact, the

nce102Δ phenotype on Pil1-GFP localization closely resembles the phenotype of *pil1(4D)* mutant cells, bearing a phosphomimicking mutant of Pil1-GFP in which four residues that are phosphorylated in the wild-type protein are mutated to aspartate (S45D, S59D, S230D, and T233D; Fig. 1 b and Fig. S4 c; Walther et al., 2007).

Therefore, we tested genetically whether Nce102 acts on eisosomes by altering Pil1 phosphorylation that could then indirectly modulate eisosome assembly. If *nce102Δ* effect is mediated by phosphorylation, we expect that a *pil1(4A)*-GFP mutant in which four residues that are required for the effect of Pkh kinases on eisosome assembly are changed to alanine (S45A, S59A, S230A, and T233A; Walther et al., 2007) blocks the effect of *NCE102* deletion. However, if Nce102's effect on eisosomes is independent of Pil1 phosphorylation state, we expect to see similar effects of *nce102Δ* on wild-type Pil1 and *pil1(4A)*. Indeed, *pil1(4A)*-GFP localization was indistinguishable between *nce102Δ* and wild-type cells, showing slightly more eisosome *pil1(4A)* assembly at the plasma membrane compared with wild-type Pil1 (Fig. 4 b). Therefore, *pil1(4A)* is epistatic to *nce102Δ*. Because Pil1 needs to get phosphorylated on residues mutated in *pil1(4A)* to develop the *nce102Δ* eisosome phenotype, we conclude that Nce102 acts upstream of Pil1 phosphorylation.

When combined with *pil1(4D)*-GFP, *nce102Δ* cells showed a similar, albeit slightly more severe phenotype than *NCE102 pil1(4D)-GFP* cells (Fig. S4 c), indicating that phosphorylation at additional sites can enhance eisosome disassembly. Previous work identified at least seven additional phosphorylation sites in Pil1, which may mediate this effect (Zhang et al., 2004; Walther et al., 2007; Luo et al., 2008). Together, *pil1(4A)* epistasis on *nce102Δ* and enhancement of the *pil1(4D)* phenotype by *nce102Δ* suggest

that Nce102 negatively regulates Pil1 phosphorylation.

Nce102 inhibits Pil1 phosphorylation

To substantiate these findings, we determined whether the phosphorylation state of Pil1 is altered in *nce102Δ* cells. To this end, we purified Pil1 fused to a tandem affinity purification (TAP) tag from wild-type and metabolically heavy lysine-labeled *nce102Δ* cells (stable isotope labeling by amino acids in cell culture [SILAC]; Fig. S2 a; Ong et al., 2002) and analyzed it by two strategies. First, we mixed proteins of Pil1-TAP eluates 1:1 and separated them by SDS-PAGE, resulting in a clearly visible doublet of Pil1, where the upper band represents phosphorylated Pil1 (Walther et al., 2007). Separate analysis of the two bands by liquid chromatography (LC) mass spectrometry (MS)/MS revealed that contaminant proteins present in both bands have a 1:1 ratio of protein from wild-type and *nce102Δ* sample, as determined by comparing mean peptide peak intensities. In contrast, Pil1 from *nce102Δ* was 30% enriched in the upper phospho-Pil1 band (1.28 ratio, Pil1 heavy vs. light) and correspondingly decreased in the lower band (0.59 ratio, Pil1 heavy vs. light; Fig. 5 a; and Fig. S2, c and d).

In a second approach, we directly mixed, digested, and analyzed Pil1 pull-down eluates by LC-MS/MS (Fig. S2 a). From this approach, we identified many unphosphorylated peptides and, for example, the phosphorylated peptide harboring T233 of Pil1 from both wild-type and *nce102Δ* cells. Importantly, the phosphopeptide was more than threefold more abundant coming from the heavy lysine-labeled *nce102Δ* samples compared with the wild-type control (Fig. 5 b; and Fig. S2, e and f). The total amount of Pil1 was equal in both experiments because unphosphorylated peptides were present in a

1:1 ratio (Fig. S2 f). Together, these data demonstrate that Pil1 was present in a roughly equimolar ratio in both pull-down eluates but that phosphorylation at T233 was more than threefold increased in *nce102Δ* cells. Therefore, the results of the two biochemical approaches converge, demonstrating that Pil1 phosphorylation is increased in *nce102Δ* cells.

Because Pil1 phosphorylation is inhibited by sphingoid bases (Zhang et al., 2004; Walther et al., 2007), we tested whether *NCE102* deletion results in a similar effect on Pil1 phosphorylation as sphingolipid depletion. To this end, we measured the relative abundance of the Pil1 T233 phosphopeptide in cells where synthesis of sphingolipids was blocked for 1 h by myriocin, a drug targeting the serine palmitoyl transferase that catalyzes the rate-limiting step of sphingolipid synthesis, compared with wild-type cells. In this experiment, we detected a twofold increase of Pil1 phosphorylation at T233 after myriocin treatment compared with wild-type cells (Fig. 5 c and Fig. S2 g). This shows that the block of sphingolipid synthesis by myriocin and *NCE102* deletion has a similar effect on Pil1 phosphorylation.

Nce102 acts on Pil1 via Pkh kinases

Several studies show that Pil1 phosphorylation is mediated by Pkh kinases (Zhang et al., 2004; Walther et al., 2007; Luo et al., 2008). Therefore, we asked whether the effect of Nce102 on Pil1 phosphorylation occurs through the Pkh kinase pathway. First, we determined the epistatic relationship between Pkh kinase mutants and *nce102Δ* using a yeast strain that harbors a deletion of *PKH2* and a temperature-sensitive allele of *PKH1* (*pkh^{ts}*; Friant et al., 2001). Already at the permissive temperature, these mutations lead to

a strong over-assembly effect on eisosomes. Specifically, *pkh^{ts}* strains display large elongated threads of Pil1 at the plasma membrane with more of the membrane covered with Pil1 (Fig. 6; Walther et al., 2007). This phenotype is also very severe at the restrictive temperature, with most of the membrane covered with Pil1 (Fig. S4 e).

Combining *pkh^{ts}* and the *nce102Δ* mutations, we found that double-mutant cells show a Pil1-GFP phenotype indistinguishable from the *pkh^{ts}* phenotype at both 24 (Fig. 6) and 37°C (Fig. S4 e). This indicates that Pkh kinases are required to obtain the *nce102Δ* phenotype and shows that Nce102 acts upstream of Pkh kinases, inhibiting them in a linear pathway.

Nce102 acts downstream of long chain bases in sphingoid base signaling

Our data suggest that Nce102 acts on Pil1 phosphorylation by inhibiting Pkh kinases. Because Pkh kinases are regulated by sphingoid bases and both, a block of sphingolipid synthesis and *nce102Δ*, lead to increased Pil1 phosphorylation, Nce102 itself may be controlled by sphingolipids, acting upstream of the Pkh kinases. Alternatively, Nce102 could be required for efficient synthesis of sphingolipids that are then sensed by the kinases by some other route. One more possibility is that Nce102 acts independently of sphingolipids to regulate Pkh kinases.

To distinguish between these possibilities, we tested whether Nce102 is required for the synthesis of sphingoid bases. If this was the case, addition of exogenous sphingoid base would rescue the *nce102Δ* phenotype. Exogenously added sphingoid bases can enter the cell and rescue a sphingoid base synthesis defect because addition of 5 μM PHS suppressed the Pil1-GFP phenotype of the *lcb1-100* mutant (which impairs sphingolipid

synthesis) both at the permissive and restrictive temperatures (Fig. 7 a). In contrast, the eisosome defect of *nce102Δ* cells was not rescued by addition of PHS under conditions that rescued the *lcb1-100* mutant phenotype (Fig. 7 a) or by a 10-fold higher concentration of PHS (unpublished data). Quantitation of eisosome number and cytosolic Pil1 levels confirmed the visual evaluation (Fig. 7 b).

These data show that Nce102 is not required for sphingoid base synthesis but rather acts downstream of it. Because PHS has no additive effect on *nce102Δ* cells, sphingolipids and Nce102 act in the same pathway (Fig. 7 b).

To further test this hypothesis, we investigated the interaction between myriocin treatment and *nce102Δ*. If both act independent from each other, we expect an additive effect between them. However, this is not the case. As shown in images and quantitation of eisosomes, myriocin has no further effect on eisosomes in *nce102Δ* cells, confirming that sphingolipid signaling and Nce102 act in the same pathway on eisosomes (Fig. 7, c and d).

We previously showed that Pil1 hyperphosphorylation caused by decreased sphingolipid synthesis causes eisosome disassembly (Walther et al., 2007). If our hypothesis is true and Nce102 is an inhibitor of Pil1 phosphorylation acting downstream of sphingolipids, we predict that overexpression of Nce102 will rescue eisosome disassembly when sphingolipid synthesis is decreased. To test this, we expressed Nce102-mars from the inducible Gal promoter in cells that have Pil1-GFP-marked eisosomes. When these cells are grown on raffinose, Nce102-mars is not expressed, and eisosomes appear normal, as these cells also express endogenous Nce102 (Fig. 8). When these cells grow on galactose, Nce102-mars is overexpressed (Fig. 8). Strikingly, when we blocked

sphingolipid synthesis in these cells by treating them with myriocin, the normal effect of disassembling eisosomes apparent in control cells was completely blocked (Fig. 8). This shows that increasing Nce102 levels blocks the effect of inhibiting sphingolipid synthesis on eisosomes.

Together, our genetic experiments thus place Nce102 in a linear pathway inhibiting Pkh kinases and suggest a relationship: sphingoid bases \rightarrow Nce102 \dashv Pkh1/2 \rightarrow Pil1 phosphorylation \rightarrow eisosome disassembly. In this scenario, Nce102 would function as part of a sensor relay for sphingoid base or sphingolipid levels.

Nce102 localization responds to changes in sphingolipid levels

Because Nce102 negatively regulates Pkh kinases that localize to eisosomes, we next tested whether Nce102 distribution between MCCs at eisosomes and the rest of the plasma membrane is affected by sphingolipid levels. To this end, we determined Nce102-GFP localization after blocking sphingolipid synthesis. Strikingly, after a 1 h incubation of cells with myriocin, the punctate pattern of Nce102-GFP localization in MCCs disappeared, and the protein distributed diffusely across the plasma membrane (Fig. 9 a). Consistently, in intensity plots of surface images, myriocin-treated cells show a rather flat distribution of the Nce102-GFP signal, whereas control samples show many Nce102-GFP peaks corresponding to MCCs at eisosomes (Fig. 9 b). Relocalization of Nce102-GFP could be reversed by addition of exogenous PHS for a short time (15 min). In this case, the MCC pattern of Nce102-GFP localization reappeared, showing an even more pronounced pattern of Nce102-GFP foci than normal (Fig. 9 b).

Nce102 relocalization could be caused by redistribution of existing protein in the

plasma membrane or new protein synthesis under conditions in which myriocin blocks the efficient incorporation of Nce102 in MCCs. To distinguish these possibilities, we added myriocin after a preincubation with the translation-blocking drug cycloheximide. During persistent translation block, Nce102 localized normally to MCCs and the remainder of the membrane (Fig. 9 c). Moreover, it still relocated from MCCs after myriocin treatment, indicating that this phenomenon is not dependent on protein synthesis (Fig. 9 c). Similarly, when PHS was added to cells in which translation was blocked, Nce102 relocation occurred normally (Fig. 9 c).

To test whether this effect is specific to the availability of sphingoid bases or a more general response to sphingolipid levels, we added aureobasidin to cells for 1 h. This drug inhibits complex sphingolipid synthesis from ceramide downstream of the formation of sphingoid bases (Nagiec et al., 1997). We observed the same Nce102-GFP redistribution in the plasma membrane after aureobasidin or myriocin addition (Fig. 9 a and Fig. S4). Consistent with the downstream block of sphingolipid synthesis by aureobasidin, addition of exogenous sphingoid bases did not result in reformation of the punctate Nce102 pattern (Fig. S4).

Together, these data suggest an equilibrium of two pools of Nce102-GFP localizing to MCCs at eisosomes or to spaces in between that is shifted by levels of sphingolipids. Consistent with this notion, addition of PHS to untreated cells shifted more Nce102-GFP into punctate structures, rendering them more pronounced (Fig. 9, a and b). In the yeast plasma membrane, many proteins are sensitive to extraction by detergents to a different level, and Nce102 was previously described operationally as an abundant component of detergent-resistant membranes (Bagnat et al., 2000). To test whether

Nce102 distribution between MCCs and the remainder of the plasma membrane observed by microscopy is reflected in its partitioning between different membrane environments, we analyzed its solubility in a buffer containing 1% Triton X-100 at 4°C. Proteins partitioning into sphingolipid/ergosterol-rich domains show lower solubility in this buffer compared with proteins embedded in mostly phospholipid bilayers. This difference can be tested in a velocity sedimentation gradient. Nce102 from untreated cells was present in most fractions of the gradient, indicating that it is localized both to detergent-resistant and other membranes (Fig. 9 d). When treated with myriocin, Nce102 partitioning changed toward the bottom of the gradient, indicating higher solubility. After short treatment of these cells with PHS, Nce102 redistributed to more detergent-insoluble membrane fractions at the top of the gradient. Pma1, a marker for MCP membranes, did not significantly alter its migration in the gradient after either myriocin or PHS treatment.

Together, these results show that relative levels of Nce102 in different plasma membrane domains are regulated by sphingolipids and that this redistribution is highly sensitive to changes in membrane composition because it can be observed after small perturbations that do not change Pma1 behavior. These data are consistent with the hypothesis that Nce102 sphingolipid-mediated redistribution is the mechanism by which Nce102 regulates Pil1 phosphorylation. In this model, Nce102 is recruited to MCCs at eisosomes under conditions of sufficient sphingolipids to repress Pkh kinase activity toward Pil1 and released from there when sphingolipid levels drop, for example, after inhibition of their synthesis by myriocin or aureobasidin. To test this, we determined the localization of Nce102-mars relative to Pkh kinases. Pkh2-GFP localizes in few very dim spots that colocalize with eisosomes and Nce102 foci (Fig. S5, a and b). Importantly,

when we blocked sphingolipid synthesis with myriocin, Nce102-mars relocated from these foci, leaving Pkh2-GFP behind (Fig. 5, c and d).

If Nce102 acts as a plasma membrane sphingolipid sensor, then its partitioning should be upstream and independent of the assembly state of eisosomes. Alternatively, Nce102 redistribution could be a consequence of eisosome disassembly after inhibition of sphingolipid synthesis. To test this directly, we used *pil1(4A)* mutant cells in which Pil1 cannot be sufficiently phosphorylated. Eisosomes are therefore resistant to activation of Pkh kinases (Walther et al., 2007). As expected, when cells that express *pil1(4A)-GFP* as their sole copy of Pil1 are incubated with myriocin, eisosomes remain stable because Pil1(4A) does not get sufficiently phosphorylated to disassemble (Fig. 9 e). To determine whether Nce102-GFP redistribution is caused by disassembly of eisosomes, we investigated the localization of Nce102-GFP in *pil1(4A)* cells. We found it to distribute normally in both MCCs and the remainder of the plasma membrane (Fig. 9 f). When we added myriocin to these cells, eisosomes remained assembled as a result of the *pil1(4A)* mutation, yet Nce102-GFP relocated to become diffusely distributed throughout the plasma membrane (Fig. 9 f). To test whether this is a general property of MCC proteins, we performed similar experiments with cells expressing Sur7-mars. When we treated these cells with myriocin, the intensity of Sur7 signal in MCC decreased as Pil1 disassembled (Fig. 9 g; not depicted), but this could be completely blocked by expressing Pil1(4A) (Fig. 9 h). Thus, Nce102-GFP has a distinct behavior from other MCC components and redistributes in the plasma membrane dependent on sphingolipids but independently of the eisosome assembly state.

DISCUSSION

We report a comprehensive screen for genes involved in Pil1-GFP localization. Recently, a similar screen using an MCC reporter identified 27 genes (Grossmann et al., 2008). Compared with that screen, we found roughly three times more genes affecting Pil1 localization ($n = 88$). It remains to be seen whether this difference is caused by different thresholding during the screen or biological differences between MCCs versus eisosomes. Because Pil1 and MCC components colocalize and *PIL1* is required for normal MCC formation, it is surprising that there is little overlap between the two screens: only *NCE102*, *SUR4*, *MNN10*, and few biological processes were found in both. Examples include retrograde transport from the Golgi apparatus to the ER (*VPS52* and *VPS54* in the MCC screen; *VPS51* and *VPS53* in the Pil1 screen). Therefore, these genes and processes likely have a global effect on plasma membrane organization affecting MCCs and eisosomes. Genes that were identified only in one screen likely perform more specific functions; future experiments will, for example, show whether *YMR086W*, *YMR031C*, or genes encoding the NatC complex are important for eisosomes but not MCCs.

Besides genes globally affecting the plasma membrane, we expected to find genes impacting eisosome organization directly as well as genes that alter sphingolipid signaling, resulting in altered Pil1 phosphorylation and assembly. In the later class, we identified *Nce102*. Besides it, also *SUR4*, *ISC1*, and *SAC1* are likely to act on eisosomes through sphingolipid signaling. Deletion of *SUR4*, required for fatty acid elongation during sphingolipid synthesis (Han et al., 2002; Paul et al., 2006), or deletion of *ISC1*, the homologue of mammalian neutral sphingomyelinase (Sawai et al., 2000), results in accumulation of complex sphingolipids. In our screen, both *isc1* and *sur4* cells showed

hyperassembled Pil1-GFP, which is the opposite effect of depleting complex sphingolipids by inhibiting their synthesis (Table S2). In addition, it was recently reported that *sac1* cells have elevated sphingoid bases and reduced levels of complex sphingolipids (Brice et al., 2009), and we found them to have fewer eisosomes and increased cytoplasmic Pil1-GFP signal (Table S2). We expect that other genes identified will also turn out to play a role in sphingolipid biology.

In this study, we focused on the function of Nce102, a multispinning plasma membrane protein required for normal eisosomes, MCC formation, and plasma membrane organization. Initially, Nce102 was identified by Cleves et al. (1996) as required for nonclassical export of mammalian galectin from yeast. The mechanism of Nce102 function in this pathway was not investigated. Because the assay used requires solubilization of cell-associated galectin using high pH, it is possible that the basis of the effect could be altered protein extractability from *nce102Δ* cells because of their altered plasma membrane.

Our experiments revealed that Nce102 has fascinating properties, suggesting that it might act as part of a sphingolipid sensor. Most remarkable, its localization is dynamic and responsive to changes in sphingolipid levels: Nce102 partitions between two domains in the plasma membrane, MCCs overlying eisosomes and the rest of the plasma membrane. We show that the distribution between these two domains is controlled by sphingolipid availability. Nce102 localization to MCCs brings it into close contact with the underlying eisosomes and Pkh kinases (Fig. S5; Walther et al., 2007). Nce102 negatively regulates the activity of these kinases, and, in the presence of sphingolipids, blocks their downstream functions. Conversely, if sphingolipid synthesis is blocked,

Nce102 redistributes away from Pkh kinases (Fig. S5), alleviating their inhibition. Therefore, we propose a model that Nce102 acts as part of a sphingolipid-sensing mechanism and that its distribution in the plasma membrane regulates Pkh kinases (Fig. 10). In the simplest hypothesis, Nce102 could simply accomplish repression of the kinases by regulated juxtaposition to them, which is a common scheme in kinase signaling. Based on filipin staining, MCCs were suggested as sites of increased ergosterol concentration in the plasma membrane (Grossmann et al., 2007), and because sterols preferentially interact with sphingolipids, it is likely that sphingolipids are also concentrated there, forming detergent-resistant, liquid-ordered membrane domains or lipid rafts (Simons and Ikonen, 1997; Malinska et al., 2003) where Nce102 was found previously (Bagnat et al., 2000). Thus, it is possible that Nce102 also reacts to ergosterol levels in the plasma membrane. However, we did not observe an effect of nonessential *erg* mutants or block of sterol synthesis on eisosomes or Nce102 localization (unpublished data). Consistent with our model, Nce102 localizes to eisosome remnants that also show increased filipin staining, likely reflecting increased concentration of ergosterol and possibly sphingolipids (Grossmann et al., 2007). Alternatively, filipin might preferentially report on free sterols not in complex with sphingolipids, and staining of MCCs could actually indicate a lower concentration of sphingolipids in this compartment. This view is supported by a recent observation that filipin staining increases if sphingolipid synthesis is blocked (Jin et al., 2008). A further alternative is that Nce102 could directly bind sphingolipids, changing its affinities to other proteins that help localize it to MCCs and/or switching its activity as a Pkh kinase inhibitor on and off. In either model, Nce102 leaves the MCC when sphingolipid levels there are low,

releasing its inhibition of Pkh kinases that now phosphorylate Pil1 and other targets. This is consistent with our observation that Nce102 detergent solubility changes after inhibition of sphingoid base synthesis, indicating that it partitions between different membrane environments. Most likely, this change corresponds to the relocalization of Nce102 from MCCs to the remainder of the membrane observed by microscopy. The interpretation of this result, however, remains vague, as most proteins in the yeast plasma membrane differ only in the degree of their resistance to Triton X-100 detergent extraction. For example, the MCP marker Pma1 was also previously used as a marker for detergent-resistant lipid rafts (Bagnat et al., 2000; Lee et al., 2002; Malinska et al., 2003). The difference in Triton X-100 solubility between Nce102 and Pma1 after myriocin treatment might therefore indicate that these proteins differently partition into such lipid rafts or that the MCP is actually more complex and contains subdomains not easily resolved by light microscopy. Consistent with the later notion, TORC2 (Tor kinase complex 2) is localized at a distinct plasma membrane domain separate from MCC and MCP and is also partially detergent resistant (Aronova et al., 2007; Berchtold and Walther, 2009).

The sensing mechanism of sphingolipids in the plasma membrane by Nce102 suggested in this study is different from a previous model positing that soluble sphingoid bases in the cytoplasm directly control Pkh kinases (Zhang et al., 2004; Liu et al., 2005). It is possible that sphingolipids control the activity of Pkh kinases at many levels. Sphingoid bases could, for example, directly regulate Pkh kinases as in vitro experiments suggest (Zhang et al., 2004), and complex sphingolipids could affect signaling via Nce102. However, the in vivo effect of direct inhibition of Pkh kinase activity toward

Pil1 by sphingoid bases is probably minor compared with the Nce102 pathway, as exogenously added PHS was not able to counteract the *nce102Δ* hyperphosphorylation effect on eisosomes.

Our model of regulation of Pkh kinases by complex sphingolipids via the transmembrane protein Nce102 would also bridge the topological barrier between the cytoplasmic Pkh kinases and complex sphingolipids mainly concentrated in the outer leaflet of the plasma membrane (van Meer et al., 2008).

Downstream of sphingolipid sensing, the Nce102–Pkh pathway regulates phosphorylation of Pil1 that, when increased, always correlated with eisosome disassembly, e.g., in *nce102Δ* cells. This effect could be blocked by mutating phosphorylated Pil1 residues to alanines that we previously found were required and sufficient for the effect of Pkh kinases on eisosomes (Walther et al., 2007). This is different from findings by Luo et al. (2008), who reported that a mutant form of Pil1 harboring five phosphosites mutated to alanine (S6A, S59A, T233A, S273A, and S299A) cannot assemble properly and argued that phosphorylation of Pil1 is important for assembly of eisosomes rather than disassembly. In this study, even a mutant that lacks these five sites and even two additional sites (S6A, S45A, S59A, S230A, T233A, S273A, and S299A) still assembles into eisosomes correctly (unpublished data). The reason for this difference is unclear but might indicate that additional pathways to the Nce102–Pkh kinase module regulate Pil1 phosphorylation in a complex fashion.

Besides phosphorylation of Pil1, Pkh kinases modify many plasma membrane functions. Therefore, as expected, *nce102Δ* cells show altered organization of the plasma membrane, as observed for MCCs, MCPs, and the endocytic foci marked by the

lipophilic dye FM4-64. Recently, it was also shown that *nce102Δ* cells have accelerated endocytosis rates of some membrane transporters (Grossmann et al., 2008). Pkh kinases also participate in processes as diverse as cortical actin patch organization, cell integrity signaling, endocytosis, and eisosome organization (Inagaki et al., 1999; Sun et al., 2000; deHart et al., 2002; Roelants et al., 2002; Zhang et al., 2004; Liu et al., 2005; Grosshans et al., 2006; Walther et al., 2007; Luo et al., 2008). Regulation of these diverse processes may help control the composition of the plasma membrane according to need, perhaps constituting part of a negative feedback loop that targets genes involved in sphingolipid synthesis. Indeed, expression of such genes, e.g., *LCB2*, *FEN1*, and *SUR4*, is strongly negatively correlated to the expression of *NCE102* when the latter is regulated in response to various physiological conditions, e.g., during diauxic shift, nitrogen depletion, or heat shock (correlations for *NCE102/SUR4* are: diauxic shift, -0.94 ; nitrogen starvation, -0.66 ; and heat shock, -0.85 ; Fig. S3, b–d; DeRisi et al., 1997; Gasch et al., 2000). In addition, after prolonged incubation with PHS, we observed Nce102-GFP signal at the vacuole (unpublished data), perhaps reflecting an adaptation to recalibrate the set level of Pkh signaling after long times with high sphingolipids levels.

An important role of Nce102 in regulation of sphingolipids is also supported by the ability of its deletion to suppress the growth defect of a mutation in the serine palmitoyl transferase subunit *TSC3* (Schuldiner et al., 2005; unpublished data) or the growth inhibition caused by myriocin (Fig. S3 a), both of which reduce the first and rate-limiting step in sphingolipid synthesis.

Salient features of the sphingolipid–Nce102–Pkh kinase signaling network are likely conserved between yeast and other eukaryotes. Nce102 shares homology with the

synptogyrin/cellugyrin protein family (Belfort et al., 2005), but the molecular roles of these proteins are not understood. In contrast, mammalian PDK1 kinases (the homologues of yeast Pkh kinases) are well characterized, and the general architecture of downstream signaling is conserved (Casamayor et al., 1999). In either system, full activation of AGC kinases, such as AKT, Sch9, serum glucocorticoid kinase, or Ypk1/2, requires phosphorylation both by PDK1 (in mammalian cells) or Pkh kinases (in yeast) and in addition by the conserved kinase complex TORC2 (Powers, 2007). For yeast, TORC2 signaling has been implicated in the regulation of sphingolipid biosynthesis (Beeler et al., 1998; Tabuchi et al., 2006; Aronova et al., 2008). This effect of TORC2 is mediated by the Pkh kinase target Ypk2 (Aronova et al., 2008). Additionally, the Slm proteins were identified as targets of both the TORC2 and Pkh kinase signaling pathways and to regulate a late step in the synthesis of complex sphingolipids (Tabuchi et al., 2006). It is therefore likely that the TORC2 and Pkh1/2 pathways collaborate to regulate sphingolipid metabolism in yeast. Given the similarity of the signaling pathway components and its architecture in higher eukaryotes, their output may also be evolutionarily conserved.

MATERIALS AND METHODS

Visual screen

To generate a library of deletion mutants each expressing Pil1-GFP, we performed a modification of the synthetic genetic array screen as described previously (Tong et al., 2001). In short, a *MAT* strain containing a chromosomal copy of Pil1-GFP marked with a *NAT^R* marker, the *CAN1* gene disrupted by a construct that encodes the MATa promoter driving expression of the *HIS3* gene and the *LYPI* gene disrupted by a construct

expressing *LEU2* from the MF promoter (KEM108), was crossed to the *MATa* deletion library BY4741 (each strain marked with *KAN^R*). Diploids were selected on G418 and nourseothricin and sporulated. From the sporulation, *MATa* haploids containing both Pil1-GFP and the deletion gene were selected with successive pinning on –HIS (selection for *MATa* cells), G418 (selection for the gene deletion from the library), canavanine (selection for haploid cells harboring *can1Δ*), S-(2-aminoethyl)-L-cysteine hydrochloride (selection for haploid cells harboring *lyp1Δ*), and nourseothricin (selection for Pil1-GFP)-containing media.

For imaging, cells were grown overnight to saturation in 384-well plates, transferred to 96-well plates, diluted, and grown for 9 h until they reached mid-log phase. Cells were transferred to glass-bottom 96-well plates coated with concanavalin A and imaged with a 40x high NA objective in an ImageXPress Micro (MDS Analytical Technologies). At least six different images were taken for each deletion strain. The images were visually inspected using the software by the microscope manufacturer and classified using three categories: increased cytosolic Pil1-GFP fluorescence, altered number or eisosomes, and altered pattern of eisosomes. Strains that showed a phenotype in this first round of screening were regrown and imaged by using a confocal microscope (LSM510; Carl Zeiss, Inc.).

Two optical mid-section and two top-section images were taken for each strain, showing 15–40 cells per image. Images were visually analyzed, and several parameters of the Pil1-GFP signal on the surface of cells were quantitated using an image interpretation script developed in MATLAB that we named EISURAN (both the source code and an executable MATLAB file can be found at

<http://www.biochem.mpg.de/en/rg/walther/news/index.html>). In short, EISURAN first subtracts background from the images and then finds the edge of a cell by image dilation. To facilitate the quantitation of signal from assembled Pil1, the script thresholds the image using Otsu's method (Otsu, 1979). From the resulting binary image, EISURAN calculates the number of positive pixels per cell, a measure for the area covered by eisosomes (percentage of cell surface covered by eisosomes). It then calculates the mean size of the connected clusters (mean pixel number per eisosome cluster on cell surface). To eliminate small background clusters, a minimum of 20 pixels are used for the lower cut off. In some conditions, very large values result caused by connection of eisosomes into very large clusters, which are sometimes string formed. To determine how much Pil1 is in individual eisosomes, EISURAN determines the mean intensity of each cluster by applying the binary image as a mask on the original image, integrating the intensity in each cluster, and averaging this intensity over all clusters in an image (mean integrated intensity per eisosome cluster on cell surface). Quantitation of eisosome number was based on the mean number of eisosomes counted by two independent observers in optical mid sections of mother cells (eisosome number; mean for the wild type = 11.5 ± 1.55).

The cytoplasmic signal was quantitated as the mean intensity of a 50 x 50-pixel area in the cytoplasm (cytoplasmic Pil1-GFP signal) visible in a confocal mid section of the cell using ImageJ (National Institutes of Health). The resulting values were averaged from at least 20 cells, analyzed by hierarchical clustering, and displayed using *R* software (<http://www.r-project.org>).

Yeast strains and plasmids

All yeast strains used as well as their genotypes are listed in Table S1. The starter strain used for the screen *Pil1-GFP::NAT^R* (KEM 108) was generated in the strain YMS196 (provided by N. Krogan, University of California, San Francisco, San Francisco, CA) by tagging Pil1 with GFP using homologous recombination. *Nce102-GFP::HIS* and *nce102Δ::NAT^R* were generated in the W303 wild-type strain by homologous recombination of PCR-generated fragments to yield strains TWY840 and TWY842, respectively (Janke et al., 2004). The *pil1Δ::KAN^R NCE102-GFP::HIS* was similarly generated by homologous recombination, transforming the *NCE102-GFP* and marker into the *pil1Δ* strain TWY226 to yield TWY836. Analogously, *nce102Δ::NAT^R Pil1-GFP* was generated by transforming a *PIL1-GFP* fragment with an HIS marker into TWY842 to yield TWY837. The *Nce102-TAP:KAN^R* strain was generated by homologous recombination after transforming an *Nce102-TAP* fragment in the S288C wild-type strain to yield TWY897 (Janke et al., 2004). Strains harboring *pkh^{ts}* mutants and Pil1-GFP were described previously (Walther et al., 2007). *nce102Δ::NAT^R* was generated by homologous recombination of a PCR fragment in a control strain with the same background as *pkh^{ts}* and used to derive a strain with *pkh1^{ts} pkh2Δ::LEU nce102Δ::NAT^R Pil1-GFP::URA* by crossing, sporulation, and selection of haploid cells to yield strain TWY932. All deletion strains were confirmed by PCR, and strains expressing tagged proteins were confirmed by PCR and Western blot analysis.

A *pil1Δ::KAN^R nce102Δ::NAT^R* strain was generated by crossing *pil1Δ* strain TWY226 with the *nce102Δ* strain TWY841. Sporulation and selection yield TWY898.

pRS306 plasmids containing the *PIL1* promoter, the wild type, or mutated ORF fused to GFP used for expression of phosphomimicking and nonphosphorylatable Pil1

were described previously (Walther et al., 2007) and were integrated into the URA locus of TWY898 to yield TWY931 and TWY934.

Pma1-GFP was created by PCR-mediated tagging in wild type or *nce102Δ::NAT^R* to generate TWY958 and TWY1049, respectively. Similarly, *SUR7-GFP* strains were generated to yield TWY956 (wild-type) and TWY1049 (*nce102Δ*).

The pGalNce102-mars plasmid was created by cloning a fusion PCR product combining the Gal-promoter, the Nce102 ORF, and the mars sequence into the NotI and HindIII sites of pRS306. This plasmid was integrated into the *URA3* locus of TWY110 to yield TWY1222.

For SILAC labeling, the lysine auxotroph S288C strain TWY70 was transformed with a Pil1-TAP fragment to get the *Pil1-TAP:KAN^R* strain TWY1004 (Janke et al., 2004). To generate a *Pil1-TAP:KAN^R nce102Δ:NAT^R* strain, TWY1004 was transformed with a *nce102Δ* fragment yielding TWY1052 (Janke et al., 2004).

Yeast culture and drug treatment

Yeast cells were grown according to standard procedure. For microscopy, cells were grown in synthetic complete medium and bound to concanavalin A–treated coverslips. Myriocin (Sigma-Aldrich) and PHS (Sigma-Aldrich) were added in concentrations as indicated and incubated for 1 h or 15 min. Cycloheximide (Sigma-Aldrich) was added in a concentration of 100 μg/ml for 1 h and 15 min before treatment with other drugs.

For SILAC labeling, Pil1-TAP–expressing yeast cells in a wild-type or *nce102Δ* background were grown in 1 l YNB liquid medium. *PIL1-TAP* cells were grown in the presence of 20 mg/l normal L-lysine, and *PIL1-TAP nce102Δ* cells were grown in the

presence of 20 mg/l L-lysine-U-¹³C₆, ¹⁵N₂ overnight with at least 10 doublings to OD₆₀₀ = 0.7.

Microscopy

For fluorescence microscopy, yeast cells were grown to OD = 0.6 in synthetic medium at 30°C unless indicated otherwise. Cells were mounted in synthetic media onto coverslips previously coated with concanavalin A and directly imaged with a spinning-disk confocal microscope (TiLL iMIC CSU22; Andor) using a back-illuminated EM charge-coupled device camera (iXonEM 897; Andor) and a 100x 1.4 NA oil immersion objective (Olympus). From this setup, 16-bit images were collected using Image iQ (version 1.9; Andor) in the linear range of the camera. For presentation, images were filtered with a smoothing filter averaging 2 pixels, converted to 8-bit images, and cropped using ImageJ software (<http://rsbweb.nih.gov/ij/>).

FM4-64 assay

To measure the formation of early FM4-64 uptake intermediates, either wild-type or *nce102Δ* cells were grown in mid-log phase to OD = 0.5. Approximately 5 ml cell culture was harvested by centrifugation and incubated on ice for 5 min. Cells were then labeled for 10 min with 40 μM FM4-64, washed three times in ice-cold medium, and resuspended in RT YPD for 5 min. Cells were killed by addition of 10 mM NaN₃ and NaF each and immediately analyzed by fluorescence microscopy.

Isolation of detergent-resistant membranes

Detergent-resistant membranes were isolated essentially as described previously (Bagnat et al., 2000). In brief, 20 ODs Nce102-TAP-expressing yeast cells were harvested by centrifugation. The pellets were washed once with water and lysed in TNE buffer (50 mM Tris-HCl, pH 7.4, 150 mM NaCl, and 5 mM EDTA) by vortexing with glass beads twice for 5 min each at 4°C. The lysate was cleared of unbroken cells by centrifugation at 500 g for 5 min and incubated with Triton X-100 (1% final) for 30 min on ice. 250 µl lysate was adjusted to 40% Optiprep by adding 500 µl of 60% Optiprep solution and overlaid with 1.2 ml of 30% Optiprep in TXNE (TNE and 0.1% Triton X-100) and 200 µl TXNE. The samples were centrifuged at 55,000 rpm for 2 h in a rotor (S55S; Sorvall), and five fractions of equal volume were collected from the top. Proteins of each fraction were precipitated with 10% trichloroacetic acid for 15 min on ice. Precipitates were resuspended in 50 µl 2x sample buffer (0.24 M Tris, pH 8.0, 8% SDS, 1 mM DTT, 40% glycerol, and 0.4% bromphenol blue) and heated at 65°C. 25-µl aliquots were loaded onto 12% SDS-PAGE gel and analyzed by Western blotting. Nce102-TAP was detected with a rabbit peroxidase antiperoxidase antibody (Sigma-Aldrich), Pma1 with a rabbit anti-Pma1 antibody (Santa Cruz Biotechnology, Inc.), and a horseradish peroxidase-coupled goat anti-rabbit IgG antibody (Santa Cruz Biotechnology, Inc.).

MS

700 ODs of light-labeled *PILI-TAP* and heavy-labeled *PILI-TAP nce102Δ* cells were harvested by centrifugation resuspended in 5 ml of buffer (150 mM KOAc, 20 mM Hepes, pH 7.4, 10% glycerol, and complete protease inhibitor cocktail [Roche]) and phosphatase inhibitor cocktail (Sigma-Aldrich) and frozen in liquid nitrogen. Total

protein was extracted by bead milling; the thawed lysates were incubated with Triton X-100 (1% final) for 30 min at 4°C and clarified by two consecutive spins of 4 min at 1,000 g. To immunopurify Pil1-TAP, equivalent amounts of the lysates of *PILI-TAP* cells and *PILI-TAP nce102Δ* cells, according to the protein concentration, were incubated with IgG conjugated to agarose beads (GE Healthcare) for 2 h, washed, and eluted by TEV cleavage and centrifugation. The eluates were mixed, reduced for 20 min at RT in 1 mM DTT, and alkylated for 30 min by 5.5 mM iodoacetamide at RT in the dark. Nu-PAGE sample buffer (Invitrogen) was added, and the sample was loaded onto 4–12% Nu-PAGE Bis-Tris SDS-PAGE gels (Invitrogen). Two Pil1 bands were excised from the gel, and proteins were digested with endoproteinase LysC in gel overnight at RT. The resulting peptides were extracted with 30% acetonitrile and 3% trifluoroacetic acid, reduced in a speed vacuum centrifuge, and desalted and concentrated on a reversed-phase column (C18 StageTip; Rappsilber et al., 2003).

In a different approach, the mixed eluates were precipitated with chloroform/methanol and resuspended in 8 M urea. Proteins were alkylated, reduced, and directly digested in solution overnight at RT with LysC. Peptides were desalted and concentrated on StageTips. Peptides were eluted from the StageTips by passage of 2x 20 µl solvent B (80% acetonitrile and 0.5% acetic acid). The volume was reduced to 4 µl in a speed vacuum centrifuge, and 2 µl solvent A* (2% acetonitrile and 1% trifluoroacetic acid) was added to acidify the sample. Peptides were separated on line to the mass spectrometer by using an HPLC system (1200; Agilent Technologies). 5-µl samples were loaded with constant flow of 500 nl/min onto a 15-cm fused silica emitter with an inner diameter of 75 µm (Proxeon Biosystems) packed in house with reverse-phase 3-µm resin

(ReproSil-Pur C18-AQ; provided by Dr. Maisch GmbH). Peptides were eluted with a segmented gradient of 10–60% solvent B over 110 min with a constant flow of 250 nl/min. The HPLC system was coupled to a mass spectrometer (linear trap quadrupole Orbitrap; Thermo Fisher Scientific) via a nanoscale LC interface (Proxeon Biosystems). The spray voltage was set to 2.2 kV, and the temperature of the heated capillary was set to 180°C.

The mass spectrometer was operated in positive-ion mode. Survey full-scan MS spectra ($m/z = 300\text{--}1,600$) were acquired with a resolution of 60,000 at $m/z = 400$ after accumulation of 1,000,000 ions. The most intense ions (up to five) from the preview survey scan delivered by the Orbitrap were sequenced by collision-induced dissociation (collision energy 35%) in the linear trap quadrupole after accumulation of 5,000 ions. Multistage activation was enabled in all MS/MS events to improve fragmentation of phosphopeptides. Maximal filling times were 1,000 ms for the full scans and 150 ms for the MS/MS. Precursor ion charge state screening was enabled, and all unassigned charge states as well as singly charged peptides were rejected. The dynamic exclusion list was restricted to a maximum of 500 entries with a maximum retention period of 90 s and a relative mass window of 10 ppm. Orbitrap measurements were performed enabling the lock mass option for survey scans to improve mass accuracy (Olsen et al., 2005). Data were acquired using the Xcalibur software (version 2.0.5).

Mass spectra were analyzed using the in house–developed software MaxQuant (version 1.0.1; Cox and Mann, 2008). The data were searched against the yeast database concatenated with reversed copies of all sequences (Moore et al., 2002; Peng et al., 2003) and supplemented with frequently observed contaminants (porcine trypsin,

Achromobacter lyticus lysyl-endopeptidase, and human keratins) using Mascot (version 2.2.0; Matrix Science; Perkins et al., 1999).

Carbamidomethylated cysteines were set as fixed, oxidation of methionine, N-terminal acetylation and phosphorylation of serines, threonines, and tyrosines as variable modification. 0.5 D was set as maximum-allowed mass deviation for MS/MS peaks, and a maximum of three missed cleavages were allowed. Maximum false discovery rates were set to 0.01 both on peptide and protein levels. Minimum-required peptide length was six amino acids. Proteins with at least two peptides (thereof one uniquely assignable to the respective sequence) were considered identified.

Online supplemental material

Fig. S1 shows a flowchart of the screening process and the quantitation of Pil1-GFP mutant phenotypes. Fig. S2 shows mass spectrometric analysis of Pil1 phosphorylation in wild-type and *nce102Δ* or myriocin-treated and -untreated control cells. Fig. S3 shows growth curves of *nce102Δ* and wild-type cells untreated or treated with myriocin as well as microarray profiles of *NCE102* versus sphingolipid biosynthesis gene expression. Fig. S4 shows Nce102-GFP localization depending on sphingolipids, phosphomimicking Pil1 mutant being enhanced by deletion of *NCE102*, and epistasis between *nce102Δ* and Pkh kinase mutants. Fig. S5 shows colocalization of Pkh2 and Nce102 depending on sphingolipid synthesis. Table S1 contains yeast strains used. Table S2 shows the phenotypes and classification of Pil1-GFP visual screen hits. Online supplemental material is available at <http://www.jcb.org/cgi/content/full/jcb.200811081/DC1>.

ACKNOWLEDGEMENTS

We thank Nevan Krogan and Dijana Avdic for help generating the *PILI-GFP* deletion library, Ron Vale for use of his high throughput microscope, and Nico Stuurman for his invaluable expertise to image the *PilI-GFP* deletion library. We also thank Stefan Jentsch, Robert Farese Jr., Lena Karotki, Natalie Krahrmer, and Doris Berchtold for discussions, Howard Riezman (University of Geneva, Geneva, Switzerland) for providing reagents, and Andrew Kruchinsky for sharing unpublished data.

This work was supported by the Max Planck Society, the German Research Association (DFG; grant WA 1669/2-1), the German-Israeli Foundation (grant G-2193-1838.9), and the Human Frontiers Science Program (to T.C. Walther). K. Moreira is a recipient of an aging training grant from National Institutes of Health/National Institute on Aging. P. Walter is a Howard Hughes Medical Institute Investigator. P.S. Aguilar is supported by the ANII (DCI-ALA/2007/19.040).

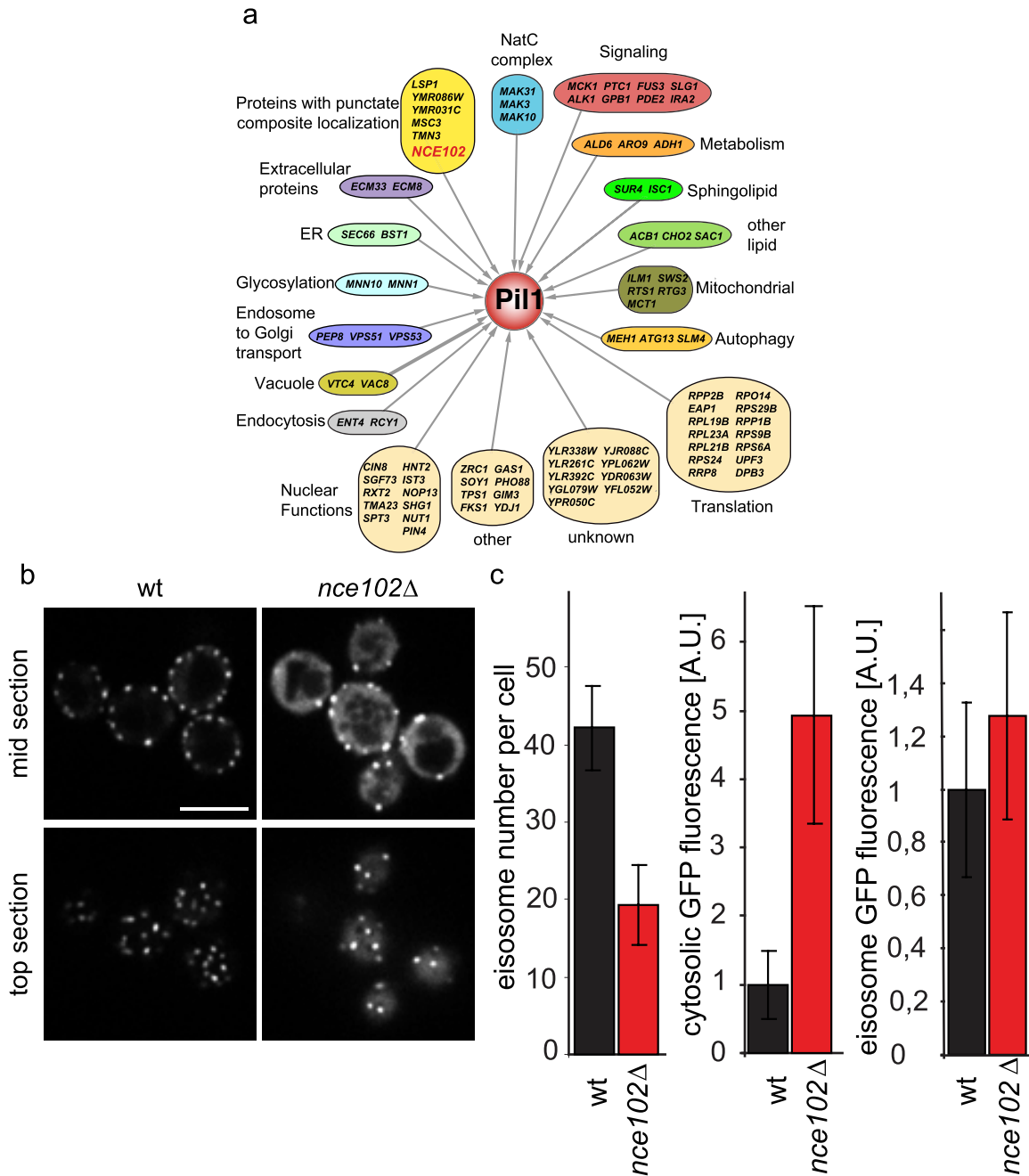


Figure 1. A functional genomic screen reveals genes required for eisosome organization. (a) Genes with a Pil1 organization phenotype shown in functional groups. (b) *Nce102* is required for normal eisosome organization. Images of Pil1-GFP expressed in wild-type (wt; left) or *nce102Δ* cells (right) are shown. (c) Number of eisosomes per mother cell (left), cytoplasmic Pil1-GFP fluorescence (middle), and Pil1-GFP fluorescence per eisosome (right). Error bars indicate SD. Bar, 5 μ m.

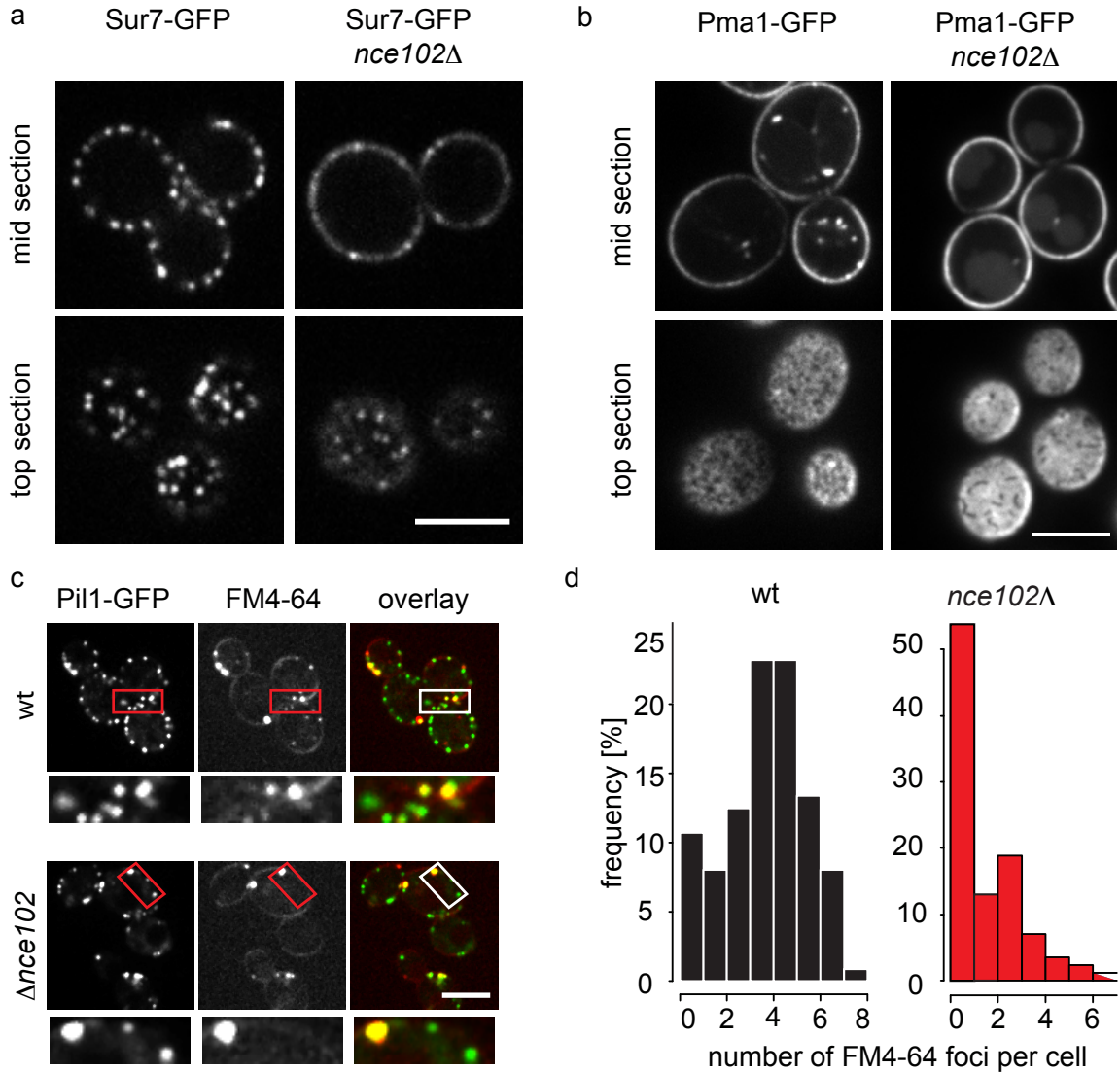


Figure 2. NCE102 is required for normal plasma membrane organization. (a and b) Sur7-GFP (a) and Pma1-GFP (b) were expressed in wild-type (wt) or *nce102Δ* cells, and representative confocal top (bottom) and mid sections (top) are shown. (c) Wild-type and *nce102Δ* cells expressing Pil1-GFP (green) were pulse labeled with FM4-64 (red) for 1 min, and representative images are shown. Boxes indicate the area magnified in the bottom panels. (d) Numbers of FM4-64 intermediates per cell ($n > 50$) from images as in c are shown as a histogram. Bars, 5 μ m.

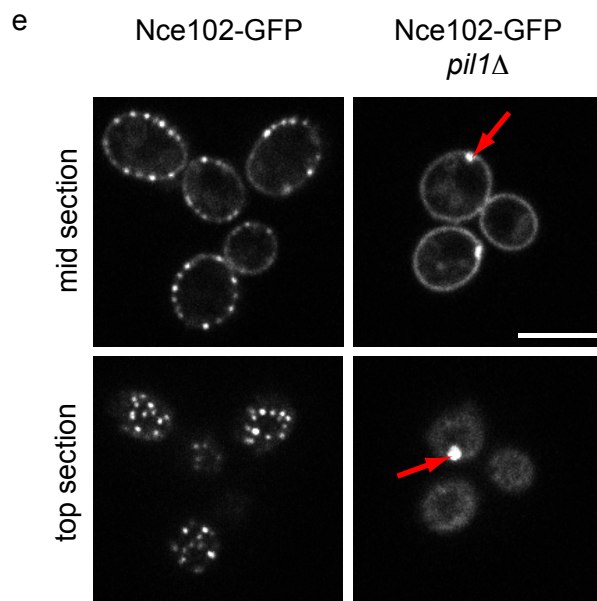
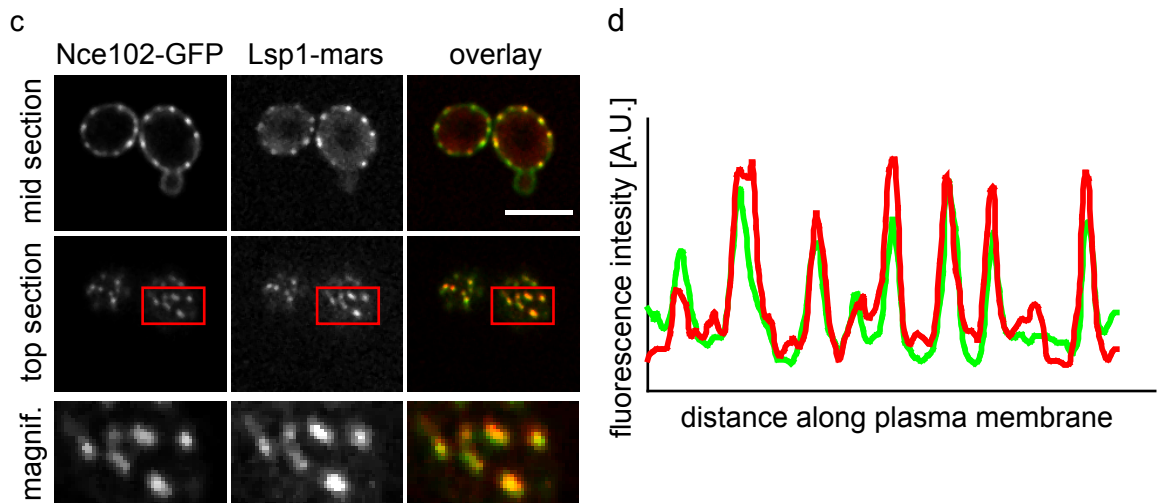
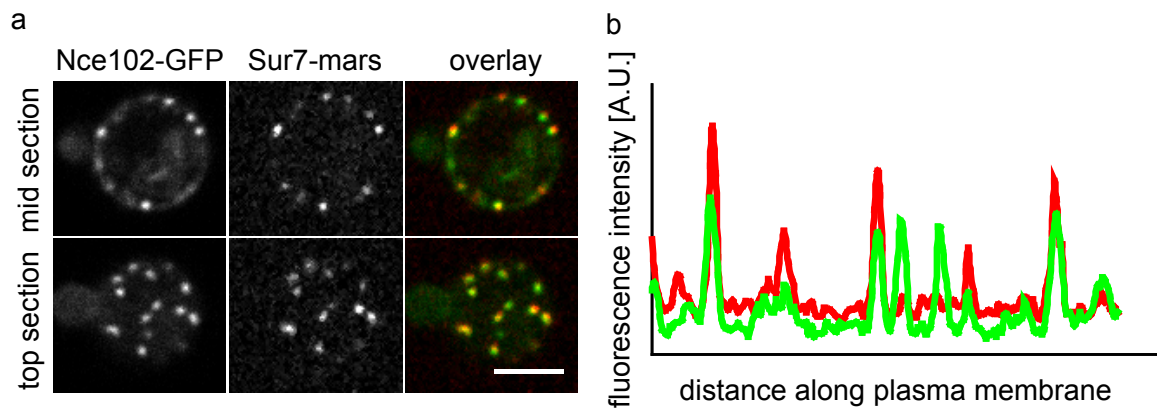


Figure 3. Nce102 localizes to both MCC and non-MCC domains in the plasma membrane. (a) Images from cells expressing Nce102-GFP (left; green in overlay) and Sur7-mars (middle; red in the overlay) are shown. (b) Intensity profiles of Nce102-GFP and Sur7-mars along the plasma membrane. (c) Images from cells expressing Nce102-GFP (left; green in overlay) and Lsp1-mars (middle; red in the overlay) are shown. Boxes indicate the area magnified in the bottom panels. (d) Intensity profiles of Nce102-GFP and Lsp1-mars along the plasma membrane. (e) Pil1 is required for normal Nce102 distribution. Wild-type (left) and *pil1Δ* (right) cells expressing Nce102-GFP are shown. Arrows highlight eisosome remnants. Bars, 5 μ m.

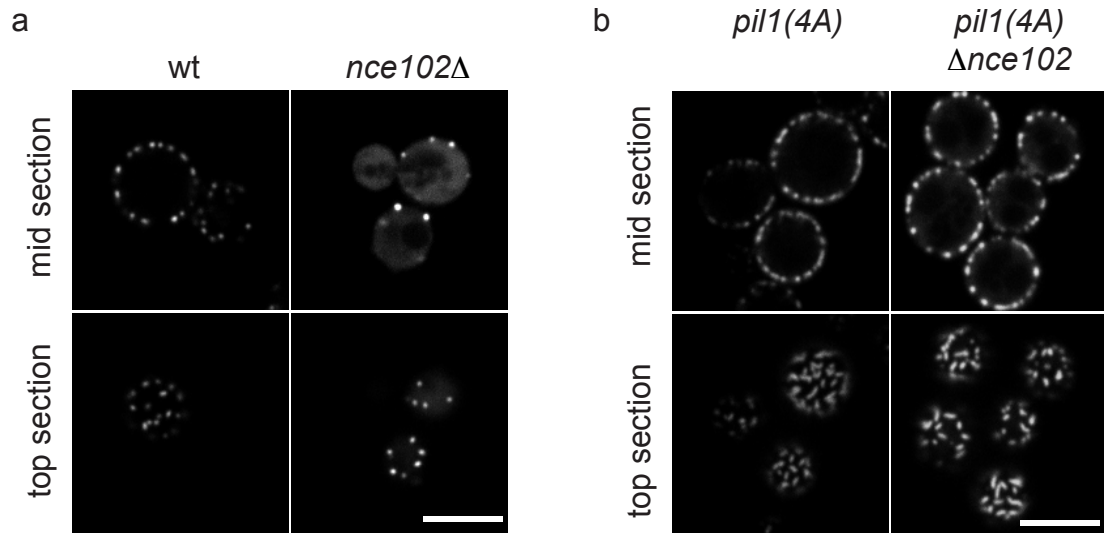


Figure 4. Nonphosphorylatable Pil1 is resistant to *nce102Δ*. (a and b) Representative top and mid sections of wild-type (wt; left) or *nce102Δ* cells (right) expressing Pil1-GFP (a) or nonphosphorylatable *pil1(4A)* fused to GFP (b) are shown. Bars, 5 μ m.

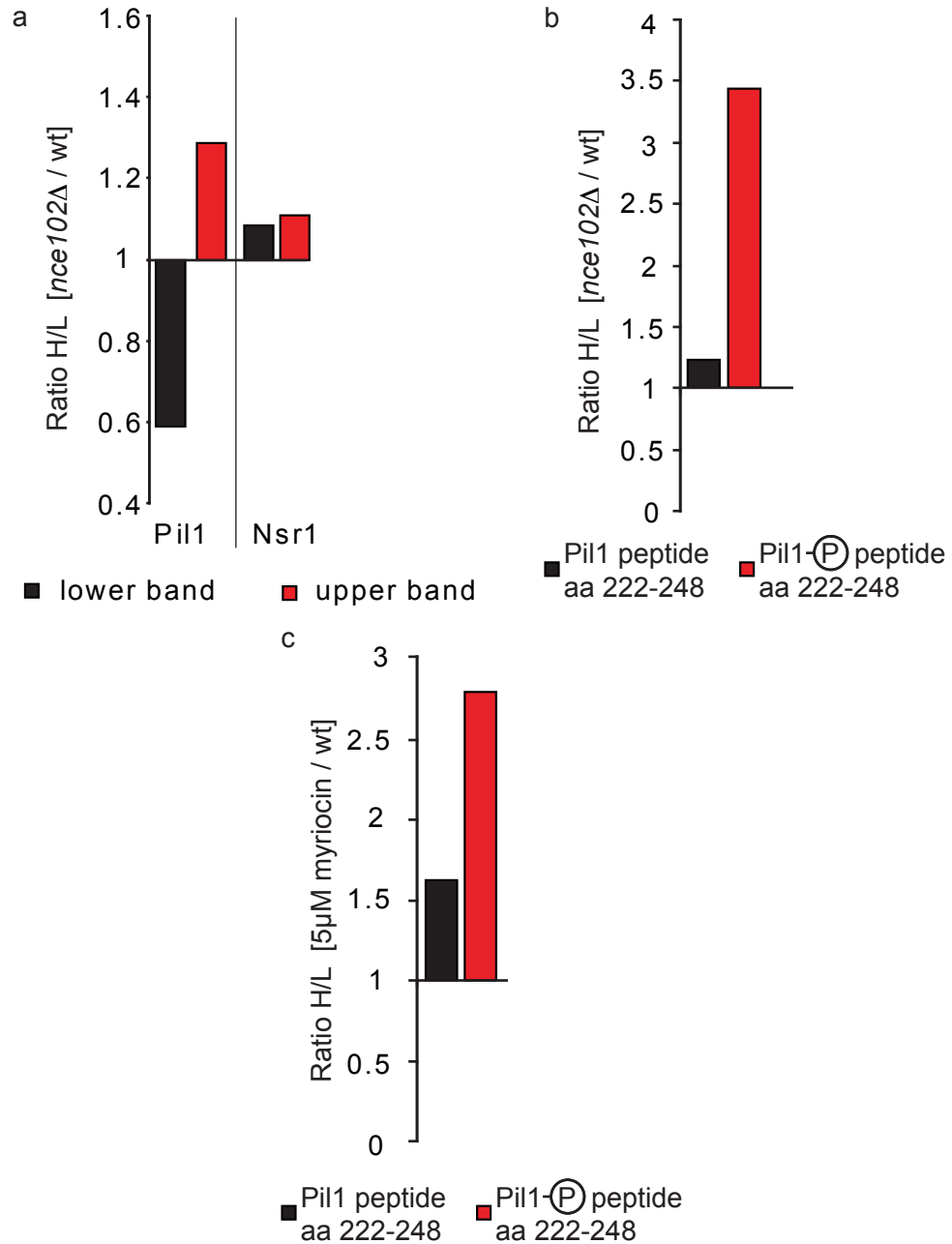


Figure 5. Pil1 phosphorylation is increased in *nce102Δ* cells. (a) Pil1-TAP was purified from SILAC-labeled wild-type and *nce102Δ* cells, mixed in equal amounts, resolved by SDS-PAGE, and two resulting Pil1 bands were separately analyzed by MS. The contaminant Nsr1 was present in a 1:1 ratio from both strains in each band. Pil1 was 1.3-fold enriched in the upper band (red) and decreased to a ratio 0.6 in the lower band (black). (b) Pil1-TAP purified from SILAC-labeled wild-type and *nce102Δ* cells was analyzed by MS. Unphosphorylated Pil1 peptide amino acids 222–248 is shown in

black, and the T233 phosphopeptide is shown in red. (c) Pil1-TAP purified from SILAC-labeled untreated cells or treated with myriocin for 1 h was analyzed as in b. Representative data of three experiments are shown. Ratio H/L denotes the mean ratio of the abundance of heavy- versus light-labeled peptides.

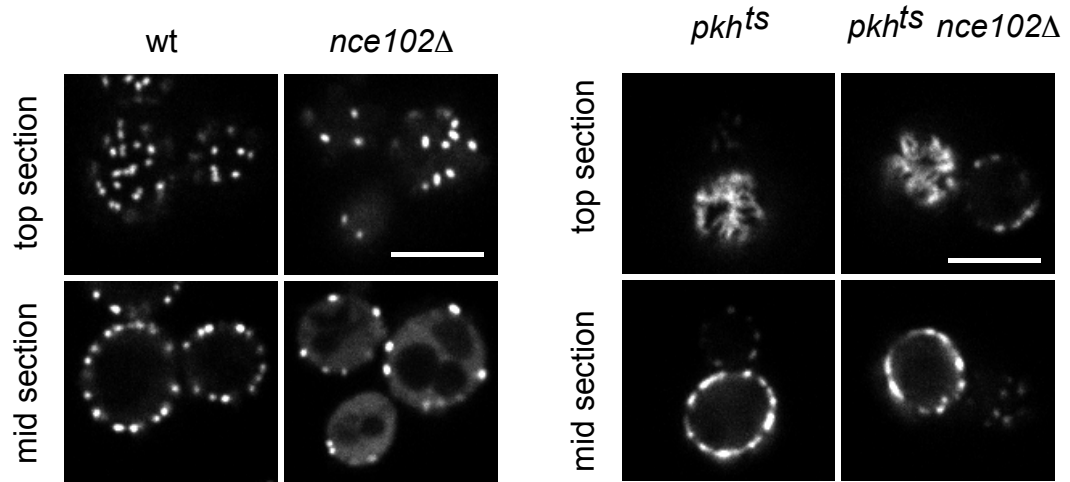


Figure 6. Mutation of Pkh kinases is epistatic to Nce102. Optical top and mid sections of wild-type (*wt*; top left), *nce102Δ* (top right), *pkh1^{ts}* (bottom left), or *pkh1^{ts} nce102Δ* (bottom right) cells expressing Pil1-GFP are shown. Bars, 5 μ m.

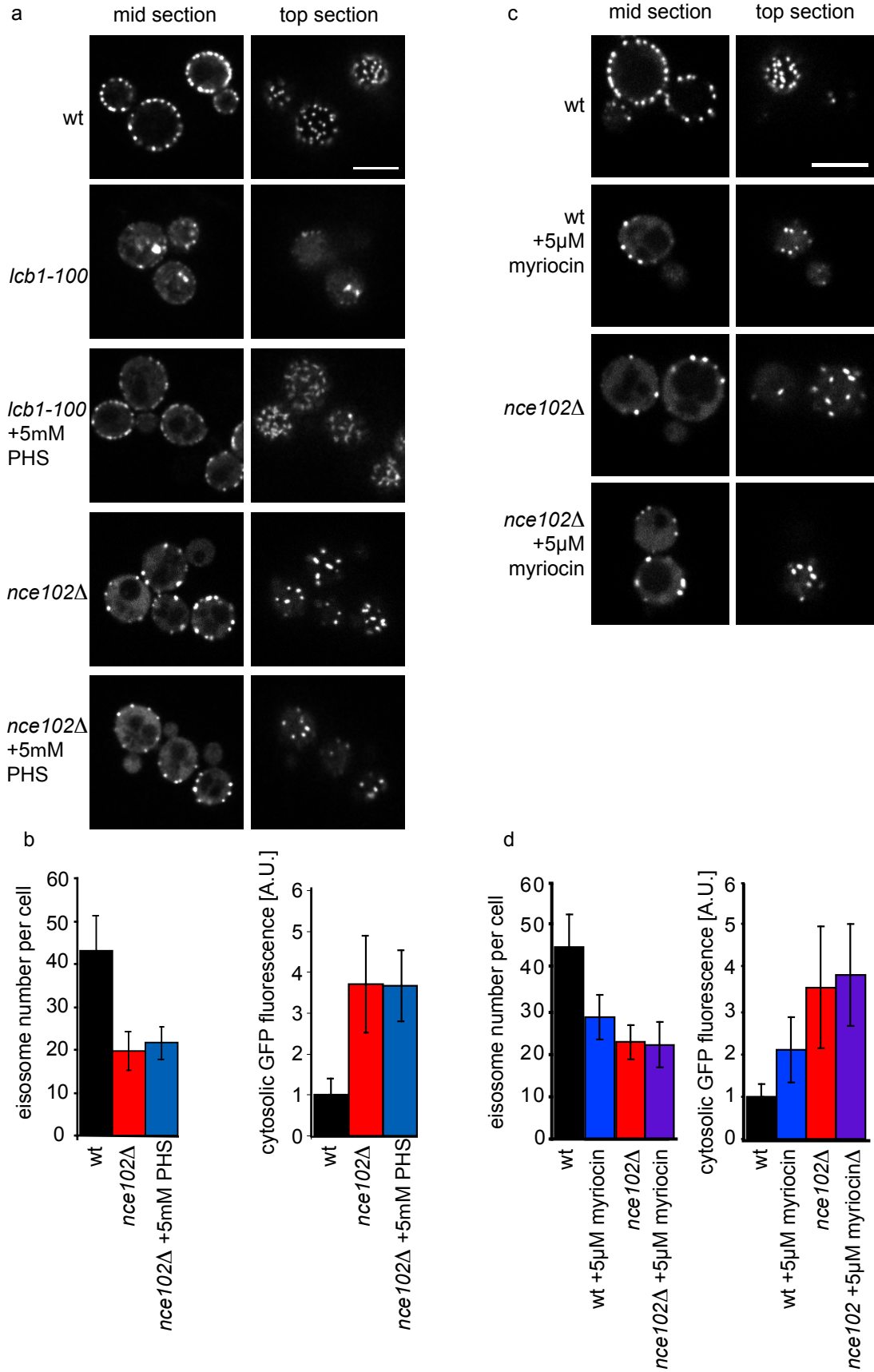


Figure 7. Nce102 and sphingolipids act in the same pathway. (a) *lcb1-100* but not *nce102Δ* is suppressed by sphingoid bases. Wild-type (wt), *lcb1-100*, or *nce102Δ* cells expressing Pil1-GFP were analyzed with or without addition of 5 μM PHS, and representative images are shown. (b) Eisosome number per mother cell (left) and cytosolic Pil1-GFP fluorescence (right) are shown. (c) Myriocin has no additive effect on *nce102Δ* cells. Wild-type and *nce102Δ* cells were treated for 1 h with 5 μM myriocin, and representative images are shown. (d) Quantitation of eisosome number per mother cell (left) and cytoplasmic Pil1-GFP fluorescence (right) of cells treated as in c. Error bars indicate SD. Bars, 5 μm.

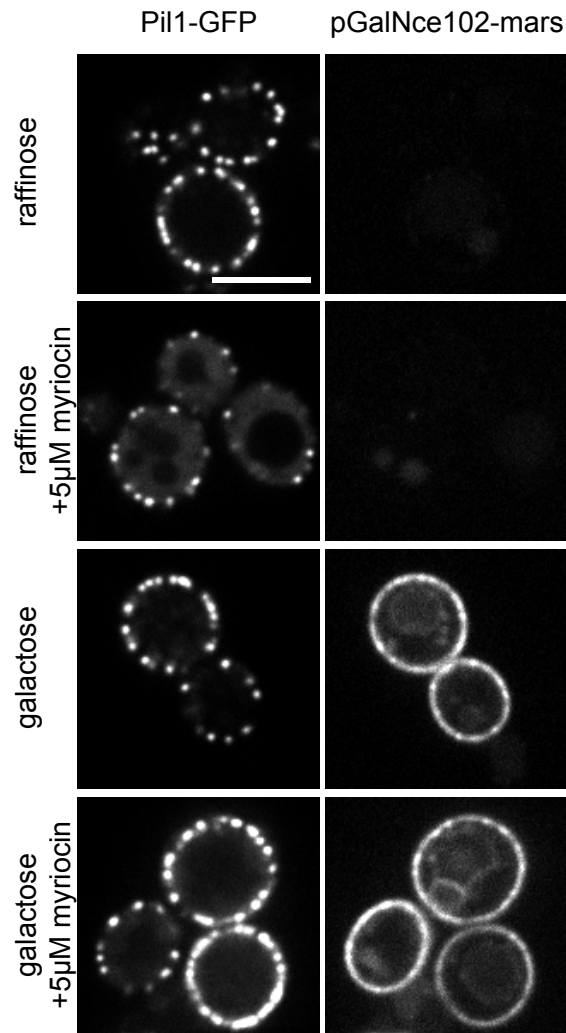


Figure 8. Overexpression of Nce102 suppresses eisosomes disassembly after sphingolipid synthesis block. Nce102-mars (right) controlled by the Gal promoter was either not expressed in raffinose-containing medium or induced in galactose-containing medium in Pil1-GFP (left) cells, which were incubated for 1 h with 5 μ M myriocin as indicated. Bar, 5 μ m.

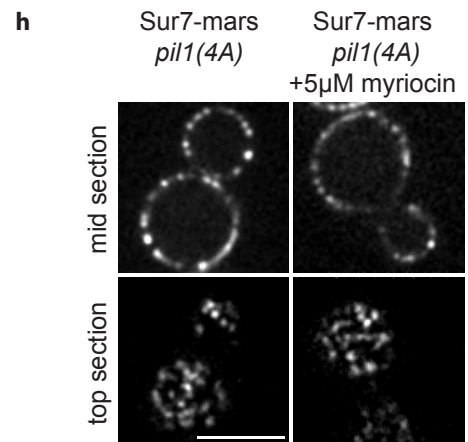
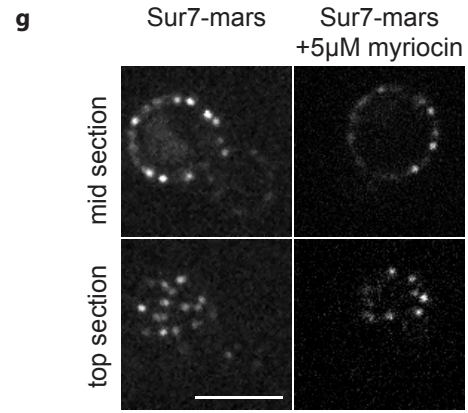
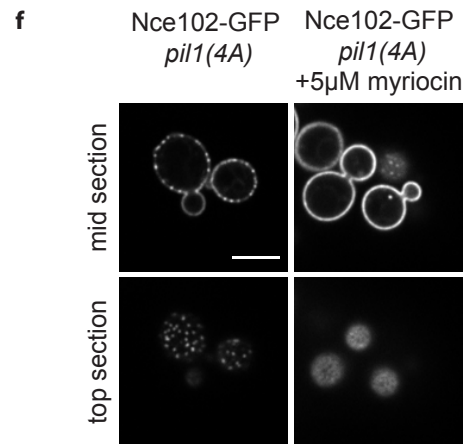
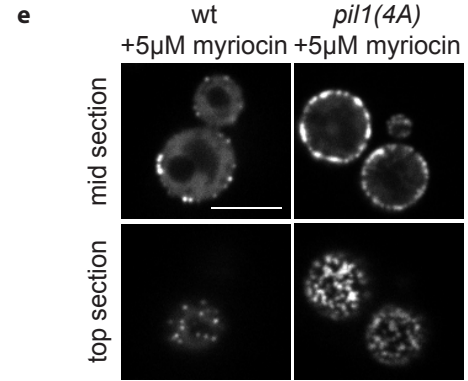
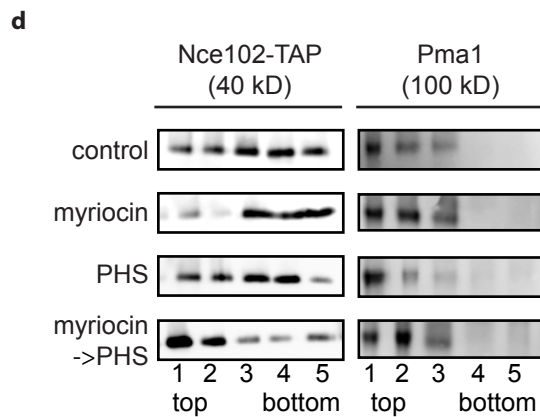
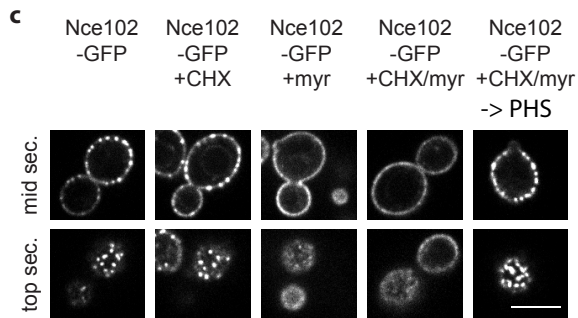
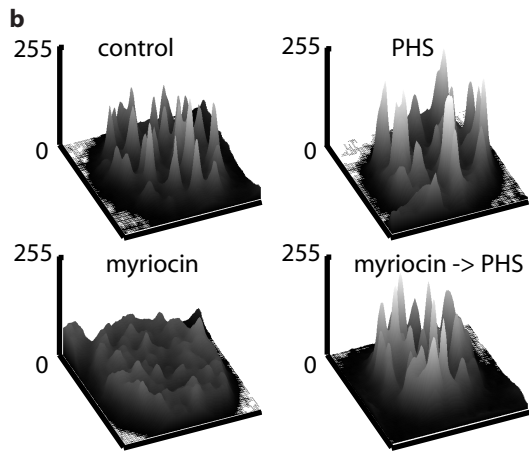
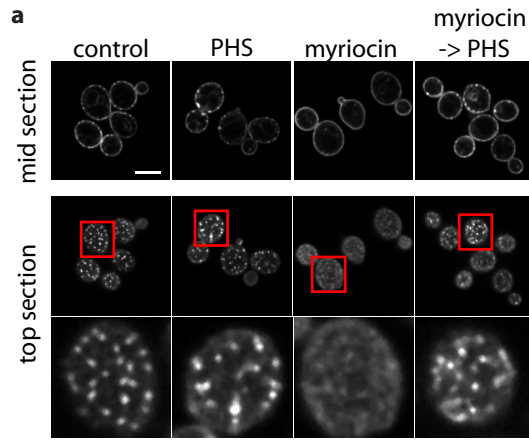


Figure 9. Nce102-GFP localization depends on sphingolipid levels. (a) Nce102-GFP was imaged under normal growth conditions (control), after addition of 5 μ M myriocin for 1 h (myriocin), after sequential treatment with 5 μ M myriocin for 1 h and 50 μ M PHS for 15 min (myriocinPHS), or after addition of 50 μ M PHS for 15 min (PHS). Boxes indicate the area magnified in the bottom panels. (b) Fluorescence intensities of the area are shown plotted against xy image coordinates. (c) Nce102 redistribution is not dependent on new protein synthesis. Nce102-GFP cells were treated with myriocin or myriocin and PHS successively as in a after 10-min preincubation and continued presence of cycloheximide (CHX). (d) Nce102 partitions into detergent-resistant membranes dependent on sphingoid bases. Untreated Nce102-TAP-expressing cells and cells treated as in (a), were lysed in buffer containing 1% Triton X-100 and analyzed by gradient centrifugation and Western blotting against TAP (left). The same blots were probed with Pma1 antibodies (right). (e) *pil1(4A)-GFP* is resistant to disassembly after myriocin treatment. *pil1(4A)-GFP*-expressing cells were imaged after 1-h 5 μ M myriocin incubation. (f) Redistribution of Nce102-GFP after myriocin treatment is independent of eisosome disassembly. Cells expressing *pil1(4A)* and Nce102-GFP were imaged before (left) and after 1 h treatment with 5 μ M myriocin (right). (g and h) Sur7-mars does not behave like Nce102 after myriocin treatment. Wild-type Pil1 (g) or *pil1(4A)* (h) cells expressing Sur7-mars were treated with myriocin and imaged. wt, wild-type. Bars, 5 μ m.

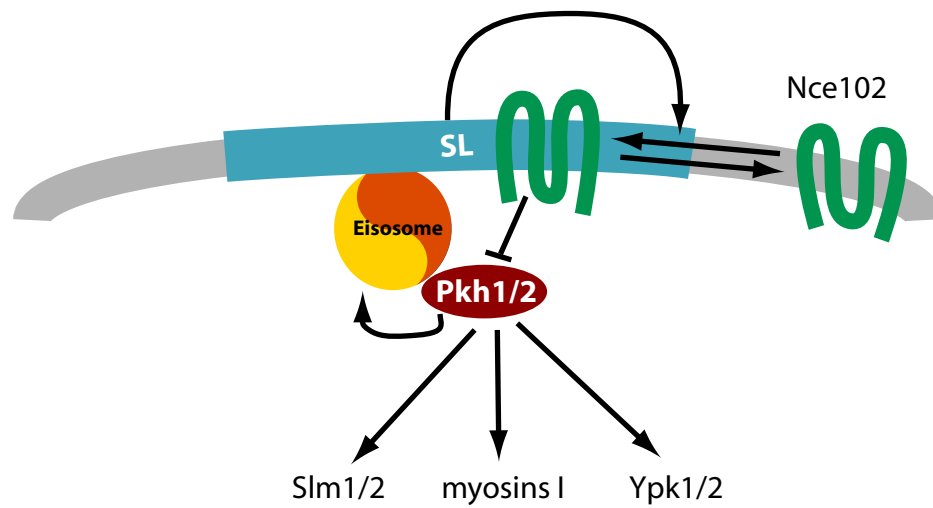
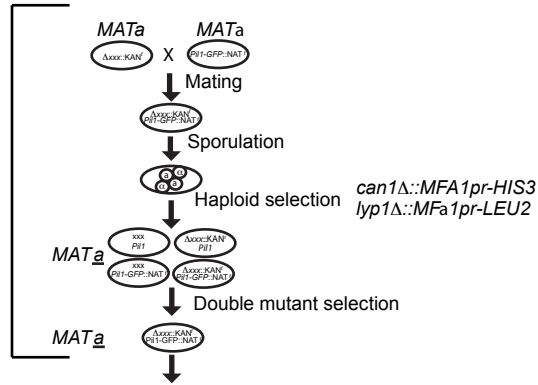


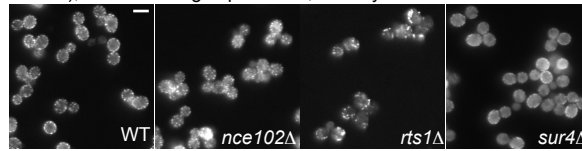
Figure 10. Model for Nce102 function in sphingolipid sensing. Nce102 (green) senses sphingolipid levels in the plasma membrane by distributing between the thick sphingolipid-rich MCC (blue) and the rest of the plasma membrane (gray) depending on sphingolipid levels. In the MCC, it inhibits Pkh kinases (red) that localize under this domain at eisosomes.

a **Screening Steps:**

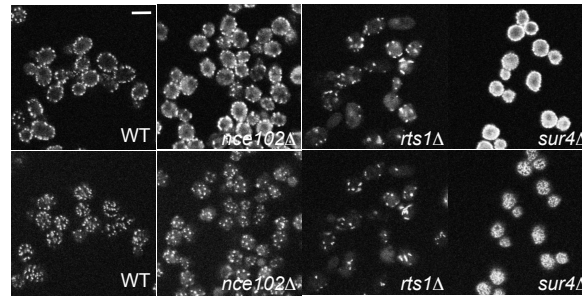
1. Generation of Pii1-GFP deletion strain library



2. Automated imaging of library epifluorescence microscopy,
40x magnification, collect 6 images per strain, visually scored



3. Repeat imaging of candidates by confocal microscopy (63x magnification);
collect two mid sections (top panels) and two surface sections (bottom panels)



4. Quantitative analysis using four parameters:

EN: eisosome number per mother cell in a cross section - manually scored

CPGS: cytoplasmic Pii1-GFP signal - manually measured

AI: average integrated intensity per eisosome cluster on cell surface - scored by EISURAN

APPC: average pixel number per eisosome cluster on cell surface - scored by EISURAN

Perc: percentage of cell surface covered by eisosomes - scored by EISURAN

b

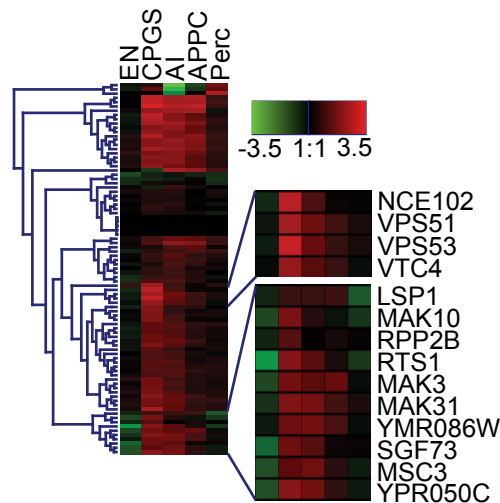


Figure S1. A visual screen for genes affecting Pil1-GFP. (a) Flowchart of the screening process. Step 1: MAT α deletion library was crossed to a MAT α strain containing a chromosomal copy of Pil1 fused to GFP, sporulated, selected for MAT α haploids by growing in media lacking histidine, and selected against diploids by growing on SAEC (Sigma-Aldrich) and canavanine (Sigma-Aldrich). Double mutants were selected by growing on media containing nourseothricin (NAT; Werner Bioagents) and geneticin (G418; Invitrogen). Step 2: cells were grown to saturation overnight in 384-well plates, diluted, and grown to mid-log phase for 9 h in 96-well plates then imaged. Cells were imaged by automated epifluorescence microscopy, and six images per strain were recorded (representative images are shown). Step 3: candidates were subjected to a second round of imaging by confocal microscopy. Images representing optical cross sections and surface views were taken for each strain and used for subsequent quantification. Step 4: eisosome number and cytoplasmic GFP signal were quantified manually in cross sections. All other parameters were quantified in surface view images using EISURAN. Bars, 5 μ m. (b) Quantitation of mutant phenotype of Pil1-GFP organization. Phenotypes quantitated as described in a were hierarchically clustered using the fold deviation from the values obtained for wild-type cells. Decreases are colored in green and the increases in red.

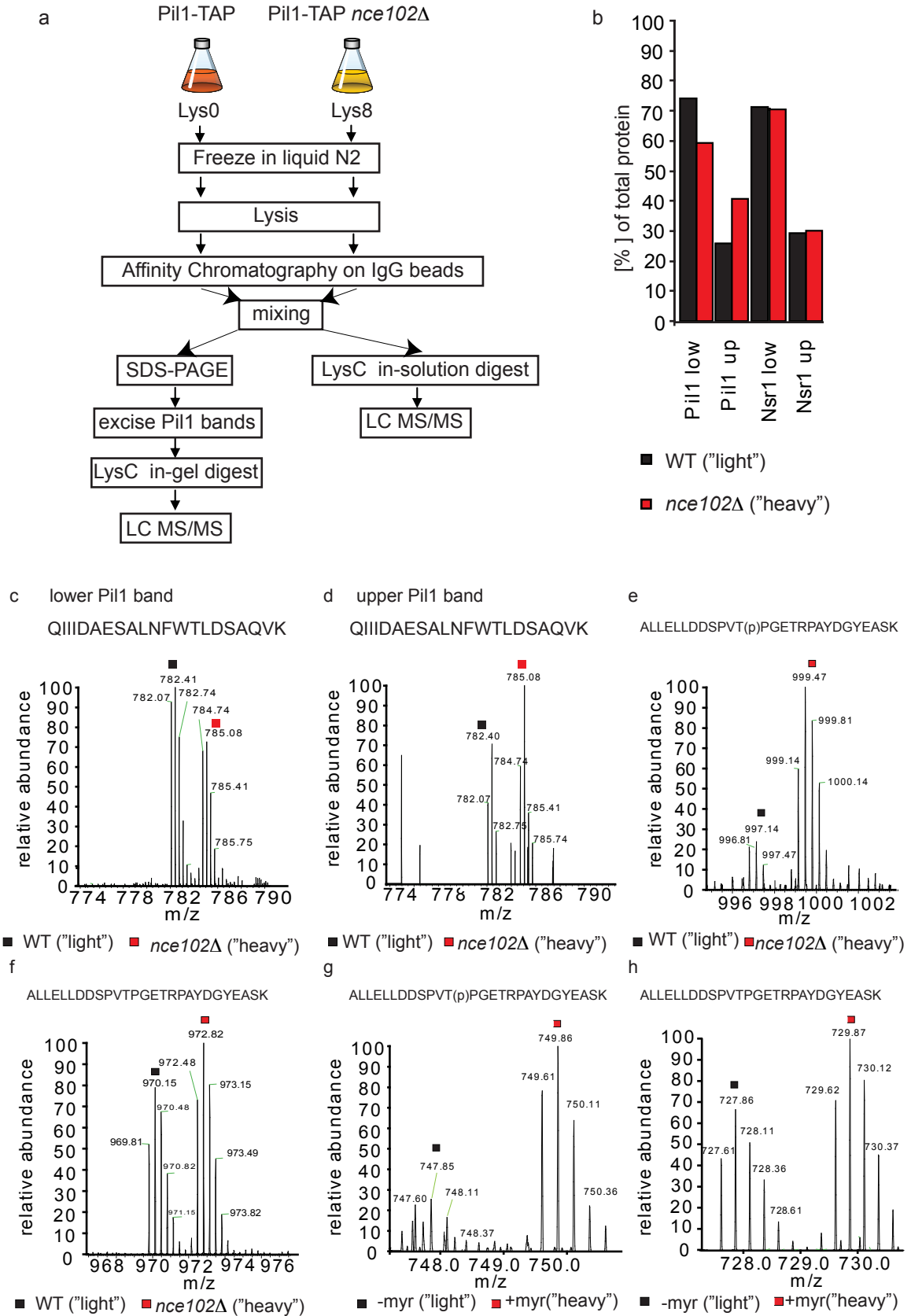


Figure S2. Mass spectrometric analysis of Pil1 shows increased Pil1 phosphorylation in *nce102Δ* - and myriocin-treated cells compared with wild-type cells. (a) Outline of the two experimental strategies (see Results and Materials and methods for details). (b) Representative percentages of Pil1 or Nsr1 protein detected in either the upper or lower band from wild-type (wt) or *nce102Δ* cells as described in a. (c and d) Representative spectra of the experiment described in Fig. 5 a . (e) Representative spectrum of phosphorylated Pil1 (amino acids 222–248) from the experiment described in Fig. 5 b . (f) Representative spectrum of Pil1 (amino acids 222–248) from the experiment described in Fig. 5 b . (g) Representative spectrum of phosphorylated Pil1 (amino acids 222–248) from the experiment described in Fig. 5 c . (h) Representative spectrum of Pil1 (amino acids 222–248) from the experiment described in Fig. 5 c . Representative data of three experiments are shown.

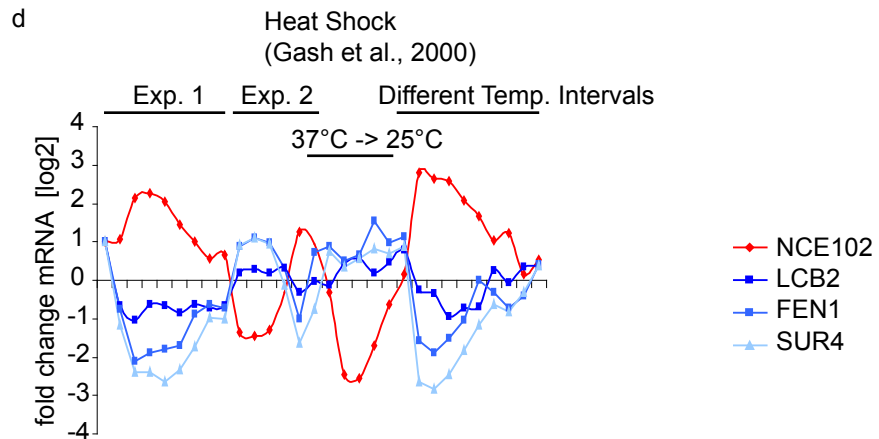
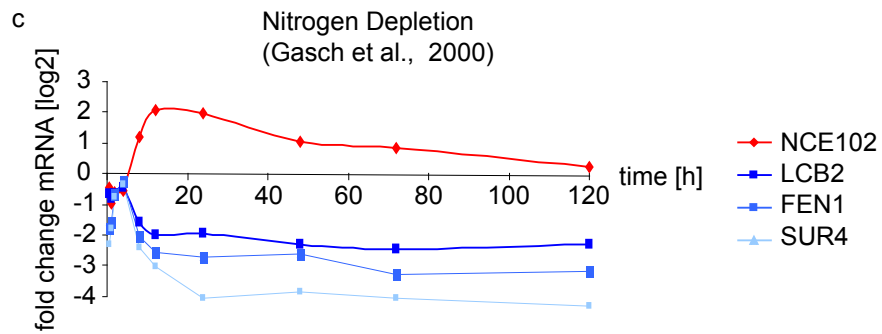
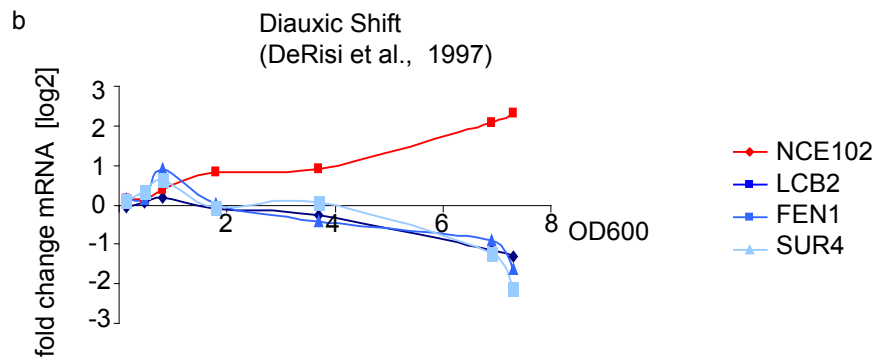
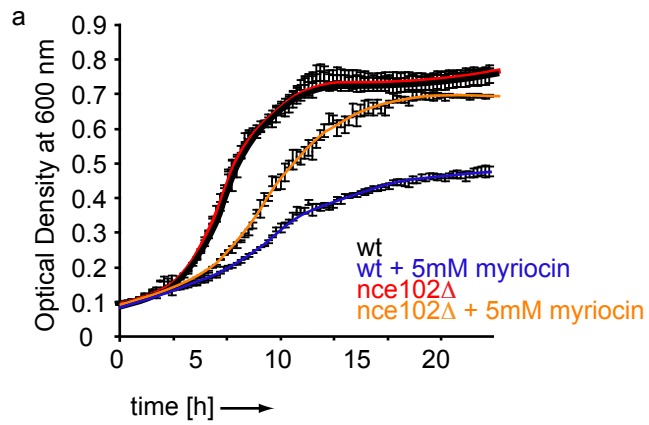


Figure S3. Relationship of NCE102 with sphingolipid metabolism. (a) *nce102Δ* enhances growth on myriocin. Wild-type (wt) and *nce102Δ* cells were grown in a BIO-SCREEN C (ILF Biosciences), and the optical density was measured at 600 nm every 15 min in either the presence or absence of 5 μM myriocin. Error bars indicate SD from the mean of three experiments. (b–d) Microarray expression analysis of *NCE102* versus genes of the sphingolipid biosynthesis pathway. (b) Relative expression levels of *NCE102*, *LCB2*, *FEN1*, and *SUR4* were retrieved from DeRisi et al. (1997. Science . 278:680–686) and plotted against the time of the experiment. (c and d) Relative expression levels of *NCE102*, *LCB2*, *FEN1*, and *SUR4* for heat shock or nitrogen starvation were retrieved from Gasch et al. (2000. Mol. Biol. Cell . 11:4241–4257), and in c, were plotted against the time of nitrogen starvation. In d, a combination of different time courses performed is shown. See Gasch et al. (2000) for details.

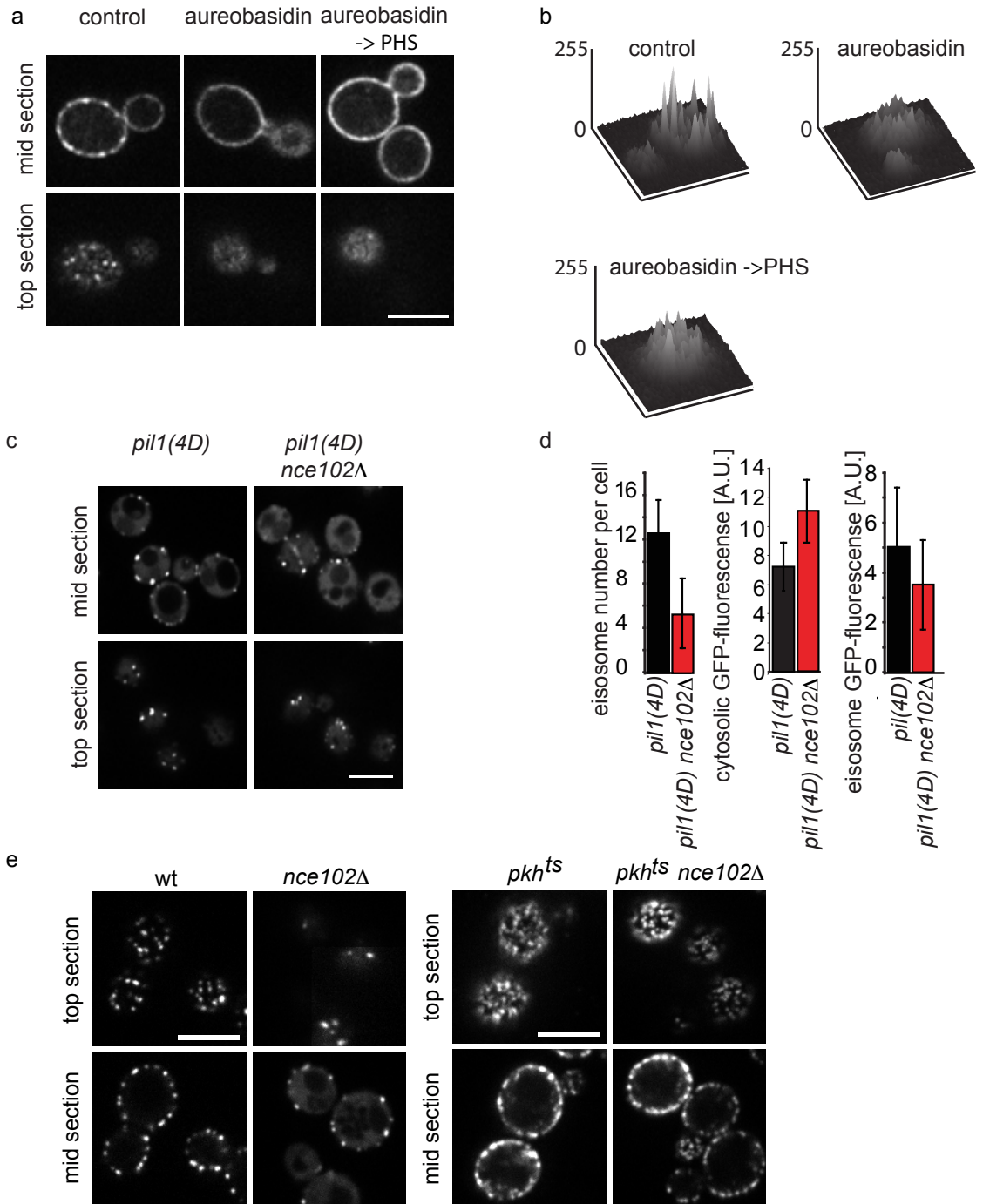


Figure S4. Localization of Nce102-GFP in response to altered sphingolipid levels or mutations of Pil1 or Pkh kinases. (a) The localization of Nce102-GFP depends on sphingolipid levels. Nce102-GFP was imaged under normal growth conditions (control) after the addition of 1 $\mu\text{g/ml}$ aureobasidin for 1 h (aureobasidin) and after the sequential treatment with 1 $\mu\text{g/ml}$ aureobasidin for 1 h and 50 μM PHS for 30 min (aureobasidin→

PHS). Representative optical top (middle) and mid section (top) are shown. (b) Fluorescence intensities of the area shown in top sections of a are plotted against the xy coordinates of the image. (c) Phosphomimicking mutants of *PIL1* are enhanced by *nce102Δ*. A phosphomimicking Pil1 (S45D, S59D, S230D, and T233D) mutant (*pil1(4D)*) fused to GFP was expressed in wild-type (left) or *Δnce102* cells (right). (d) The phenotype of the *pil1(4D)* mutant is enhanced, as can be seen in the quantitation of eisosome number per mother cell (left), the cytoplasmic fluorescence (middle), and *pil1(4D)-GFP* fluorescence per cell (right). (e) Pkh kinase mutation is epistatic to *nce102Δ*. Analogously to Fig. 6, shift to the restrictive temperature (37 °C) did not result in a phenotype of *nce102Δ* when combined with the *pkh1^{ts} pkh2Δ* mutation. The transiently slightly improved appearance of eisosomes in *pkh1^{ts} pkh2Δ* strains might be due to a short spike in sphingolipid synthesis, counteracting the inactivation of the kinases (Dickson et al. 1997. J. Biol. Chem. doi:10.1074/jbc.272.48.30196). wt, wild-type. Bars, 5 μm.

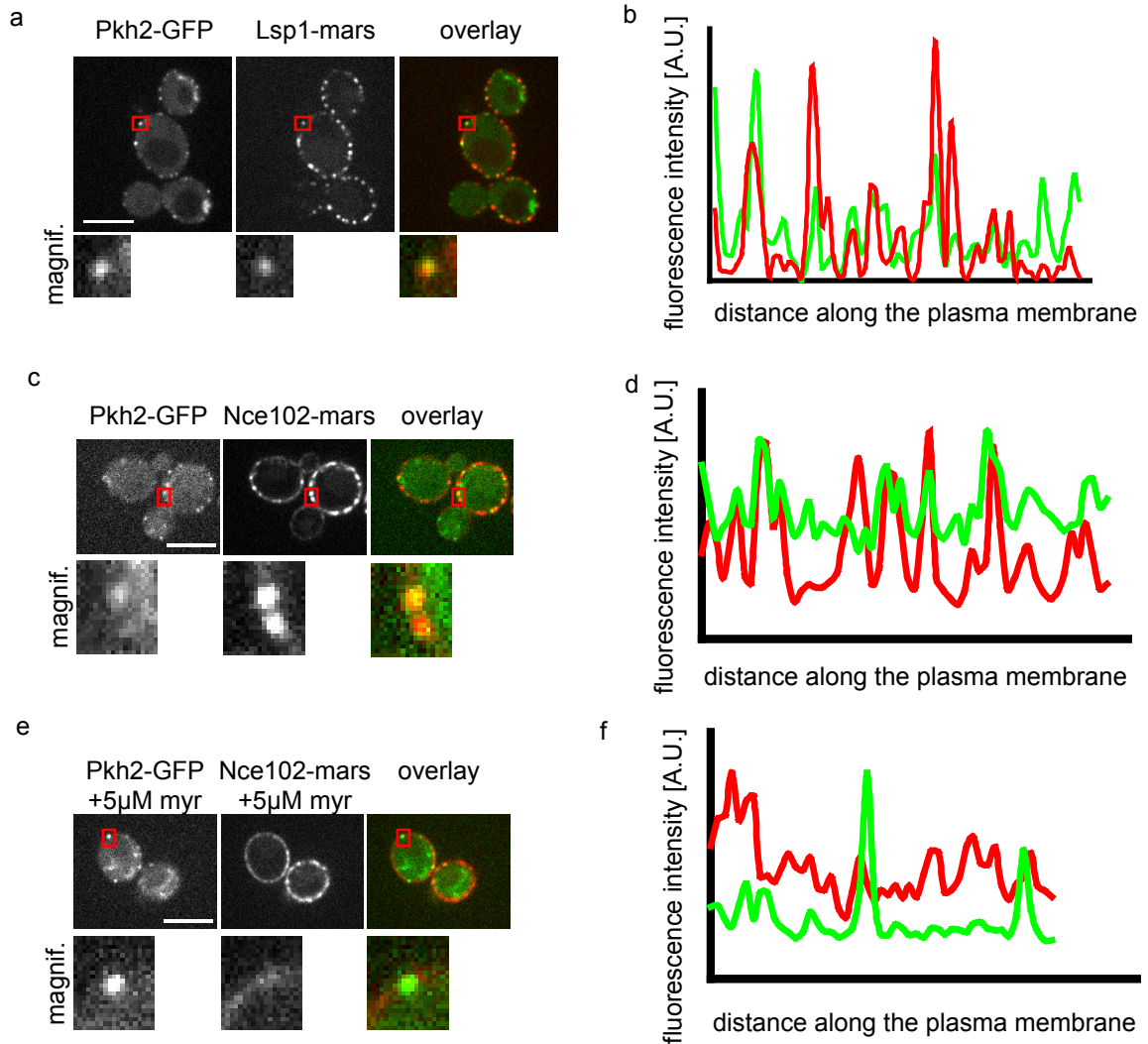


Figure S5. Pkh2 and Nce102 colocalization depends on sphingolipid synthesis. (a) Pkh2-GFP colocalizes with Lsp1-mars foci. Pkh2-GFP (left; green in the overlay) was expressed from its endogenous promoter in cells harboring Lsp1-mars (middle; red in the overlay). Representative confocal mid sections (top) are shown. Bottom panels show the indicated magnified section of the images. (b) Intensity profiles for Pkh2-GFP and Lsp1-mars overlap. A line profile along the plasma membrane was generated for both channels, and the overlay is shown. (c) Pkh2-GFP colocalizes with Nce102-mars foci. Pkh2-GFP (left; green in the overlay) was expressed from its endogenous promoter in cells harboring Nce102-mars (middle; red in the overlay). Representative confocal midsections (top) are shown. Bottom panels show the indicated magnified section of

the images. (d) Intensity profiles for Pkh2-GFP and Nce102-mars overlap. A line profile along the plasma membrane was generated for both channels, and the overlay is shown. (e) Nce102-mars separates from Nce102-GFP after myriocin treatment. Cells expressing Pkh2-GFP and Nce102-mars as shown in a were treated for 1 h with myriocin and imaged. Representative confocal midsections (top) are shown. Bottom panels show the indicated magnified section of the images. (f) Intensity profiles for Pkh2-GFP and Nce102-mars after myriocin treatment. A line profile along the plasma membrane was generated for both channels and the overlay is shown. Bars, 5 μm .

Strains	Genotype	Source
RH5412	<i>MAT_a pkh2Δ::LEU2 pkh1_{ts} trp1 lys2 his2 ura3 leu2 bar1</i>	Friant et al. 2001
TWY520	<i>MAT_a pkh2Δ::LEU2 pkh1_{ts} Pil1-GFP::URA trp1 lys2 his2 leu2 bar1</i>	Walther et al., 2007
TWY932	<i>MAT_a nce102Δ::NAT^R pkh2Δ::LEU2 pkh1_{ts} Pil1-GFP::URA trp1 lys2 his2 leu2 bar1</i>	this study
TWY841	<i>MAT_α nce102Δ::NAT^R ura3 trp1 leu2 his3 ade2 can1-100</i>	this study
TWY842	<i>MAT_a nce102Δ::NAT^R ura3 trp1 leu2 his3 ade2 can1-100</i>	this study
TWY893	<i>MAT_α nce102Δ::NAT^R trp1 lys2 bar1 ura3 leu2</i>	this study
TWY894	<i>MAT_a nce102Δ::NAT^R trp1 lys2 bar1 ura3 leu2</i>	this study
TWY1045	<i>MAT_a pil1Δ::KAN^R nce102Δ::NAT^R pil(4D)-GFP::URA trp1 leu2 his3 ade2 can1-100</i>	this study
TWY934	<i>MAT_a pil1Δ::KAN^R nce102Δ::NAT^R pil(4A)-GFP::URA trp1 leu2 his3 ade2 can1-100</i>	this study
TWY898	<i>MAT_a pil1Δ::KAN^R nce102Δ::NAT^R ura3 trp1 leu2 his3 ade2 can1-100</i>	this study
TWY836	<i>MAT_a pil1Δ::KAN^R NCE102-GFP::HIS ura3 trp1 leu2 his3 ade2 can1-100</i>	this study
TWY955	<i>MAT_a pil1Δ::KAN^R NCE102-GFP::HIS pil(4A)-MARS::URA trp1 leu2 his3 ade2 can1-100</i>	this study
RH3809	<i>MAT_a his4 lcb1-100 leu2 ura3 bar1</i>	Friant et al. 2000
TWY493	<i>MAT_a PIL1-GFP::URA his4 lcb1-100 leu2 ura3 bar1</i>	Walther et al., 2007
TWY839	<i>MAT_α LSP1-MARS::NAT^R NCE102-GFP::HIS ura3 trp1 leu2 his3 ade2 can1-100</i>	this study
TWY838	<i>MAT_a NCE102-GFP::HIS ura3 trp1 leu2 his3 ade2 can1-100</i>	this study
TWY840	<i>MAT_α NCE102-GFP::HIS ura3 trp1 leu2 his3 ade2 can1-100</i>	this study
TWY897	<i>MAT_a NCE102-TAP::KAN^R his3 leu2 lys2 ura3</i>	this study
TWY110	<i>MAT_a PIL1-GFP::HIS ura3 trp1 leu2 his3 ade2 can1-100</i>	Walther et al., 2006
TWY837	<i>MAT_a PIL1-GFP::HIS nce102Δ::NAT^R ura3 trp1 leu2 his3 ade2 can1-100</i>	this study
TWY1052	<i>MAT_a PIL1-TAP::KAN^R nce102Δ::NAT^R his3 leu2 lys2 ura3</i>	this study
TWY1004	<i>MAT_a PIL1-TAP::KAN^R his3 leu2 lys2 ura3</i>	this study
TWY1049	<i>MAT_a PMA1-GFP::HIS nce102Δ::NAT^R ura3 trp1 leu2 his3 ade2 can1-100</i>	this study
TWY958	<i>MAT_a PMA1-GFP::HIS ura3 trp1 leu2 his3 ade2 can1-100</i>	this study
TWY1048	<i>MAT_α SUR7-GFP::HIS nce102Δ::NAT^R ura3 trp1 leu2 his3 ade2 can1-100</i>	this study
TWY956	<i>MAT_a SUR7-GFP::HIS ura3 trp1 leu2 his3 ade2 can1-100</i>	this study
TWY70	<i>MAT_a his3 leu2 lys2 ura3</i>	Walther et al., 2006
TWY138	<i>MAT_a ura3 trp1 leu2 his3 ade2 can1-100</i>	Walther et al., 2006
TWY139	<i>MAT_α ura3 trp1 leu2 his3 ade2 can1-100</i>	Walther et al., 2006
TWY1242	<i>MAT_a NCE102-GFP::HIS Sur7-MARS::NAT^R ura3 trp1 leu2 his3 ade2 can1-100</i>	this study
TWY1222	<i>MAT_a PIL1-GFP::KAN^R PgalNCE102-MARS::URA ura3 trp1 leu2 his3 ade2 can1-100</i>	this study
TWY1240	<i>MAT_a pil1Δ::KAN^R NCE102-GFP::HIS pil(4A)-MARS::URA trp1 leu2 his3 ade2 can1-100</i>	this study
TWY1091	<i>MAT_a PKH2-GFP::KAN^R NCE102-MARS::NAT^R ura3 trp1 leu2 his3 ade2 can1-100</i>	This study
KEM108	<i>MAT_α Pil1-GFP::NAT^R can1Δ::MFA1pr-HIS3 mfa1::Mfa1pr-LEU2 his3 leu2 met15 ura3 LYS2</i>	This study
YMS196	<i>MAT_α can1Δ::MFA1pr-HIS3 mfa1::Mfa1pr-LEU2 his3 leu2 met15 ura3 LYS2</i>	Krogan Lab, Tong et al., 2001

Table S1. Yeast strains used in this study

CHAPTER 4

PEN1 PROMOTES EISOSOME NUCLEATION AND ELONGATION

INTRODUCTION

The plasma membrane is a highly dynamic structure that must orchestrate the movement of molecules into and out of the cell. It was recently found in *Saccharomyces cerevisiae*, that the plasma membrane is highly organized by stable lateral microdomains. These membrane compartments (MCs) contain several transporters, permeases, and protein complexes, in addition these compartments have been shown to coordinate endocytosis and cell signaling (Malinska et al., 2003; Grossmann et al., 2008; Berchtold et al., 2009). One such compartment is called MCC (membrane compartments containing the arginine permease Can1); this compartment is characterized by discrete foci distributed on the plasma membrane that are rich in ergosterol and share eisosome membrane components (Malinska et al., 2003; Grossmann et al., 2007, 2008; Fröhlich, Moreira et al., 2009).

Eisosomes are large molecular structures organized in a distinctive punctate pattern below the plasma membrane, colocalizing with MCCs. Their main characteristics are that they are large structures homogenous in size, very stable and have a constant density. Mother cells contain between 25-45 eisosomes depending on their size. During biogenesis these are deposited in a polarized fashion from bud neck to bud tip. These were shown to mark sites of endocytosis in yeast by following FM4-64 and hexose transporter internalization. Loss of their organization affects the rate of internalization of protein and lipid cargo, causes large aberrant membrane invaginations, collapse of ergosterol rich MCCs (Walther, et al., 2006; Moreira et al. 2008, Malinska et al., 2003; Grossmann et al., 2008).

Eisosomes are composed mainly of two highly homologous cytoplasmic phosphoproteins: Pil1 and Lsp1. Pil1 emerged as the main organizer of eisosomes

because its deletion alone causes all other known eisosome components to collapse into a few remnants as well as into mislocalized pools characterized by a diffusely cytoplasmic localization of the soluble proteins and homogenous membrane localization of membrane proteins. In addition, timely and controlled expression levels are important to give eisosomes their characteristics (Walther et al., 2006; Moreira et al., 2008). We previously conducted a genome-wide genetic screen to identify genes that participate in eisosome organization, acting upstream of Pil1. We identified 88 genes that when deleted resulted in the abnormal distribution of Pil1-GFP (Fröhlich, Moreira et al., 2009).

We were interested in identifying a novel eisosomal component and the best candidate that as a GFP-fusion showed a pronounced peripheral punctate localization was Ymr086w (Huh et al., 2003). Ymr086w is a previously uncharacterized soluble protein found in two other genomic screens to interact with ribosomes, and its expression is repressed by cAMP levels (Fleischer et al., 2006; Tadi et al., 1999). Also, Ymr086w was recently found to form a complex with eisosomal components Pil1 and Lsp1 and colocalized with eisosomes (Deng et al., 2009).

We propose that the function of Ymr086w is to nucleate eisosomes and provide a framework for Pil1 assembly. In addition, overnucleation of Ymr086w molecules cause eisosomes to elongate along a longitudinal axis. Thus we name it Pen1 for promotes eisosome nucleation. In this study we found that deposition of Pen1 in growing buds is not polarized and that the deposition does not display a lag phase as is characteristic of Pil1 deposition. Moreover, Pen1 deposition precedes that of Pil1 and is independent to Pil1. Also, *PEN1* deletion caused a delay in eisosome formation, resulting in sporadic deposition of smaller eisosomes. By contrast, Pen1 overexpression caused the formation

of larger and morphologically altered elongated eisosomes. This elongating activity was inhibited by a single point mutation in Pen1, suggesting that this activity may be controlled by modifications to this residue. Together these results, lead to a model of eisosome assembly in which eisosomes have a longitudinal axis that is controlled by nucleating low levels of Pen1 molecules. This nucleating structure then serves as a platform that promotes the timely assembly of Pil1 molecules.

RESULTS

Pen 1 is required for normal eisosome and membrane organization.

To explore the role of Pen1 in eisosome formation, we investigated the localization of Pil1-GFP in *pen1Δ* cells compared with wild-type cells. In agreement with the systematic genome-wide screen, confocal images showed a high cytoplasmic Pil1-GFP signal combined with fewer and dimmer eisosomes (Fig. 1 a). Preliminary studies of the plasma membrane by electron micrograph also showed that *pen1Δ* cells have multiple curled membrane protrusions at the cell periphery (Fig. 1 b). These protrusions are smaller and more abundant than the aberrant invaginations seen in *pill1Δ* cells. We hypothesize that these protrusions correspond to the eisosome remnants seen in *pill1Δ* cells.

Pen 1 functions as an eisosome nucleator.

To investigate the function of Pen1 in eisosome assembly, we followed the subcellular localization of Pen1 by fluorescence microscopy. Pen1 was previously shown to colocalize with the eisosome component Lsp1 (Deng et al., 2009). As expected and consistent with this study we also found that Pen1 colocalizes with the eisosome

component Pil1 (Fig. 2 a). However, we did find that Pen1 was more prominent in the buds compared to Pil1. In addition, the abundance of Pen1 is significantly lower than Pil1; there is a 13-fold difference in the intensity of Pen1-GFP containing eisosomes compared to Pil1-GFP containing eisosomes (Fig. 2 c). Therefore, we estimated that each eisosome contains 2,000-5,000 molecules of Pil1 and 130-330 molecules of Pen1.

Next, we followed the deposition of Pen1-GFP in differently sized buds and compared it to Pil1-GFP deposition. In contrast to Pil1-GFP, we found that Pen1-GFP is present early in small buds in a diffused pattern at the plasma membrane with some nucleated eisosomes (Fig. 2 b, top panel). Medium buds are fully colonized with Pen1-GFP containing eisosomes and did not resemble the polarized distribution that Pil1-GFP containing eisosomes show (Fig. 2 b, middle panel). Large buds were also fully colonized with Pen1-GFP containing eisosomes similarly to Pil1-GFP containing eisosomes. This indicates that Pen1 deposition precedes that of the key organizer, Pil1 and thus is a good candidate for an eisosome nucleator.

To refine this idea further, we quantified the number of Pen1-GFP containing eisosomes in different sized buds and plotted them against the bud surface area (Fig. 2 d, yellow dots). Similar to the measurements for Pil1-GFP or Lsp1-GFP containing eisosomes, we found a positive correlation between the number of eisosomes and size of the bud (Fig. 2 d, green and yellow dots respectively). In contrast to the deposition of Pil1 or Lsp1, however, Pen1 is deposited in buds smaller than $17\mu\text{m}^2$, again highlighting that Pen1 enters eisosomes before Pil1. This observation combined with the low abundance of Pen1 lead to the idea that Pen1 does not form a significant bulk of eisosome assembly, but instead it is needed as a seeding molecule.

The nucleator hypothesis predicts that the deposition of Pen1 in eisosomes should be independent of Pil1, as it was the case in very small buds. We tested this prediction by looking at Pen1-GFP localization in $\Delta pil1$ cells. To our surprise, we found that Pen1 did not form eisosomes, instead it was diffusely localized throughout the plasma membrane, had a few eisosome remnants and a patchy distribution. These patches were more concentrated and abundant in smaller buds (Fig. 3 a). This result was unexpected for a cytoplasmic protein; Pen1 does not have any predicted transmembrane domains. Yet, it did not diffuse to the cytoplasm like the other soluble protein Lsp1 does in $pil1\Delta$ cells. We concluded that Pen1 can associate to the plasma membrane and nucleate loosely packed patches independent of Pil1. However, the stabilization of these patches into eisosomes assemblies requires the presence of Pil1.

Next, we explored the idea that Pen1 could be localized to the membrane by interactions with Nce102. Nce102 is a transmembrane protein that localizes to eisosomes to modulate the phosphorylation state of Pil1 (Fröhlich, Moreira et al., 2009). This is the only eisosome component with a transmembrane domain that was found in the genomic-wide screen to also affect eisosome organization. So, we looked at the localization of Pen1-GFP in $pil1\Delta nce102\Delta$ cells. We did not see a significant change in the localization of Pen1 however, demonstrating that it is not Nce102 anchoring Pen1 to the plasma membrane (Fig. 3 b). The other integral plasma membrane eisosomal protein Sur7, is another candidate to be tested in the future. Deletion of the Sur7 family: Sur7, Ynl194, and Ydl222 but not deletion of Sur7 alone, causes a loss of eisosome organization (personal communication with Tobias Walther). This effect is attributed to the fact that this group of proteins affects the synthesis and composition of sphingolipids, which plays

a major role in the assembly state of Pil1 (Young et. al., 2002 and Walter et al., 2007).

Together our results are consistent with a nucleation model. We show that Pen1 is the first eisosomal component found to precede Pil1 deposition during eisosome assembly. Small quantities of Pen1 are incorporated into eisosomes in small buds before Pil1 deposition, however these structures are not stable in the complete absence of Pil1 as *pil1Δ* cells only have loose Pen1 assemblies. This leads to the conclusion that Pen1 diffuses at the membrane and collides to form seeding platforms for eisosome assembly that are then capped by Pil1 molecules.

Pen1 overexpression results in elongated eisosomes.

Next, we predicted that overexpressing Pen1 would increase nucleation of eisosomes, and we expected either more or brighter eisosomes as these assemblies became larger. To test this idea, we expressed Pen1 under the *CUPI* promoter, this promoter's expression level can be tuned by the addition of copper into the media, and followed eisosome formation with Pil1-GFP. This promoter is leaky and even with no copper induction there is enough Pen1 to form normal eisosomes (Fig. 4 a, top panel). We grew cells in 100μM CuSO₄ overnight and found that mother cells had rod shaped eisosomes, while daughter cells had fewer yet normal, round eisosomes (Fig. 4 a, bottom panel). These rods were parallel to the membrane and very homogenous in length within a cell, but some cells had longer eisosomes than others (Fig. 4 e). It is possible that the overnucleation of eisosomes in the mother cells over multiple generations sequestered the available Pil1 into these structures away from the new ones in daughter cells. The amount of Pil1-GFP was quantified by Western blot and did not change in the inducible

strains compared to wild-type under either condition (Fig. 4 b), thus Pil1 was redistributed amongst larger and longer structures in the induced condition. This result shows that the increased abundance of Pen1 molecules during nucleation, forms larger platforms for eisosome assembly.

We also expected Pen1 to form an elongated patch when overexpressed, so we placed Pen1-GFP under the copper inducible system to follow its assembly during copper induction. Again, we found that under uninduced conditions there was enough Pen1 to form normal eisosomes (Fig. 4 c, top panel). As we grew cells in higher CuSO₄ concentrations overnight, eisosomes got longer (Fig. 4 c, middle panels). At 900 μM CuSO₄ eisosomes became highly filamentous (Fig. 4 c, bottom panel). We quantified the amount of Pen1 overexpressed under the different conditions by western blot (Fig. 4 d), increasing the expression of Pen1 by 3-fold over its concentration in wild-type control cells (0 μM CuSO₄) is not enough to induce rod formation but increasing it 7-fold (100 μM CuSO₄) overcomes the threshold to induce rod formation.

Our results uncovered a new eisosome property that is controlled by Pen1. It appears from these studies that eisosome geometry has an axis along which they can be extended. Their normal geometry looks round by fluorescent imaging, because of the limits that this method confers. Because this property now becomes visible in overnucleated eisosomes, we hypothesized that the eisosomes formed in the absence of Pen1 may also have an aberrant assembly. To test this, we measured the intensity of Pil1-GFP containing eisosomes in *pen1Δ* cells compared to wild-type cells and plotted it as a function of the frequency of individual intensities. We found with high frequency that the eisosomes formed in *pen1Δ* cells were smaller and less uniform than those formed in

wild-type cells. We measured the integrated Pil1-GFP fluorescence intensities of individual eisosomes for *pen1Δ* cells with an average of 12 +/- 5 A. U. and for wild-type cells with an average of 19 +/- 3 A. U. (Fig. 5 a, top and middle panels respectively). This result shows that in the absence of Pen1, Pil1 patches are smaller, possibly not reaching their regular size as a result of uncontrolled assembly. In cells overexpressing Pen1 however, the patches with the lowest intensities resemble that of wild-type cells (Fig. 5 lower panel). As these patches elongate, they also get brighter, thus the graph shows some eisosomes with large intensities, resulting in an average intensity of 36 +/- 13 A. U. Our results indicate that the rods initially start with a normal length that then increases over generations. We can then predict that mother cells with the most bud scars have the longest eisosomes.

Pen1 nucleating function is compromised in *pen1(F2A)-GFP* mutant.

We previously speculated that some eisosome components may be N-terminal acetylated after identifying all subunits (*MAK3*, *MAK10*, and *MAK31*) of the NatC (N alpha-terminal acetyltransferase complex C) complex in our genetic screen for genes affecting eisosome organization (Fröhlich et al., 2009). Mutations in either of the subunits resulted in a phenotype similar to *PEN1* deletion; fewer eisosomes and an increased cytoplasmic Pil1-GFP pool. The NatC complex prefers substrates with specific amino acids on the second position: Met-Ile, Met-Leu, Met-Trp, and Met-Phe (Polevoda and Sherman, 2001). Neither of the known eisosome components however, showed this preference except for Pen1 (Met-Phe). We next tested a possible connection between Pen1 function and N-terminal acetylation. To this end, we substituted the Phe2 of Pen1-GFP with an alanine

(*pen1(F2A)-GFP*). We expressed *pen1(F2A)-GFP* or *PEN1-GFP* from a plasmid, integrated in the URA locus of *pen1Δ* cells to follow eisosome formation. To our surprise, both of these alleles were overexpressed ~8-fold when compared to a wild-type Pen1 tagged at the endogenous locus (Fig. 6 b). It seems that the URA locus is much more transcriptionally active than the endogenous *PEN1* locus. This level of expression is enough to induce rod formation, as is seen in the cells expressing *PEN1-GFP* from the integrative plasmid (Fig 6 a, left panels). The cells expressing Pen1 harboring the F2A mutation however did not form rods (Fig 6 a, right panels). This result suggests that N-terminal acetylation of Pen1 plays a role in eisosome nucleation. It is possible that this modification may increase the nucleation activity of Pen1. Thus when this residue is modified and the protein is overexpressed, it promotes the nucleation of multiple Pen1 assemblies into one long platform. Alternatively, this amino acid may play a role in the interaction between individual Pen1 subunits limiting the number of molecules that can assemble together. To confirm our results, we would then expect that the deletion of a NatC subunit will be resistant to the elongating activity of Pen1 overexpression. In addition, mass spectrometry studies will help elucidate whether this residue is modified or not and whether a disruption of this modification causes a change in the interaction profile of Pen1.

DISCUSSION

Eisosome organization has been shown to affect the rate of endocytosis and membrane integrity (Walther et al., 2006, Grossmann et al., 2008). We originally found that Pil1 is the main organizer of eisosome size and density (Moreira et al., 2008). Since then, we

have identified 88 candidate genes that also play a role in their organization (Fröhlich et al., 2009). We focused this study on one candidate, a previously uncharacterized gene, Ymr086w, which we called Pen1 for promotes eisosome nucleation. We propose a model of eisosome assembly in which Pen1 molecules nucleate and form patches at the plasma membrane, these assemble laterally to provide a platform of the correct size and shape and to promote Pil1 assembly (Fig. 7, middle column). Until Pen1 entered the picture, no protein incorporated into eisosomes before Pil1 was known. Cells lacking *PEN1* have overall increased cytoplasmic Pil1 deposition, with fewer and smaller eisosomes mainly in mother cells. This contradicts our previous conclusion that eisosomes have a minimum size (Moreira et al., 2009). This may be explained if, in the absence of Pen1, the assembly of Pil1 is due to a random aggregation of molecules rather than organized assembly, resulting in smaller structures (Fig7, left column).

Alternatively, Pen1 may be the molecule determining the lower limit of eisosome size. Pen1 nucleation is then required to promote timely and orderly eisosome assembly to ensure that cells have all eisosomes in place before they have finished growing.

It is still unclear how eisosomes are anchored to the plasma membrane. Pen1 seems to function early in the assembly chain however, because it localizes to the plasma membrane in the absence of Pil1 despite being predicted as a cytoplasmic protein, and not containing any transmembrane domains. Pen1 does have a proline-rich stretch (aa 52 - aa 60) that is predicted to be bound by SH3-domain containing proteins. These proteins are known to mediate protein-protein interactions required to assemble complexes. Studying the interactions of Pen1 with adaptor proteins or membrane proteins may help elucidate the order of eisosome assembly and its connection to the plasma membrane.

We show that Pen1 alone can be assembled into patches, but it needs Pil1 to maintain a tight structure. It is possible that in wild-type cells Pil1 functions as a cap that assembles over the Pen1 patches which are needed to provide a mold for the structure to mature. This way, when Pil1 is completely absent, as in *Δpil1* cells, Pen1 makes more diffused patches that cannot mature into eisosomes.

It came as a surprise to find that Pen1 overexpression forms rod-shaped eisosomes instead of nucleating more eisosomes. Because the available Pil1 needs to be distributed among these structures, it is possible that the limited availability of Pil1 can only support the assembly of fewer but larger structures rather than more and smaller structures. Our previous finding that the availability of Pil1 determines the density of eisosomes while these maintain a minimum size supports this idea (Moreira et al., 2009). In the presence of Pen1, Pil1 maintains the minimal size requirement for assembly; so any assembly that exceeds Pil1 availability will not mature. Our findings reveal a novel property of eisosomes; they have an axis going through that under certain conditions can be extended. We have previously seen the growth of eisosomes as an increase of patch brightness by increasing Pil1 levels; this may be due to a longitudinal assembly of Pil1 molecules in layers. But in this study, we observe a lateral assembly of Pen1. The lateral assembly may then serve as a platform for the longitudinal assembly of other eisosome components. Small amounts of Pen1 ensure that these structures remain short. One way to make rod shaped eisosomes is that any excess Pen1, is added to the initial nucleating structure like links to a chain making these structures longer (Fig7, right column). Alternatively, increased amounts of Pen1 make larger nucleating patches for Pil1 to land on and stabilize the assembly. This elongating hypothesis is consistent with a recent

study were they found that the MCC (membrane compartment of Can1), which colocalizes with eisosomes, forms elongated furrow-like invagination of roughly 200-300 nm in length and 50 nm in diameter. In addition, Pil1 and Sur7 proteins were localized to these furrows by electron microscopy and these furrows disappeared in *Apil1* cells (Stradalova et al., 2009). It would be interesting to find a correlation between Pen1 overexpression and an increase the length of these furrows, this would suggest that eisosomes can influence the shape of these membrane compartments. Electron microscopy studies of cells containing overnucleated eisosomes are currently being conducted to study this idea.

It remains unclear if the nucleation of eisosomes has directionality, but the assembly of additional links to the chain is inhibited by the F2A mutation in Pen1. We have not fully explored whether this phenomenon is due to lack of N-terminal acetylation at this residue, but Pen1 is a good candidate for this modification and the convergence of the phenotype with that of the knock-outs of the N-acetylation machinery is highly suggestive. It is interesting that knocking down the N-terminus acetylation machinery results in a *Δpen1* phenotype, while the *pen1(F2A)* mutant can still form normal eisosomes. We believe that this mutation may render Pen1 less active, thus inhibiting rod formation yet providing enough activity to nucleate normal eisosomes due to its increased abundance. Alternatively, the NatC mutants may have pleiotropic effects on eisosome assembly as dynamic protein modifications during eisosome biogenesis may orchestrate the assembly of multiple molecules. We cannot reconcile the contradicting finding by Stradalova et al. 2009, that deletion of the NatC subunit Mak3 or an overlapping ORF encoding Ypr050c also results in elongated MCC patches seen by electron and

fluorescence microscopy. We were not able to reproduce this result, as our *Δmak3* mutant has few eisosomes, some filamentous remnants with a high cytoplasmic Pil1 localization.

We have so far modeled eisosome assembly as a linear sequence of events given the components identified. This is the first observation of an eisosome component preceding Pil1 in deposition that has an effect in eisosome formation and shape, providing us with molecular handles and taking us a step closer to understanding the assembly of this large complex. This process may in fact be far more complex, and we still need to uncover the connection of eisosome components to the plasma membrane and most importantly how the different assembly states may affect the interaction with endocytic effectors during internalization.

MATERIALS AND METHODS

Yeast strains

Genotypes of all strains used in this study are listed in Table 1. The Pil1-GFP strain was described previously (TW110, Walther et al., 2006). The PIL1-GFP *pen1Δ* (KEM120) and *pen1Δ* strain (KEM121), were made by homologous recombination of PCR-generated fragments in strain TW110 and CRY2 respectively (Janke et al., 2004). The Pil1-GFP Pen1-Cherry (KEM122) and Pen1-GFP (KEM123) strains were similarly generated by homologous recombination, transforming the *PEN1*-fluorophore and marker fragment into TW110 and CRY2 respectively. Also, Pil1 knocked out was made by introducing the LEU3 marker into the PIL1 locus by homologous recombination into KEM123 to generate KEM124, and the NAT marker was introduced into the NCE102

locus of KEM124 to generate KEM 125. The copper inducible strains KEM126 and KEM127 were made by replacing the endogenous promoter of *PIL1* with the *CUP1* promoter into TWY110 and KEM123. Pen1-GFP and *pen1(F2A)-GFP* were cloned onto a pRS306 plasmid and integrated into the URA locus of KEM121 to make KEM128 and KEM129 respectively.

Microscopy

Live cell microscopy was performed by mounting yeast cells on concanavalin A covered coverslips. Images were taken at room temperature on a Zeiss LSM510 confocal microscope and on a Nikon TE2000U inverted microscope with a Yokogawa CSU22 Spinning Disk Confocal from Solamere Technology Group. Images were processed with ImageJ (<http://rsb.info.nih.gov/ij/index.html>).

Surface area calculation for buds were described previously in Moreira et al., 2008. Eisosome brightness was calculated by integrating the pixel intensity of a spot and subtracting the integrated density of an equivalent area for background using ImageJ.

Molecular Biology

Western blots were done by preparation of cell extracts in 8M urea 50 mM HEPES pH 7.4. Pil1-GFP and Pen1-GFP were detected by a chemiluminescent method (Pierce ECL Western Blotting Substrate, Thermo Fisher Scientific Inc.) using an antibody against GFP (Roche #11814460001 mouse monoclonal antibody) at 1:2,000 dilution; and Pgk1 was detected using a monoclonal mouse antibody (Invitrogen, #A6457) at 1:5,000 dilution. This step was followed by an HRP-conjugated goat secondary antibody diluted at

1:10,000. The blots were incubated with ECL substrate, exposed to a film and developed. Films were scanned and individual bands were quantified using ImageQuant TL.

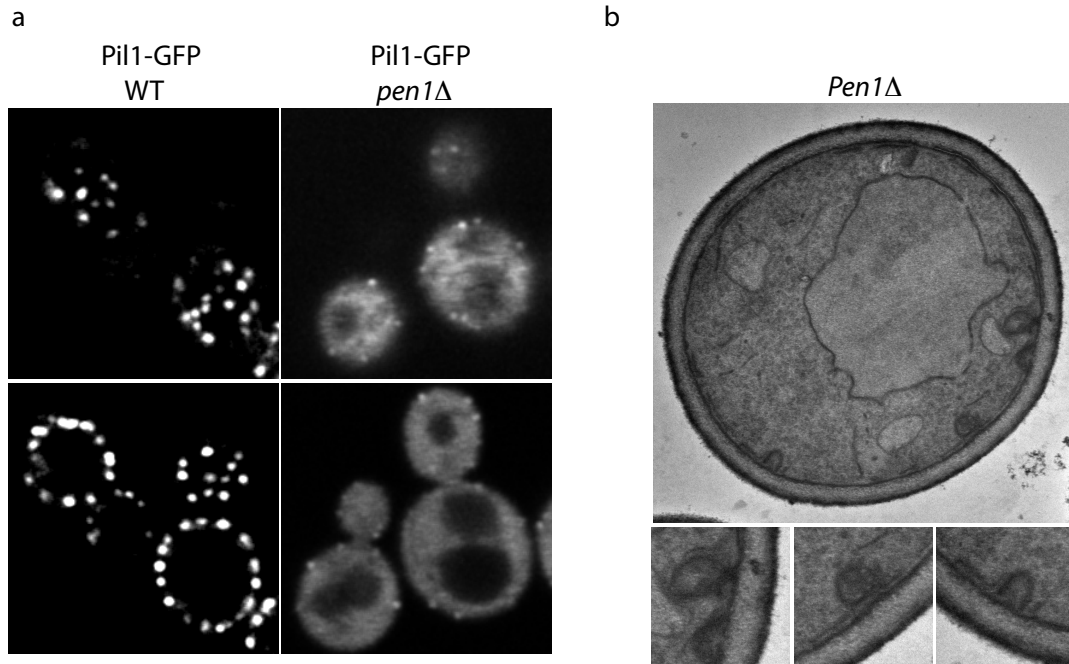


Figure 1. Pen1 is required for normal eisosome and membrane organization. (a) confocal images of Pil1-GFP in wild-type cells (WT; left) and *pen1*Δ cells (right). Representative top view images and mid sections are shown. (b) electron micrographs of *pen1*Δ cells, three inserts from the larger image.

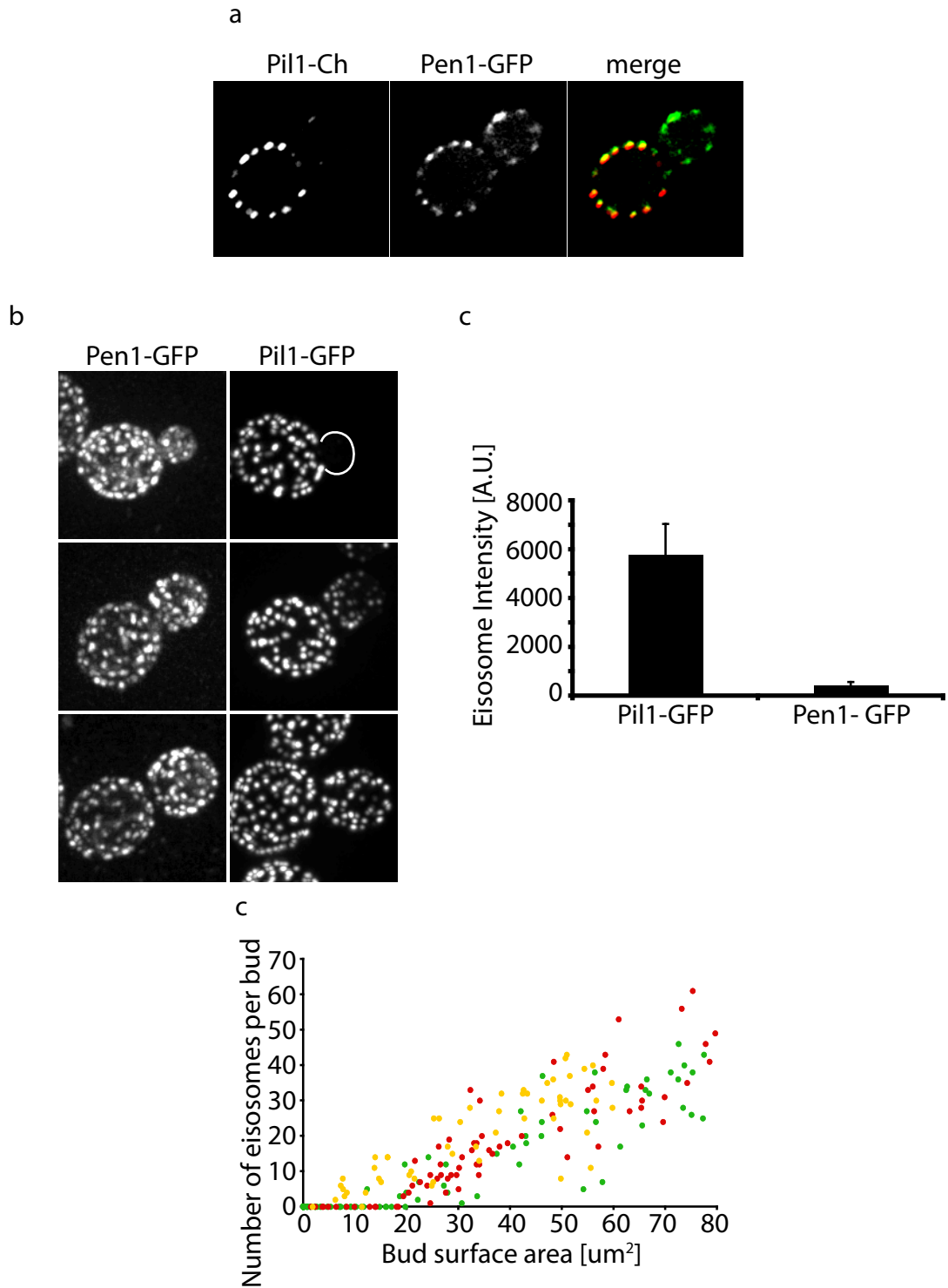


Figure 2. Pen1 colocalizes with eisosomes and its deposition precedes that of Pil1.

(a) Confocal mid section images of wild-type cells expressing Pil1-Cherry and Pen1-GFP. (b) Confocal 3D projections of wild-type cells expressing Pen1-GFP (left) or

Pil1-GFP (right). Representative images of small (top), medium (middle) and large (bottom) buds. (c) Integrated GFP fluorescence intensity of individual eisosomes from cells expressing Pil-GFP or Pen1-GFP. (d) Number of eisosomes where counted in cells expressing either Lsp1-GFP (red), Pil1-GFP (green), and Pen1-GFP (yellow) and are shown as a function of the bud cell surface.

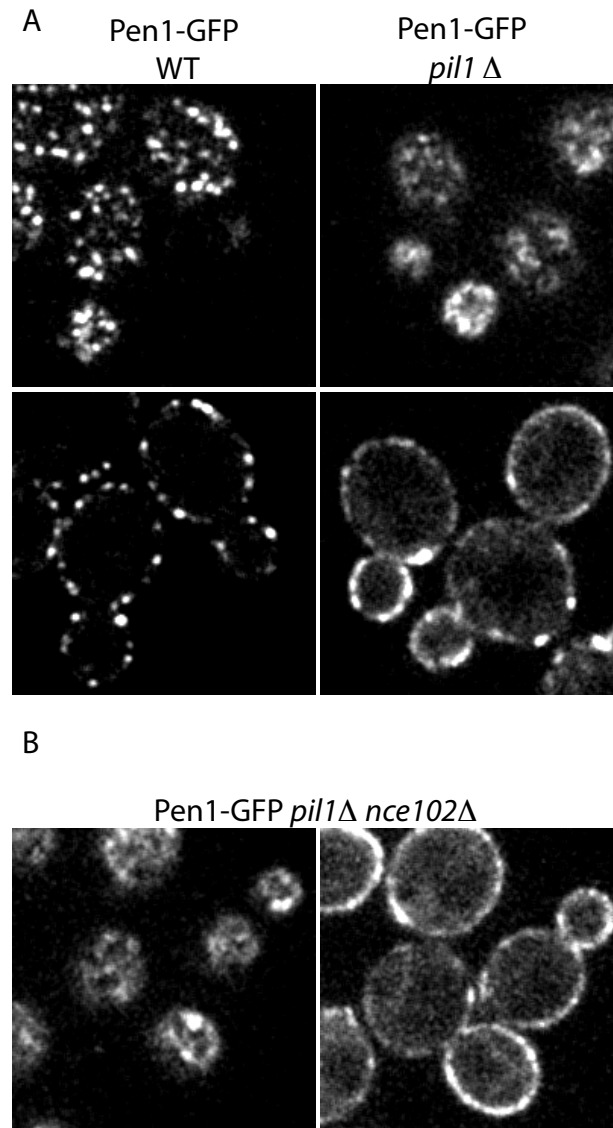


Figure 3. Pen1 localizes to the plasma membrane independent of Pil1 and Nce102.

(a) Confocal images of wild-type cells (left) and *pil1* Δ cells (right) expressing Pen1-GFP. (b) Confocal images of *pil1* Δ *nce102* Δ cells expressing Pen1-GFP. Representative top view and mid sections are shown for all images.

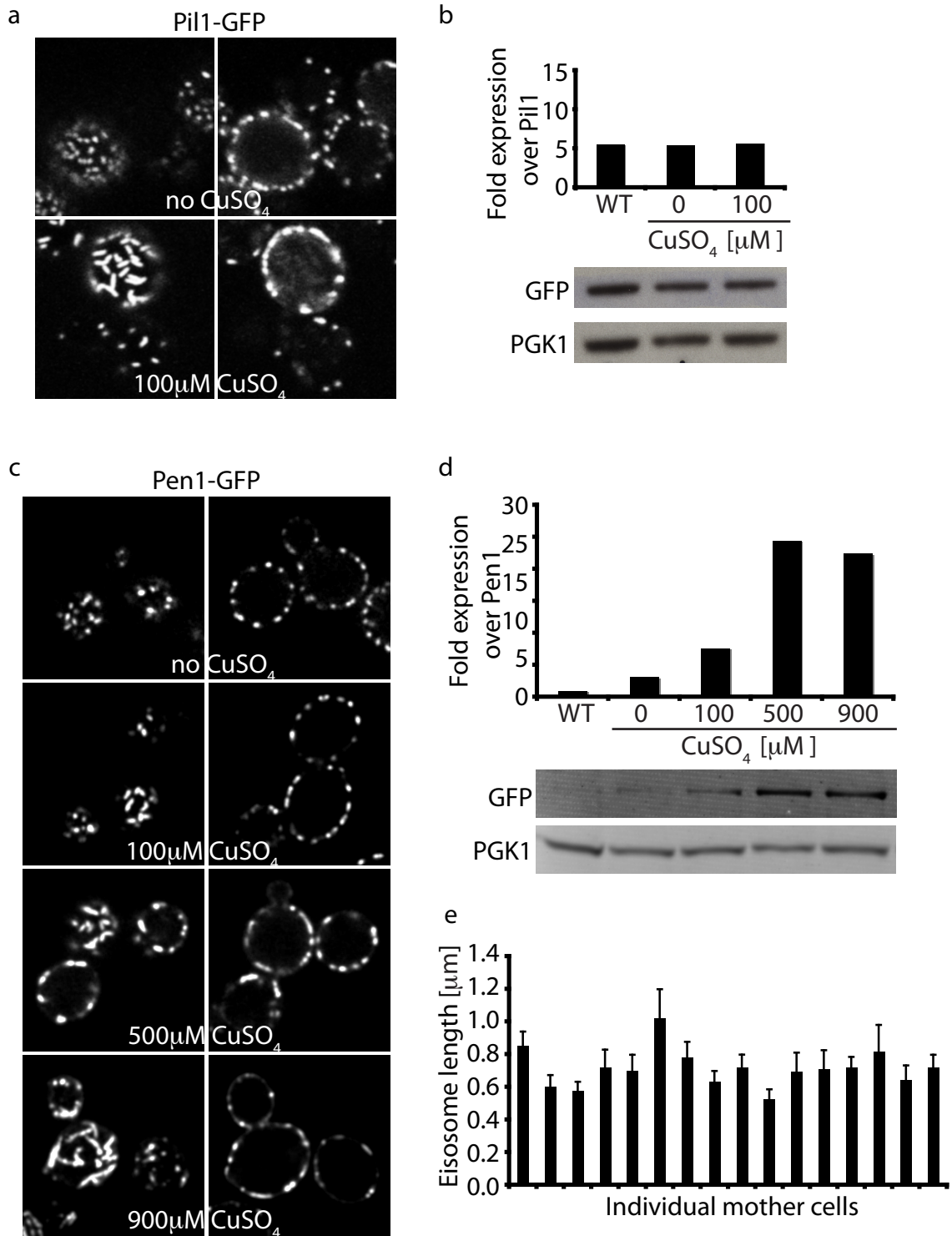


Figure 4. Pen1 overexpression causes eisosomes to nucleate into rods. (a) confocal images of cells expressing Pil1-GFP and Pen1 expressed under the CUP1 promoter. Cells grown under 0 μM CuSO_4 (top) and 100 μM CuSO_4 (bottom). (b) Western blots and the quantitation of relative abundance of Pil1-GFP to Pgc1 from cells described and

treated as in (a) normalized to wild-type “WT” levels of Pil1-GFP. (c) Titration of CuSO_4 of cells expressing Pen1-GFP under control of the CUP1 promoter treated with 0, 100, 500, and 900 μM CuSO_4 . (d) Western blots and the quantitation of relative abundance of Pen1-GFP to Pgk1 from cells described and treated as in (c) and normalized to wild-type “WT” levels of Pen1-GFP. Confocal top view (left) and mid section (right) are shown for all images. (e) Eisosome length from individual mother cells was measured from confocal top view images. Ten eisoosome lengths from each cell were averaged and plotted, the standard deviations are shown as errors, $n = 16$.

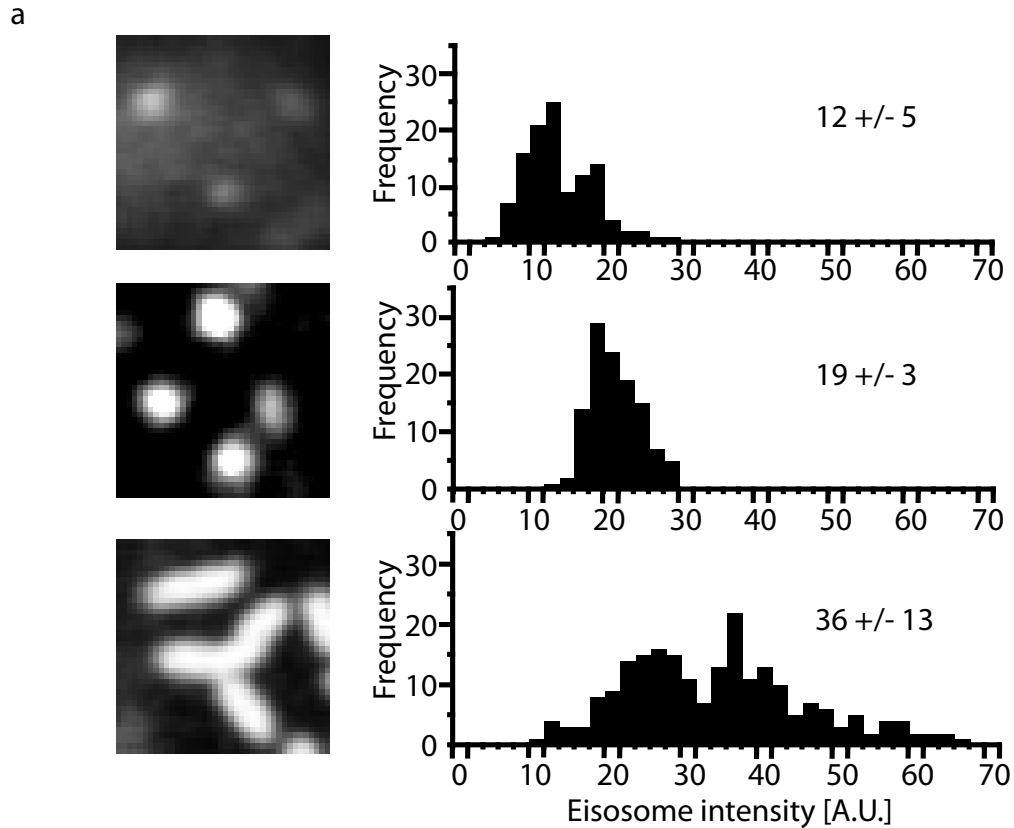


Figure 5. Eisosome brightness increases with increased Pen1 expression levels.

Left panel shows confocal top view images of *pen1Δ* (top), wild-type (middle) and Pen1 overexpressing cells, copper inducible Pen1 incubated at 100 μ M CuSO₄ (bottom), all expressing Pil1-GFP (bottom). Right panel shows the distribution of fluorescence intensities of Pil1-GFP patches as a function of the number of spots with that intensity from *pen1Δ* (top), wild-type (middle) and Pen1 overexpressing cells (bottom).

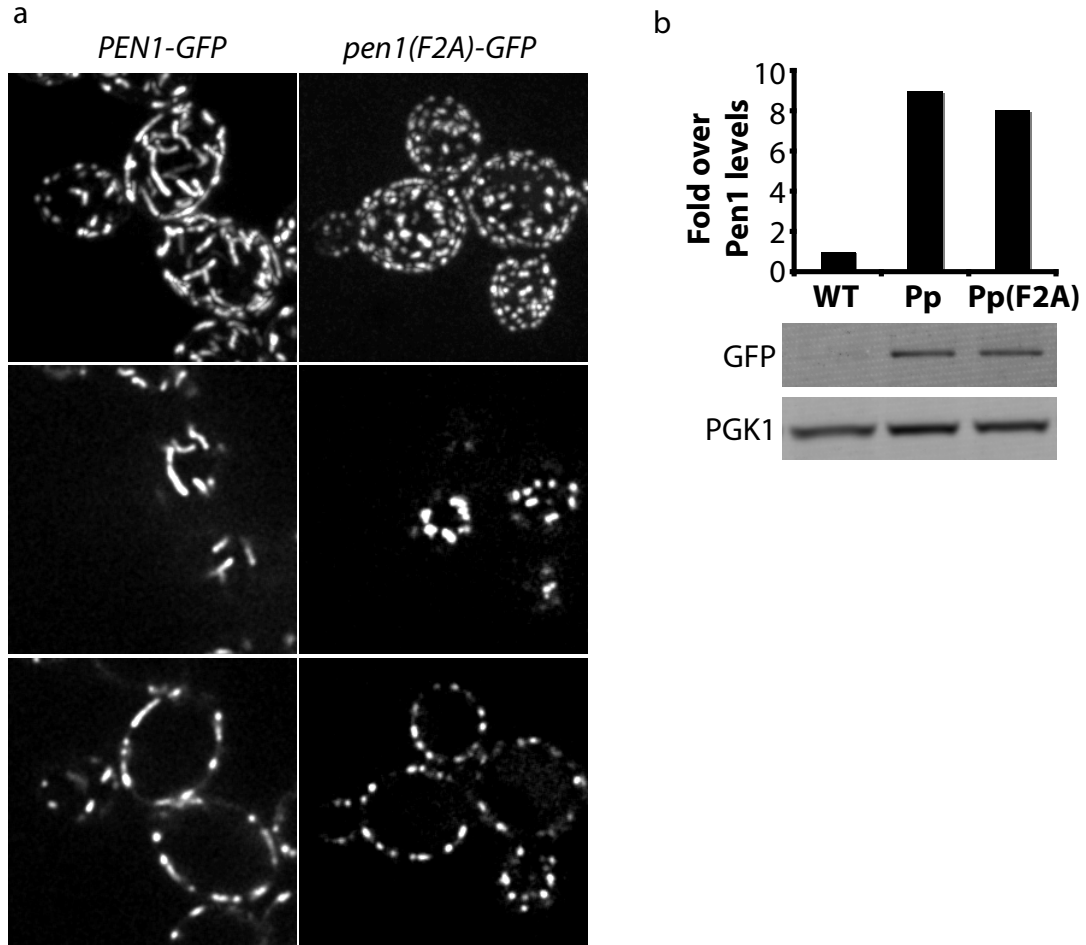


Figure 6. Pen1 nucleating function is compromised in *pen1(F2A)* mutant cells.
 (a) Confocal images of *Δpen1* cells bearing an integrative plasmid in the URA locus expressing *PEN1-GFP* or *pen1(F2A)-GFP*. 3D projections (top), top view (middle), mid section (bottom). (b) Western blots and the quantitation of relative abundance of Pen1-GFP “Pp” and *pen1(F2A)-GFP* “Pp(F2A)” to Pgc1 (cells expressing the integrative plasmid as in a), normalized to wild-type “WT” levels of Pen1-GFP tagged at the genomic locus.

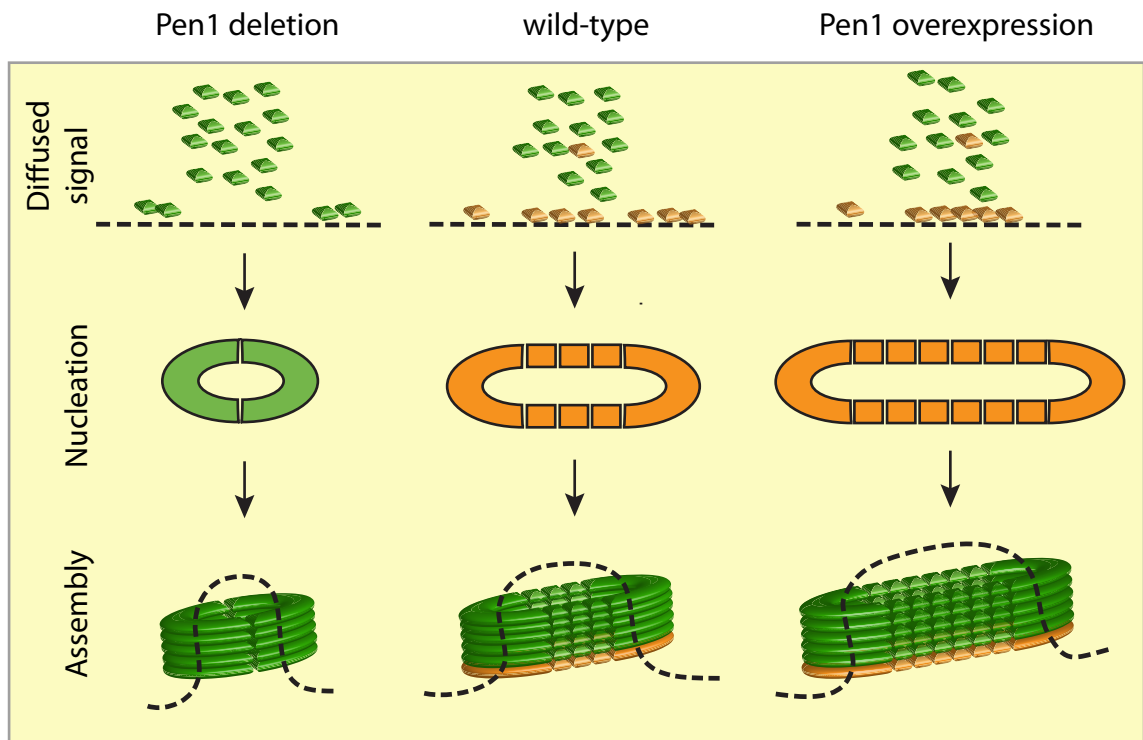


Figure 7. Eisosome nucleation and assembly model. Diagram depicting the nucleation and assembly of an eisosome in *pen1Δ* (left), wild-type (middle) and Pen1 overexpressing cells (right). Top of panel shows diffuse Pil1 (green) and Pen1 (orange) molecules in the cytoplasm and the membrane (dashed line). Nucleation step: lateral aggregation of Pil1 or Pen1 molecules at the plasma membrane (2D diagram). Assembly step: subsequent longitudinal assembly of Pil1 molecules stacking around the folding plasma membrane (3D diagram).

Supplemental Table I. Strains used in this study.	
Strain	Genotype
CRY1 ^{a,b}	<i>MATα ade2-1 can1-100 his3-11,15 leu2-3,112 trp1-1 ura3-1</i>
CRY2 ^{a,b}	<i>MATα ade2-1 can1-100 his3-11,15 leu2-3,112 trp1-1 ura3-1</i>
TWY110 ^c	<i>MATα PIL1-GFP::HIS3</i>
KEM120	<i>MATα PIL1-GFP::HIS3 pen1Δ ::NAT^R</i>
KEM121	<i>MATα pen1Δ ::NAT^R</i>
KEM122	<i>MATα PIL1-GFP::HIS3 PEN1-Cherry::KAN^R</i>
KEM123	<i>MATα PEN1-GFP::HIS3</i>
KEM124	<i>MATα PEN1-GFP::HIS3 pil1Δ ::LEU3</i>
KEM125	<i>MATα PEN1-GFP::HIS3 pil1Δ ::LEU3 nce102Δ ::NAT^R</i>
KEM126	<i>MATα PIL1-GFP::HIS3 NAT::pCUP1-PEN1</i>
KEM127	<i>MATα NAT::pCUP1-PEN1-GFP::HIS3</i>
KEM128	<i>MATα pen1Δ ::NAT^R URA3::PEN1-GFP</i>
KEM129	<i>MATα pen1Δ ::NAT^R URA3::pen1(F2A)-GFP</i>

^aAll strains used in this study were derived from CRY1 and CRY2, these strains are wild-type W303

^bWilcox et al. 1992

^cWalther et al. 1996

REFERENCES

- Alvarez FJ, L.M. Douglas, J.B. Konopka. 2009. The Sur7 protein resides in punctate membrane subdomains and mediates spatial regulation of cell wall synthesis in *Candida albicans*. *Commun Integr Biol.* 2(2):76-7.
- Alvarez, F.J., L.M. Douglas, A. Rosebrock, and J.B. Konopka. 2008. The eisosome protein Sur7 regulates plasma membrane organization and prevents intracellular cell wall growth in *Candida albicans*. *Mol. Biol. Cell.* doi: 10.1091/mbc.E08-05-0479.
- Anderson, R.G., and K. Jacobson. 2002. A role for lipid shells in targeting proteins to caveolae, rafts, and other lipid domains. *Science.* 296:1821-5.
- Aronova, S., K. Wedaman, S. Anderson, J. Yates, 3rd, and T. Powers. 2007. Probing the membrane environment of the TOR kinases reveals functional interactions between TORC1, actin, and membrane trafficking in *Saccharomyces cerevisiae*. *Mol Biol Cell.* 18:2779-94.
- Aronova, S., K. Wedaman, P.A. Aronov, K. Fontes, K. Ramos, B.D. Hammock, and T. Powers. 2008. Regulation of ceramide biosynthesis by TOR complex 2. *Cell Metab.* 7:148-58.
- Bacon, D.W. and D.G. Watts. 1971. Estimating the transition between two intersecting straight lines. *Biometrika.* 58:525-534.
- Bagnat, M., S. Keranen, A. Shevchenko, A. Shevchenko, and K. Simons. 2000. Lipid rafts function in biosynthetic delivery of proteins to the cell surface in yeast. *Proc Natl Acad Sci U S A.* 97:3254-9.
- Bagnat, M., and K. Simons. 2002. Cell surface polarization during yeast mating. *Proc Natl Acad Sci U S A.* 99:14183-8.
- Beeler, T., D. Bacikova, K. Gable, L. Hopkins, C. Johnson, H. Slife, and T. Dunn. 1998. The *Saccharomyces cerevisiae* TSC10/YBR265w gene encoding 3-ketosphinganine reductase is identified in a screen for temperature-sensitive suppressors of the Ca²⁺-sensitive *csg2Delta* mutant. *J Biol Chem.* 273:30688-94.
- Belfort, G.M., K. Bakirtzi, and K.V. Kandror. 2005. Cellugyrin induces biogenesis of synaptic-like microvesicles in PC12 cells. *J Biol Chem.* 280:7262-72.
- Berchtold, D., and T.C. Walther. 2009. TORC2 plasma membrane localization is essential for cell viability and restricted to a distinct domain. *Mol Biol Cell.* 20:1565-75.

- Bishop, A.C., J.A. Ubersax, D.T. Petsch, D.P. Matheos, N.S. Gray, J. Blethrow, E. Shimizu, J.Z. Tsien, P.G. Schultz, M.D. Rose, J.L. Wood, D.O. Morgan, and K.M. Shokat. 2000. A chemical switch for inhibitor-sensitive alleles of any protein kinase. *Nature*. 407:395-401.
- Brice, S.E., C.W. Alford, and L.A. Cowart. 2009. Modulation of Sphingolipid Metabolism by the Phosphatidylinositol-4-phosphate Phosphatase Sac1p through Regulation of Phosphatidylinositol in *Saccharomyces cerevisiae*. *J Biol Chem*. 284:7588-96.
- Brickner, J.H., Walter, P. 2004. Gene recruitment of the activated INO1 locus to the nuclear membrane. *PLoS Biol*. 2(11):e342.
- Broadie, K. 2004. Synapse scaffolding: intersection of endocytosis and growth. *Curr Biol*. 14:R853-5
- Casamayor, A., P.D. Torrance, T. Kobayashi, J. Thorner, and D.R. Alessi. 1999. Functional counterparts of mammalian protein kinases PDK1 and SGK in budding yeast. *Curr Biol*. 9:186-97.
- Cleves, A.E., D.N. Cooper, S.H. Barondes, and R.B. Kelly. 1996. A new pathway for protein export in *Saccharomyces cerevisiae*. *J Cell Biol*. 133:1017-26.
- Cox, J., and M. Mann. 2008. MaxQuant enables high peptide identification rates, individualized p.p.b.-range mass accuracies and proteome-wide protein quantification. *Nat Biotechnol*. 26:1367-72.
- Daquinag, A., M. Fadri, S.Y. Jung, J. Qin, and J. Kunz. 2007. The yeast PH domain proteins Slm1 and Slm2 are targets of sphingolipid signaling during the response to heat stress. *Mol Cell Biol*. 27:633-50.
- deHart, A.K., J.D. Schnell, D.A. Allen, and L. Hicke. 2002. The conserved Pkh-Ypk kinase cascade is required for endocytosis in yeast. *J Cell Biol*. 156:241-8.
- Delley, P. A., and Hall, M. N. 1999. Cell wall stress depolarizes cell growth via hyperactivation of RHO1. *J. Cell Biol*. 147:163-174
- Deng, C., X. Xiong, and A.N. Krutchinsky. 2009. Unifying fluorescence microscopy and mass spectrometry for studying protein complexes in cells. *Mol Cell Proteomics*.
- DeRisi, J.L., V.R. Iyer, and P.O. Brown. 1997. Exploring the metabolic and genetic control of gene expression on a genomic scale. *Science*. 278:680-6.
- Dickson, R.C., E.E. Nagiec, M. Skrzypek, P. Tillman, G.B. Wells, and R.L. Lester. 1997. Sphingolipids are potential heat stress signals in *Saccharomyces*. *J Biol Chem*. 272:30196-200.

- Eggeling C, C. Ringemann, R. Medda, G. Schwarzmann, K. Sandhoff, S. Polyakova, V.N. Belov, B. Hein, C. von Middendorff, A. Schönle, S.W. Hell. 2009. Direct observation of the nanoscale dynamics of membrane lipids in a living cell. *Nature*. 457:1159–1162.
- Eisenkolb, M., C. Zenzmaier, E. Leitner, R. Schneiter. 2002. A specific structural requirement for ergosterol in long-chain fatty acid synthesis mutants important for maintaining raft domains in yeast. *Mol. Biol. Cell*. 13:4414–4428.
- Fischer, M., I. Haase, E. Simmeth, G. Gerisch, and A. Müller-Taubenberger. 2004. A brilliant monomeric red fluorescent protein to visualize cytoskeleton dynamics in Dictyostelium. *FEBS Lett*. 577:227-32.
- Friant, S., R. Lombardi, T. Schmelzle, M.N. Hall, and H. Riezman. 2001. Sphingoid base signaling via Pkh kinases is required for endocytosis in yeast. *Embo J*. 20:6783-92.
- Gasch, A.P., P.T. Spellman, C.M. Kao, O. Carmel-Harel, M.B. Eisen, G. Storz, D. Botstein, and P.O. Brown. 2000. Genomic expression programs in the response of yeast cells to environmental changes. *Mol Biol Cell*. 11:4241-57.
- Girao H, M.I. Geli, F.Z. Idrissi. 2008. Actin in the endocytic pathway: From yeast to mammals. *FEBS Lett*. 18;582(14):2112-9
- Gourlay, C.W., H. Dewar, D.T. Warren, R. Costa, N. Satish, K.R. Ayscough. 2003. An interaction between Sla1p and Sla2p plays a role in regulating actin dynamics and endocytosis in budding yeast. *J Cell Sci*. 116:2551–2564.
- Grosshans, B.L., H. Grotzsch, D. Mukhopadhyay, I.M. Fernandez, J. Pfannstiel, F.Z. Idrissi, J. Lechner, H. Riezman, and M.I. Geli. 2006. TEDS site phosphorylation of the yeast myosins I is required for ligand-induced but not for constitutive endocytosis of the G protein-coupled receptor Ste2p. *J Biol Chem*. 281:11104-14.
- Grossmann, G., J. Malinsky, W. Stahlschmidt, M. Loibl, I. Weig-Meckl, W.B. Frommer, M. Opekarova, and W. Tanner. 2008. Plasma membrane microdomains regulate turnover of transport proteins in yeast. *J Cell Biol*. 183:1075-88.
- Grossmann, G., M. Opekarova, J. Malinsky, I. Weig-Meckl, and W. Tanner. 2007. Membrane potential governs lateral segregation of plasma membrane proteins and lipids in yeast. *Embo J*. 26:1-8.
- Han, G., K. Gable, S.D. Kohlwein, F. Beaudoin, J.A. Napier, and T.M. Dunn. 2002. The *Saccharomyces cerevisiae* YBR159w gene encodes the 3-ketoreductase of the microsomal fatty acid elongase. *J Biol Chem*. 277:35440-9.

- Ho, Y., A. Gruhler, A. Heilbut, G.D. Bader, L. Moore, S.L. Adams, A. Millar, P. Taylor, K. Bennett, K. Boutilier, L. Yang, C. Wolting, I. Donaldson, S. Schandorff, J. Shewnarane, J. Vo, J. Taggart, M. Goudreault, B. Muskat, C. Alfarano, D. Dewar, M. Z. Lin, K. Michalickova, A.R. Willems, H. Sassi, P.A. Nielsen, K.J. Rasmussen, J.R. Andersen, L.E. Johansen, L.H. Hansen, H. Jespersen, A. Podtelejnikov, E. Nielsen, J. Crawford, V. Poulsen, B.D. Sorensen, J. Matthiesen, R.C. Hendrickson, F. Gleeson, T. Pawson, M.F. Moran, D. Durocher, M. Mann, C.W. Hogue, D. Figgeys, M and Tyers. 2002. Systematic identification of protein complexes in *Saccharomyces cerevisiae* by mass spectrometry. *Nature*. 415, 180–183.
- Huh, W.K., J.V. Falvo, L.C. Gerke, A.S. Carroll, R.W. Howson, J.S. Weissman, and E.K. O'Shea. 2003. Global analysis of protein localization in budding yeast. *Nature*. 425:686-91.
- Idrissi, F.Z., H. Grotzsch, I.M. Fernandez-Golbano, C. Presciatto-Baschong, H. Riezman, M.I. Geli. 2008. Distinct acto/myosin-I structures associate with endocytic profiles at the plasma membrane. *J Cell Biol* 180:1219–1232.
- Inagaki, M., T. Schmelzle, K. Yamaguchi, K. Irie, M.N. Hall, and K. Matsumoto. 1999. PDK1 homologs activate the Pkc1-mitogen-activated protein kinase pathway in yeast. *Mol Cell Biol*. 19:8344-52.
- Janke, C., M.M. Magiera, N. Rathfelder, C. Taxis, S. Reber, H. Maekawa, A. Moreno-Borchart, G. Doenges, E. Schwob, E. Schiebel, and M. Knop. 2004. A versatile toolbox for PCR-based tagging of yeast genes: new fluorescent proteins, more markers and promoter substitution cassettes. *Yeast*. 21:947-62.
- Jenkins, G.M., A. Richards, T. Wahl, C. Mao, L. Obeid, Y. Hannun. 1997. Involvement of yeast sphingolipids in the heat stress response of *Saccharomyces cerevisiae*. *J Biol Chem*. 272:32566–32572.
- Jin, H., J.M. McCaffery, and E. Grote. 2008. Ergosterol promotes pheromone signaling and plasma membrane fusion in mating yeast. *J Cell Biol*. 180:813-26.
- Jonsdottir, G.A., R. Li. 2004. Dynamics of yeast myosin I: evidence for a possible role in scission of endocytic vesicles. *Curr. Biol*. 14:1604–1609.
- Kaksonen, M., C. P. Toret, D.G. Drubin. 2003. A modular design for the clathrin- and actin-mediated endocytosis machinery, *Cell* 123:305–320.
- Kaksonen, M., Y. Sun, D.G. Drubin. 2003. A pathway for association of receptors, adaptors, and actin during endocytic internalization, *Cell* 115:475–487.

- Koh, T.W., P. Verstreken, and H.J. Bellen. 2004. Dap160/intersectin acts as a stabilizing scaffold required for synaptic development and vesicle endocytosis. *Neuron*. 43:193-205.
- Kübler, E., H. G. Dohlman, and M. P. Lisanti. 1996. Identification of Triton X-100 insoluble membrane domains in the yeast *Saccharomyces cerevisiae*: lipid requirements for targeting of heterotrimeric G protein subunits. *J. Biol. Chem.* 271:32975-32980.
- Lee, M.C., S. Hamamoto, and R. Schekman. 2002. Ceramide biosynthesis is required for the formation of the oligomeric H⁺-ATPase Pma1p in the yeast endoplasmic reticulum. *J Biol Chem.* 277:22395-401.
- Lenne, P.F., L. Wawrezynieck, F. Conchonaud, O. Wurtz, A. Boned, X.J. Guo, H. Rigneault, H.T. He, D. Marguet. 2006. Dynamic molecular confinement in the plasma membrane by microdomains and the cytoskeleton meshwork. *EMBO J.* 25:3245–3256.
- Lew, D.J., Reed, S.I. 1993. Morphogenesis in the yeast cell cycle: regulation by Cdc28 and cyclins. *J Cell Biol.* 120(6):1305-20
- Liu, K., X. Zhang, R.L. Lester, and R.C. Dickson. 2005. The sphingoid long chain base phytosphingosine activates AGC-type protein kinases in *Saccharomyces cerevisiae* including Ypk1, Ypk2, and Sch9. *J Biol Chem.* 280:22679-87.
- Luo, G., A. Gruhler, Y. Liu, O.N. Jensen, and R.C. Dickson. 2008. The sphingolipid long-chain base-Pkh1/2-Ypk1/2 signaling pathway regulates eisosome assembly and turnover. *J Biol Chem.* 283:10433-44.
- Malinska, K., J. Malinsky, M. Opekarova, and W. Tanner. 2003. Visualization of protein compartmentation within the plasma membrane of living yeast cells. *Mol Biol Cell.* 14:4427-36.
- Malinska, K., J. Malinsky, M. Opekarova, and W. Tanner. 2004. Distribution of Can1p into stable domains reflects lateral protein segregation within the plasma membrane of living *S. cerevisiae* cells. *J Cell Sci.* 117:6031-41.
- Marie, B., S.T. Sweeney, K.E. Poskanzer, J. Roos, R.B. Kelly, and G.W. Davis. 2004. Dap160/intersectin scaffolds the periaxonal zone to achieve high-fidelity endocytosis and normal synaptic growth. *Neuron*. 43:207-19.
- Mayor S, M. Rao. 2004. Rafts: scale-dependent, active lipid organization at the cell surface. *Traffic*. 2004 Apr;5(4):231-40.
- Moore, R.E., M.K. Young, and T.D. Lee. 2002. Qscore: an algorithm for evaluating SEQUEST database search results. *J Am Soc Mass Spectrom.* 13:378-86.

- Munn, A. L., H. Riezman. 1994. Endocytosis is required for the growth of vacuolar H(+)-ATPase-defective yeast: identification of six new END genes. *J. Cell Biol.* 127: 373–386.
- Munro S. 2003. Lipid rafts: elusive or illusive?. *Cell.* 14;115(4):377-88.
- Nagiec, M.M., E.E. Nagiec, J.A. Baltisberger, G.B. Wells, R.L. Lester, and R.C. Dickson. 1997. Sphingolipid synthesis as a target for antifungal drugs. Complementation of the inositol phosphorylceramide synthase defect in a mutant strain of *Saccharomyces cerevisiae* by the AUR1 gene. *J Biol Chem.* 272:9809-17.
- Newpher, T.M., S.K. Lemmon. 2006. Clathrin is important for normal actin dynamics and progression of Sla2p-containing patches during endocytosis in yeast. *Traffic* 7:574–588.
- Oehlen, L.J., D.I. Jeoung, and F.R. Cross. 1998. Cyclin-specific START events and the G1-phase specificity of arrest by mating factor in budding yeast. *Mol Gen Genet.* 258:183-98.
- Olsen, J.V., L.M. de Godoy, G. Li, B. Macek, P. Mortensen, R. Pesch, A. Makarov, O. Lange, S. Horning, and M. Mann. 2005. Parts per million mass accuracy on an Orbitrap mass spectrometer via lock mass injection into a C-trap. *Mol Cell Proteomics.* 4:2010-21.
- Ong, S.E., B. Blagoev, I. Kratchmarova, D.B. Kristensen, H. Steen, A. Pandey, and M. Mann. 2002. Stable isotope labeling by amino acids in cell culture, SILAC, as a simple and accurate approach to expression proteomics. *Mol Cell Proteomics.* 1:376-86.
- Otsu, N. 1979. A threshold selection method form gray-level histograms. *IEEE Trans. Sys.* 9:62-66.
- Paul, S., K. Gable, F. Beaudoin, E. Cahoon, J. Jaworski, J.A. Napier, and T.M. Dunn. 2006. Members of the Arabidopsis FAE1-like 3-ketoacyl-CoA synthase gene family substitute for the Elop proteins of *Saccharomyces cerevisiae*. *J Biol Chem.* 281:9018-29.
- Peng, J., J.E. Elias, C.C. Thoreen, L.J. Licklider, and S.P. Gygi. 2003. Evaluation of multidimensional chromatography coupled with tandem mass spectrometry (LC/LC-MS/MS) for large-scale protein analysis: the yeast proteome. *J Proteome Res.* 2:43-50.

- Perkins, D.N., D.J. Pappin, D.M. Creasy, and J.S. Cottrell. 1999. Probability-based protein identification by searching sequence databases using mass spectrometry data. *Electrophoresis*. 20:3551-67.
- Peter B.J., K.M. Kent, I.G. Mills, Y. Vallis, P.J.G. Butler, P.R. Evans, H.T. McMahon . 2004. BAR domains as sensors of membrane curvature: the amphiphysin BAR structure. *Science* 303:495–499.
- Powers, T. 2007. TOR signaling and S6 kinase 1: Yeast catches up. *Cell Metab*. 6:1-2.
- Prior, I.A., C. Muncke, R.G. Parton, J.F. Hancock. Direct visualization of Ras proteins in spatially distinct cell surface microdomains. *J Cell Biol*. 2003;160:165–170
- Rappsilber, J., Y. Ishihama, and M. Mann. 2003. Stop and go extraction tips for matrix-assisted laser desorption/ionization, nanoelectrospray, and LC/MS sample pretreatment in proteomics. *Anal Chem*. 75:663-70.
- Robertson, A.S., E., Smythe, K.R. Ayscough. 2009. Functions of actin in endocytosis. *Cell Mol Life Sci*. 66(13):2049-65.
- Roelants, F.M., P.D. Torrance, N. Bezman, and J. Thorner. 2002. Pkh1 and pkh2 differentially phosphorylate and activate ypk1 and ykr2 and define protein kinase modules required for maintenance of cell wall integrity. *Mol Biol Cell*. 13:3005-28.
- Rodriguez-Boulan, E., G. Kreitzer, and A. Musch. 2005. Organization of vesicular trafficking in epithelia. *Nat Rev Mol Cell Biol*. 6:233-47.
- Sawai, H., Y. Okamoto, C. Luberto, C. Mao, A. Bielawska, N. Domae, and Y.A. Hannun. 2000. Identification of ISC1 (YER019w) as inositol phosphosphingolipid phospholipase C in *Saccharomyces cerevisiae*. *J Biol Chem*. 275:39793-8.
- Schuldiner, M., S.R. Collins, N.J. Thompson, V. Denic, A. Bhamidipati, T. Punna, J. Ihmels, B. Andrews, C. Boone, J.F. Greenblatt, J.S. Weissman, and N.J. Krogan. 2005. Exploration of the function and organization of the yeast early secretory pathway through an epistatic miniarray profile. *Cell*. 123:507-19.
- Sharma, P., R. Varma, R.C. Sarasij, Ira, K. Gousse, G. Krishnamoorthy, M. Rao , S. Mayor S. Nanoscale Organization of Multiple GPI-Anchored Proteins in Living Cell Membranes. *Cell*. 2004;116:577–589.
- Simons, K., and E. Ikonen. 1997. Functional rafts in cell membranes. *Nature*. 387:569-72.
- Simons, K., and D. Toomre. 2000. Lipid rafts and signal transduction. *Nat Rev Mol Cell Biol*. 1:31-9.

- Simons, K., and W.L. Vaz. 2004. Model systems, lipid rafts, and cell membranes. *Annu Rev Biophys Biomol Struct.* 33:269-95.
- Sivadon, P., M.F. Peypouquet, F. Doignon, M. Aigle, M. Crouzet. 1997. Cloning of the multicopy suppressor gene SUR7: evidence for a functional relationship between the yeast actin-binding protein Rvs167 and a putative membranous protein. *Yeast.* 30;13(8):747-61.
- Spellman, P.T., G. Sherlock, M.Q. Zhang, V.R. Iyer, K. Anders, M.B. Eisen, P.O. Brown, D. Botstein, and B. Futcher. 1998. Comprehensive identification of cell cycle-regulated genes of the yeast *Saccharomyces cerevisiae* by microarray hybridization. *Mol Biol Cell.* 9:3273-97.
- Sun, Y., R. Taniguchi, D. Tanoue, T. Yamaji, H. Takematsu, K. Mori, T. Fujita, T. Kawasaki, and Y. Kozutsumi. 2000. Sli2 (Ypk1), a homologue of mammalian protein kinase SGK, is a downstream kinase in the sphingolipid-mediated signaling pathway of yeast. *Mol Cell Biol.* 20:4411-9.
- Tabuchi, M., A. Audhya, A.B. Parsons, C. Boone, and S.D. Emr. 2006. The phosphatidylinositol 4,5-bisphosphate and TORC2 binding proteins Slm1 and Slm2 function in sphingolipid regulation. *Mol Cell Biol.* 26:5861-75.
- Tong, A.H., G. Lesage, G.D. Bader, H. Ding, H. Xu, X. Xin, J. Young, G.F. Berriz, R.L. Brost, M. Chang, Y. Chen, X. Cheng, G. Chua, H. Friesen, D.S. Goldberg, J. Haynes, C. Humphries, G. He, S. Hussein, L. Ke, N. Krogan, Z. Li, J.N. Levinson, H. Lu, P. Menard, C. Munyana, A.B. Parsons, O. Ryan, R. Tonikian, T. Roberts, A.M. Sdicu, J. Shapiro, B. Sheikh, B. Suter, S.L. Wong, L.V. Zhang, H. Zhu, C.G. Burd, S. Munro, C. Sander, J. Rine, J. Greenblatt, M. Peter, A. Bretscher, G. Bell, F.P. Roth, G.W. Brown, B. Andrews, H. Bussey, and C. Boone. 2004. Global mapping of the yeast genetic interaction network. *Science.* 303:808-13.
- Ubersax, J.A., E.L. Woodbury, P.N. Quang, M. Paraz, J.D. Blethrow, K. Shah, K.M. Shokat, and D.O. Morgan. 2003. Targets of the cyclin-dependent kinase Cdk1. *Nature.* 425:859-64.
- Valdez-Taubas, J., and H.R. Pelham. 2003. Slow diffusion of proteins in the yeast plasma membrane allows polarity to be maintained by endocytic cycling. *Curr Biol.* 13:1636-40.
- van Meer, G., D.R. Voelker, and G.W. Feigenson. 2008. Membrane lipids: where they are and how they behave. *Nat Rev Mol Cell Biol.* 9:112-24.
- Vida, T.A., and S.D. Emr. 1995. A new vital stain for visualizing vacuolar membrane dynamics and endocytosis in yeast. *J Cell Biol.* 128:779-92.

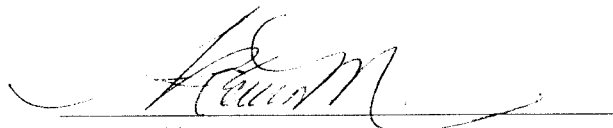
- Walther, T.C., J.H. Brickner, P.S. Aguilar, S. Bernales, C. Pantoja, and P. Walter. 2006. Eisosomes mark static sites of endocytosis. *Nature*. 439:998-1003.
- Walther, T.C., P.S. Aguilar, F. Frohlich, F. Chu, K. Moreira, A.L. Burlingame, and P. Walter. 2007. Pkh-kinases control eisosome assembly and organization. *Embo J*. 26:4946-55.
- Warren, D.T., P.D. Andrews, C.W. Gourlay, K.R. Ayscough. 2002. Sla1p couples the yeast endocytic machinery to proteins regulating actin dynamics. *J Cell Sci*. 115:1703-1715.
- Wesp, A., L. Hicke, J. Palecek, R. Lombardi, T. Aust, A.L. Munn, H. Riezman. 1997. End4p/Sla2p interacts with actin-associated proteins for endocytosis in *Saccharomyces cerevisiae*. *Mol Biol Cell*. 8:2291-2306.
- Wilcox, C.A., Redding, K., Wright, R., Fuller, R.S. 1992. Mutation of a tyrosine localization signal in the cytosolic tail of yeast Kex2 protease disrupts Golgi retention and results in default transport to the vacuole. *Mol Biol Cell*. 3(12):1353-71.
- Young, M.E., T.S. Karpova, B. Brugger, D.M Moschenross, G.K. Wang, R. Schneiter, F.T. Wieland, J.A. Cooper. 2002. The Sur7p family defines novel cortical domains in *Saccharomyces cerevisiae*, affects sphingolipid metabolism, and is involved in sporulation. *Mol Cell Biol*. 22:927-934
- Zanolari, B., S. Friant, K. Funato, C. Sutterlin, B. J. Stevenson, and H. Riezman. 2000. Sphingoid base synthesis requirement for endocytosis in *Saccharomyces cerevisiae*. *EMBO J*. 19:2824-2833.
- Zhang, X., R.L. Lester, and R.C. Dickson. 2004. Pil1p and Lsp1p negatively regulate the 3-phosphoinositide-dependent protein kinase-like kinase Pkh1p and downstream signaling pathways Pkc1p and Ypk1p. *J Biol Chem*. 279:22030-8.

Publishing Agreement

It is the policy of the University to encourage the distribution of all theses, dissertations, and manuscripts. Copies of all UCSF theses, dissertations, and manuscripts will be routed to the library via the Graduate Division. The library will make all theses, dissertations, and manuscripts accessible to the public and will preserve these to the best of their abilities, in perpetuity.

Please sign the following statement:

I hereby grant permission to the Graduate Division of the University of California, San Francisco to release copies of my thesis, dissertation, or manuscript to the Campus Library to provide access and preservation, in whole or in part, in perpetuity.



Author Signature

01-11-00
Date